Durham E-Theses

Some semiconducting properties of Barium Titanate

David L. Ridpath

ABSTRACT

A number of single crystals of barium titanate have been grown by the flux melt process. These have been rendered semiconducting by reduction in hydrogen at $800^{\circ}C$ for times up to 15 min.

The resistivity, Seebeck coefficient and optical absorption coefficient have been measured in these crystals to obtain information about the conduction processes. The temperature of the tetragonal to cubic transition in the reduced crystals has been measured and is shown to be consistent with the results of the resistivity and Seebeck data.

The results obtained are consistent with the theory that electrical conduction in these crystals is in the small polaron hopping mode with a drift mobility at room temperature of about $4 \times 10^{-4} cm^2/V.s.$ with polaron concentrations reaching a peak of $4.18 \times 10^{20} cm^{-3}$.

The variation of polaron concentration with reduction time is similar to that obtained by Arend et al. by chemical analyses.

SOME   SEMICONDUCTING   PROPERTIES

OF   BARIUM   TITANATE.

by

David   L.   Ridpath ,   B . A . (Oxon.).

being   a   thesis

submitted   for   the   degree

of   Doctor   of   Philosophy.

UNIVERSITY   OF   DURHAM

1969

Acknowledgements

Contents

Copy of Ridpath & Wright, J.Mats.Sci.$\underline{3}$,335,(1968) bound at end

                                                of thesis.

Crystals as grown before removal from crucible. (see Chapter 3)
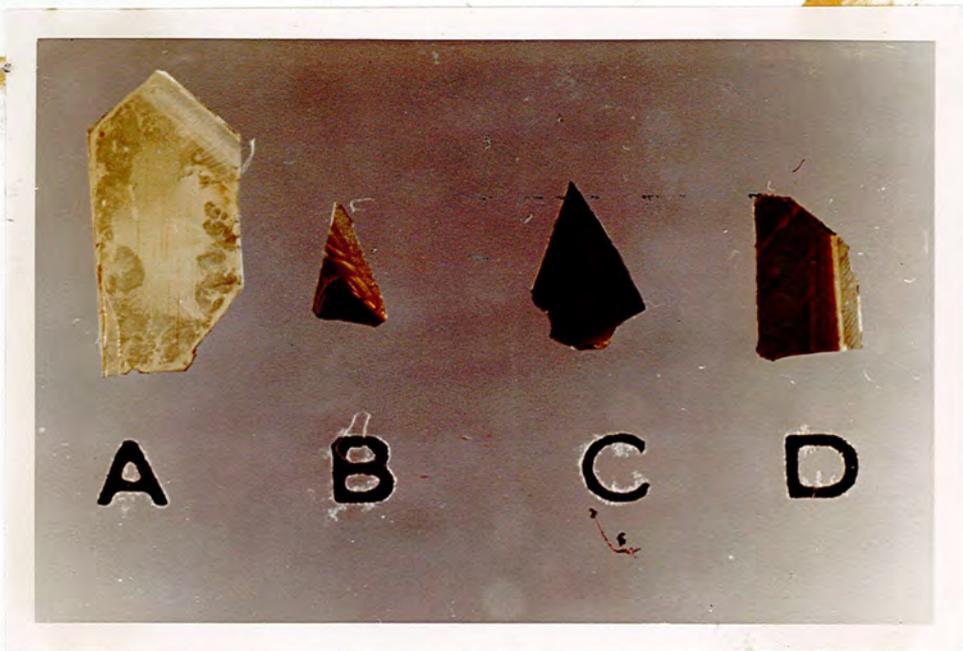
Crystals heat treated in hydrogen for successively longer periods.
(see Chapter 5)

Chapter 1
Introduction

1.The purpose of the research programme.

This thesis reports a programme of research performed on single crystal barium titanate. This, it was intended should be complementary to a similar programme on barium titanate ceramics carried out at the Central Electricity Research Laboratories, Leatherhead. The present work was sponsored by these laboratories.

When this programme commenced, the interest in barium titanate was in its use as an insulator for power lines. It was hoped that the work would assist in the design of insulators which would have positive temperature coefficients of resistivity. These could, perhaps, be constructed in such a way that controlled Joule heating would prevent ice forming on them during cold weather. Chapter 2 will explain how the positive temperature coefficient of resistance occurs in barium titanate ceramics.

The Central Electricity Generating Board had, too, an interest in semiconducting mixed oxide ceramics for possible use as electrodes in magnetohydrodynamic generators. Although the present work was not expected to yield results which would concern these applications directly, it was felt that further information on single crystal conduction in barium titanate would be of general interest to the sponsors, while also being suitable for a higher degree in a university department.

Outside the electricity supply industry, barium titanate
semiconducting ceramics are produced as positive temperature
coefficient resistors for use in the electronics industry
where they find application as protective devices in solid state
circuitry. High resistivity barium titanate ceramics are
extensively used for record player transducers. A knowledge of
conduction mechanisms in the semiconducting bulk material could
prove useful in the design of these components.

2.The research programme.

The basic interests of the programme were the conduction
parameters in the bulk material. The measurements necessary to
derive these parameters are the Hall coefficient from which the
carrier concentration can be derived; the resistivity which
yields the mobility and the Seebeck coefficient which enables
one to calculate the effective mass of the electrons. The
present programme sought to measure these properties in single
crystals treated in various ways to make them semiconducting.

The first task was to grow some single crystals and to
determine in what ways they could most easily be made semiconducting.
The way in which this was done is described in chapter 3. The
resistivity and Hall effect measurements are reported in chapter
6 and the Seebeck coefficient measurements are described in
chapter 7.

In the course of these measurements, however, there turned
out to be a number of other properties of which details would be

useful in explaining the results. Chapter 4, then, reports the measurement of the variation in the ferroelectric Curie point temperature with the semiconducting properties and Chapter 5 shows the effect of the semiconducting properties on the optical absorption coefficient. The results of brief experiments to detect photoconductivity in the semiconducting crystals are also presented in Chapter 5. Routine measurements of the two-probe resistance were made and proved to show a hitherto unreported effect at temperatures of about 450°C. This effect is briefly described in Chapter 8 but is not developed since it was not considered relevant to the main body of the programme.

An appendix describes attempts to produce compounds in which the oxygen atoms of the titanate were replaced by sulphur.

In Chapter 9, the results of all the measurements reported in the previous chapters are discussed and analysed. Various conclusions are arrived at concerning the conduction mechanisms in these crystals and suggestions are made for continuation of the work.

Chapter 2 describes various properties of single crystal and of ceramic barium titanate which are relevant to the present programme.

3. Nomenclature and units.

Wherever possible, the symbols and units recommended by the Systeme Internationale have been used. A list of these symbols can be found in reference 1.1.

It has been the custom in solid state physics to use mixed units such as $cm^2/V.s.$ for mobility. In deference to accepted usage, these units are continued here but it must be pointed out that the equations are all in c.g.s. units and as such, the values of all quantities in other units must be multiplied by the appropriate factor before the equations will apply.

Throughout the thesis, the following conventions are used to refer to figures, equations and references.

Figures: a figure is denoted by a number, being the number of the chapter in which the figure is included and a lower case letter denoting order within that chapter. The second figure in chapter 3 is thus denoted 3.b.

Equations: an equation is denoted again by the number of the chapter in which it is to be found but now followed by a capital letter to denote the equation within that chapter. The fourth equation in chapter 6 is therefore denoted 6.D.

References: references are denoted by two numbers, the first denoting the chapter in which the reference is made and the second indicating order within the chapter. (4.8.) then represents the 8th reference in chapter 4. The references at the end of the thesis are listed in numerical rather than alphabetical order.

Chapter 2
Some relevant Properties of Barium Titanate

1.General properties of barium titanate.

Barium titanate as made commercially is a white powder.
When sintered into a solid ceramic, however, it becomes a
hard, brittle, pale yellow material. The single crystals are
also pale yellow with a high refractive index.

The pure material has a high melting point (1600°C) and
is stable in air and water at moderate temperatures.

The ferroelectric properties were discovered simultaneously
in the U.S.A. (2.1.) and in the U.S.S.R. (2.2.) in 1946.
Coupled with the ferroelectric properties, the material has a
large d_{31} piezoelectric coefficient which has led to widespread
use of the ceramic material in record player transducers.

The theoretical density is 6.1 gms/c.c. and the measured
density is 5.9 gms/c.c. as determined by Rase and Roy (2.3.).
Typical ceramic densities range from 5.0 to 5.6 gms/c.c.

2.Crystal structure.

Barium titanate has two high temperature modifications,
cubic and hexagonal, of which only the former has any significance
here since the latter does not lead to the ferroelectric,
tetragonal phase at lower temperatures. The cubic form undergoes
spontaneous changes to tetragonal at about 120°C and to lower

forms of symmetry at lower temperatures. It is these non-cubic
forms which are ferroelectric.

(a) Cubic (space group Pm3m)

The cubic phase exhibits the perovskite unit cell. The
arrangement of ions in this form is shown in fig.2.a. The
barium ions are situated at the cube corners, the oxygen ions
at the cube face centres and the single titanium ion at the body
centre. The unit cell, therefore, corresponds to the empirical
formula, $BaTiO_3$. It is useful to note at this point that the
titanium ion is situated at the centre of six, octahedrally placed
oxygen ions. This is shown more clearly in fig.2.b. The cell
edge is of length about 4 angstroms at $120^{\circ}C$.

(b) Tetragonal (space group P4mm)

At the Curie point, the transition to tetragonal involves
only small changes in the ionic positions. The axial ratio is
only about 1.01. The new structure is derived from the cubic one
by stretching the unit cell along one of the cell edges. All the
ions are displaced in the c direction in such a way that the
oxygen ions are still at the face centres. In section 3 of this
chapter, however, it will be seen that the titanium atom receives
a non-proportional displacement, which leads to the ferroelectric
properties. The lack of a centre of symmetry in the new structure
leads to the piezoelectric properties. The structures in the
cubic and tetragonal phases were first ascertained by Megaw
(2.4.). The general distortion in the tetragonal phase is shown
diagramatically in fig.2.c. and the displacements of the individual
ions are shown in fig.2.d.
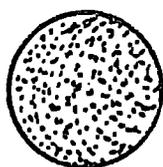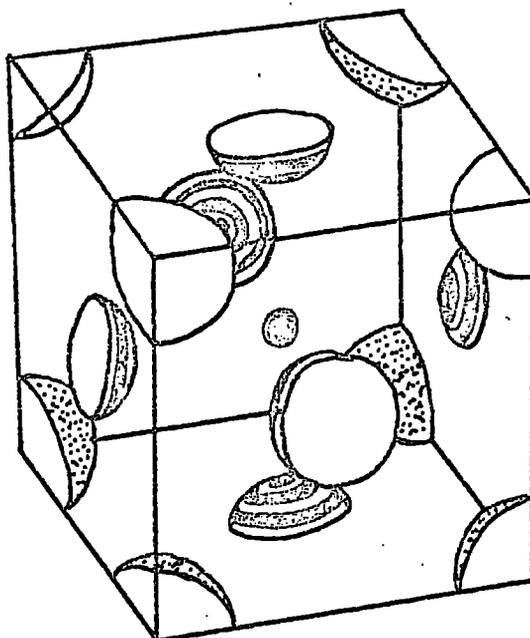
Fig. 2.a.   The arrangement of ions within the $BaTiO_3$ unit cell.
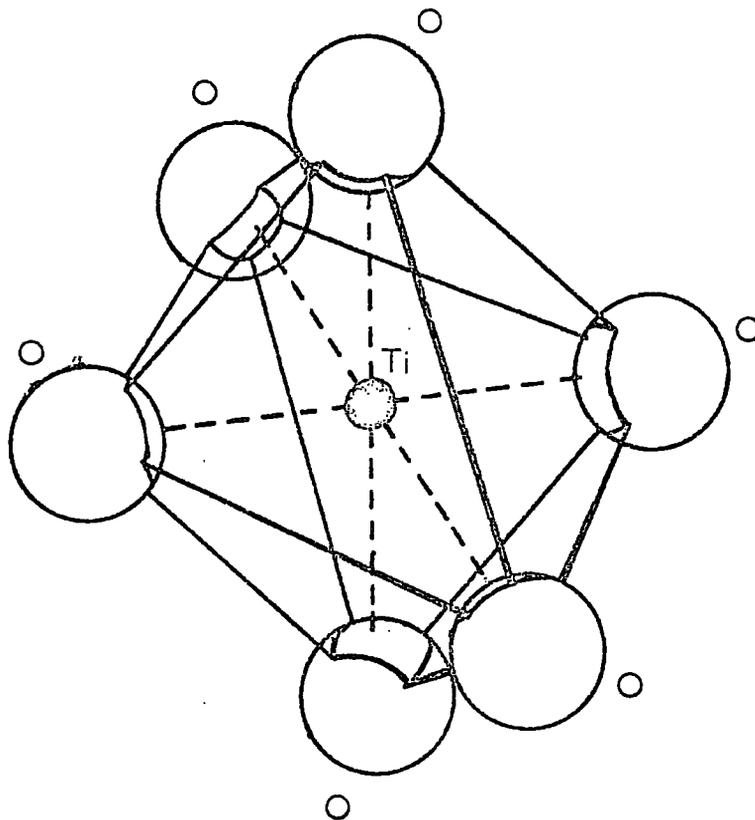
Fig. 2.b.   The octahedron of oxygen ions.
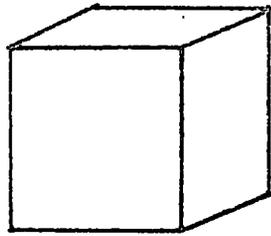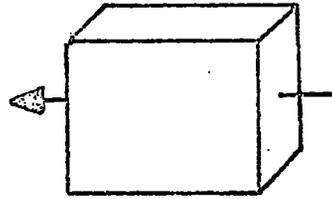
Cubic   Tetragonal
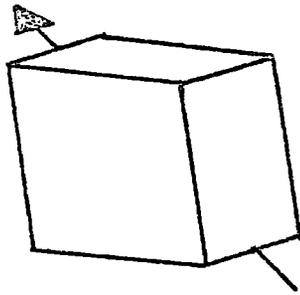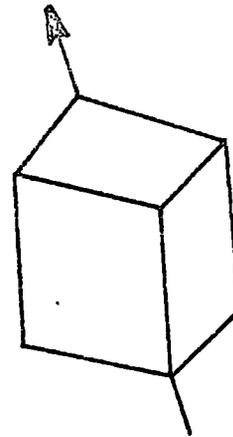
Orthorhombic   Rhombohedral

Fig. 2.c.   Distortion in various phases of $BaTiO_3$.

Tetragonal
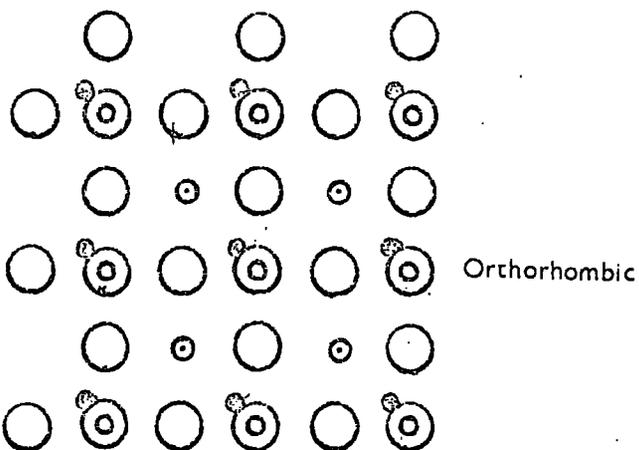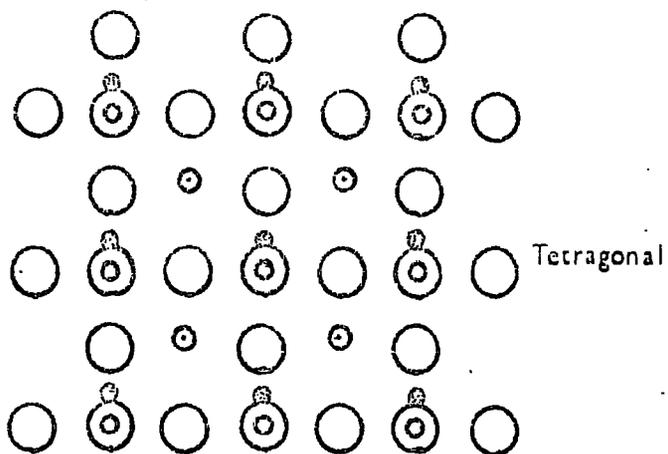
Orthorhombic

Oxygen at height $\pm \frac{a}{2}$

Oxygen at height 0

Barium at height $\pm \frac{a}{2}$

Titanium at height 0

Fig. 2.d.   Displacements of ions in the lower symmetries.

(c)Orthorhombic and Rhombohedral (space groups Bmm2 and R3m)

At lower temperatures ($0^{o}C$ and $-90^{o}C$ respectively) there are further phase changes, firstly to orthorhombic and then to rhombohedral. These represent changes to successively lower orders of symmetry. The change to orthorhombic is essentially a distortion similar to that which occurs at the Curie point but along a second cube edge direction. The further change to rhombohedral represents a further distortion along the third cube edge. These structures were determined by Rhodes (2.5.) in 1949. The distortions concerned in these changes are shown in fig.2.c. and the arrangements of ions is shown in fig.2.d.

The structure of barium titanate then can be considered to be cubic with small distortions occuring in each of the three cube edge directions as the temperature is lowered. The lattice constants of the material are shown in fig.2.e. as a function of temperature.

3.Crystal Habits.

The crystalline growth habits of barium titanate grown from solution in molten potassium fluoride have been well described by deVries (3.8.). There are three types of crystal found in flux melt runs. Near the surface of the solution, dendritic forms are found; at the bottom of the crucible, there are clusters of small equant crystals with sides of up to 2.m.m. length; growing from the equant crystals are found the "butterfly" twins on which all the experiments in this work were made. The form of these butterfly twins is shown in fig.2.f. together with
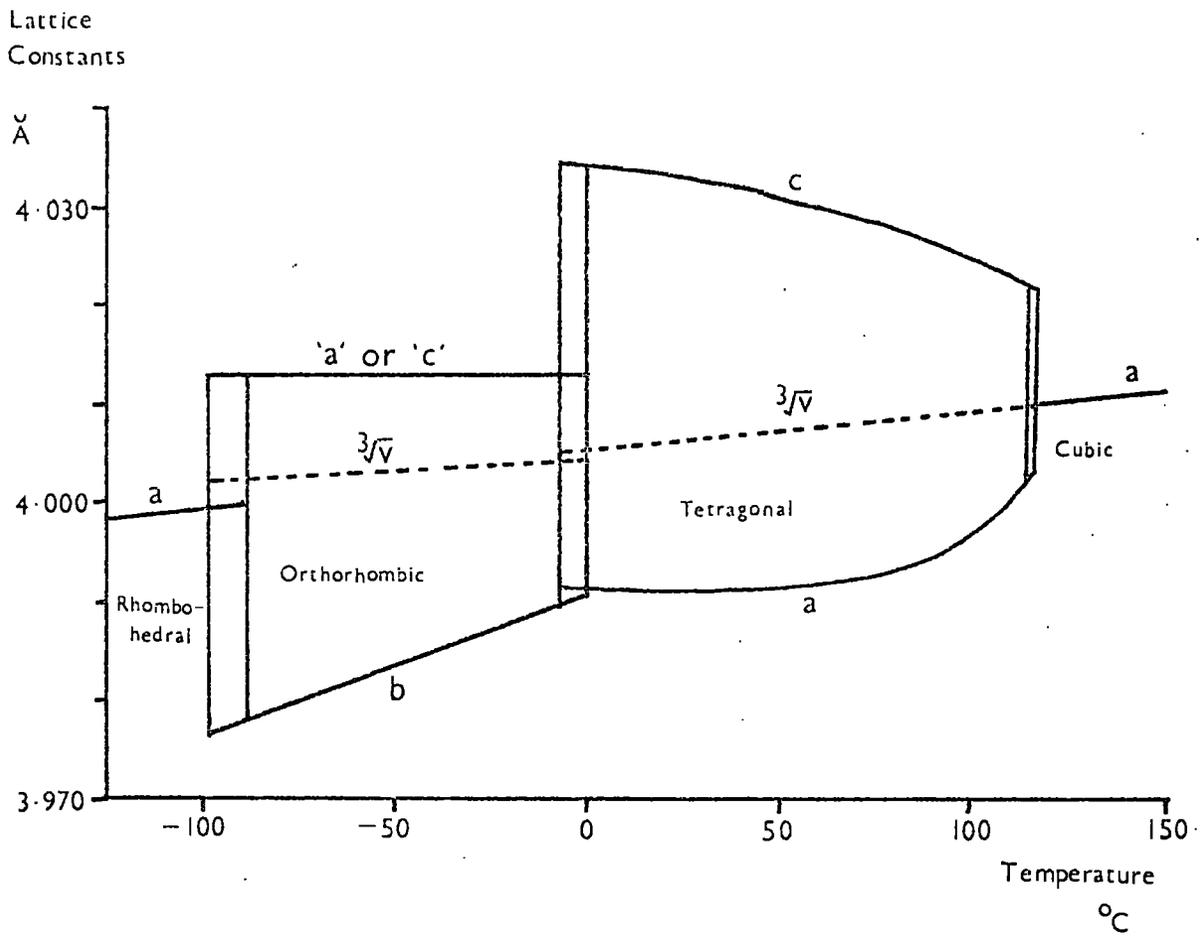
Fig. 2.e.   Lattice constants of BaTiO₃ as a function of temperature.

Small

Angle

Twin

Large

Angle

Twin

Crucible

Dendrites

Flux

Twinned Plates

Cubes
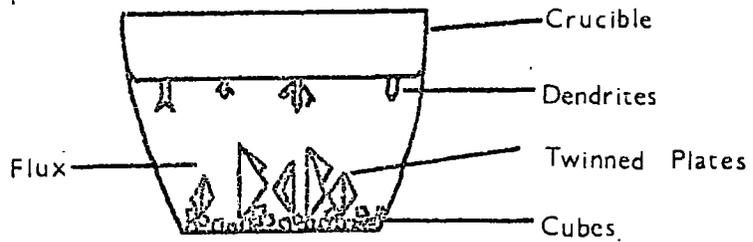
Crystals in Crucible

Fig. 2.f.   Butterfly twins and cross section of growth crucible.

a cross-section of the crucible showing the positions of the various habits during growth.

Devries showed that the formation of butterfly wing habit was due to a stacking fault in the initial stages of growth caused by the inclusion of iron impurities in the lattice. The nature of this fault is a disturbance of the usual A-B-C-A-B-C-.. stacking such that a C layer is omitted. The stacking then being A-B-C-A-B-A-B-C-.., a twin boundary is set up. Two of these boundaries are involved in the large angle twins and four such boundaries are involved in the small angled twins.

The plate nature of these butterfly twins, together with their relatively greater size makes them suitable for many of the experiments to be described later. All crystal growth runs were therefore aimed at producing these crystals.

4.Ferroelectricity.

There have been several attempts to find a theoretical model for the phase changes which occur in barium titanate and with them several explanations for the ferroelectric phenomenon as observed in this material (Mason and Matthias (2.6.), Devonshire (2.7.), Slater (2.8.) and Jaynes (2.9.)). It is not necessary here to go into these theories in detail but a simplified explanation of why the phase changes occur will be given.

The position of the titanium ion is, as stated in section 2 above, at the centre of an octahedron of oxygen ions. The position of the titanium inside this group of six oxygen ions will depend on the Coulomb field set up by them. The electronic configurations of the oxygen ions is such that the effect of ions outside the octahedron is small. The group of oxygen ions acts as a screen around the titanium ion.

The potential field set up by the six oxygen ions contains quadratic and fourth power terms. In the region above the transition temperature, the quadratic terms are dominant and the potential field in which the titanium ion finds itself is as shown in fig.2.g. At the Curie point, the fourth power terms are of the same magnitude as the quadratic terms and there is a large region of space within the octahedron at which the potential seen by the titanium ion is essentially constant. This situation is again seen in fig.2.g. At lower temperatures, the quadratic terms dominate and the field is as shown in the bottom diagram of fig.2.g. The titanium ion now drops into the potential minimum on one side of the central maximum. There will, of course, be six of these minima and the choice of these is fortuitous, depending on thermal vibration.

When one titanium ion has moved into the potential minimum displaced from the centre of the unit cell, however, this distorts the field in the neighbouring unit cells in such a way that the titanium ions in these cells are encouraged to distort in the same direction. Furthermore, the oxygen ions in the direction of displacement of the titanium ion will be forced away from the
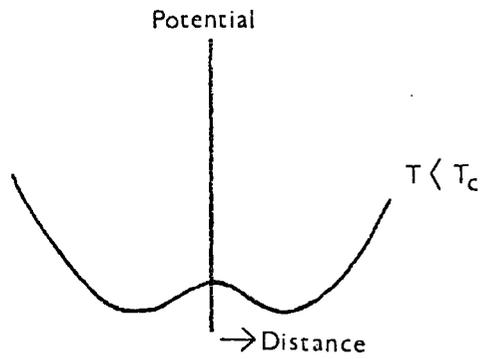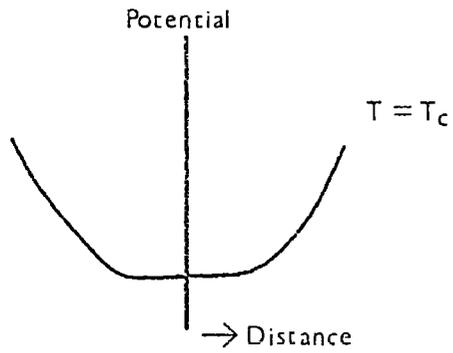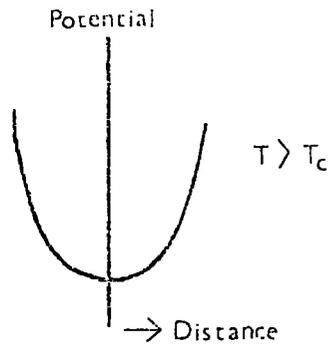
Fig. 2.g.   Titanium ion potential as a function of position in
(100) direction.

cube centre and the four oxygen ions in a plane perpendicular
to the direction of displacement of the titanium ion will be
able to move towards the cube centre. In this way, large regions
of a crystal will have all their titanium ions displaced in one
direction, which becomes the c axis for that particular region.
In most cases, there are in fact several nucleations for this
mechanism and there will be a number of ferroelectric domains
within the crystal.

It is now clear that the unit cells will have a spontaneous
electric dipole moment and so the material will be ferroelectric.

The theory of Jaynes, however, ignores the potential within
the octahedron of oxygen ions. He considers the electronic
structure of the octahedron itself. By calculating the pertubation
of the electronic structure of the octahedra under an electric
field, he finds the conditions for a spontaneous polarization.

This theory appears to be more self consistent than the
earlier ones. In chapter 4, this theory will be more fully dealt
with and an attempt will be made to use it to explain the observed
change in the Curie point of chemically reduced crystals.

5.Dielectric constant and spontaneous polarization.

The dielectric constant of a material is a measure of its
ability to adapt to an external electric field. In barium titanate,
at the Curie point, the titanium ions are in a very flat potential

well as illustrated in fig.2.g. The application of an external
electric field will result in a large shift in the position
of the titanium ions in the crystal and hence a strong dipole
moment will be set up in each unit cell to counteract the
external field. The polarizability of the lattice is therefore
very high and the dielectric constant becomes correspondingly
high.

The polarizability of the lattice declines on both sides
of the Curie point. Above the Curie point, the dielectric
constant declines according to the Curie-Weiss law,

$$\varepsilon - 1 = \frac{C}{T - T_c}$$

where ε is the dielectric constant, T_c is a temperature near
the Curie point and C is a constant having dimensions of temperature
and with a value for barium titanate in the order of 10^5 ^{o}K.

There is also a spontaneous electric polarization in the
temperature region below the Curie point. The displacements of
the titanium ions from the centres of their respective unit cells
give rise to permanent electric dipole moments. This is shown
together with the dielectric constant in the curves after Cross
(2.10) in fig.2.h.
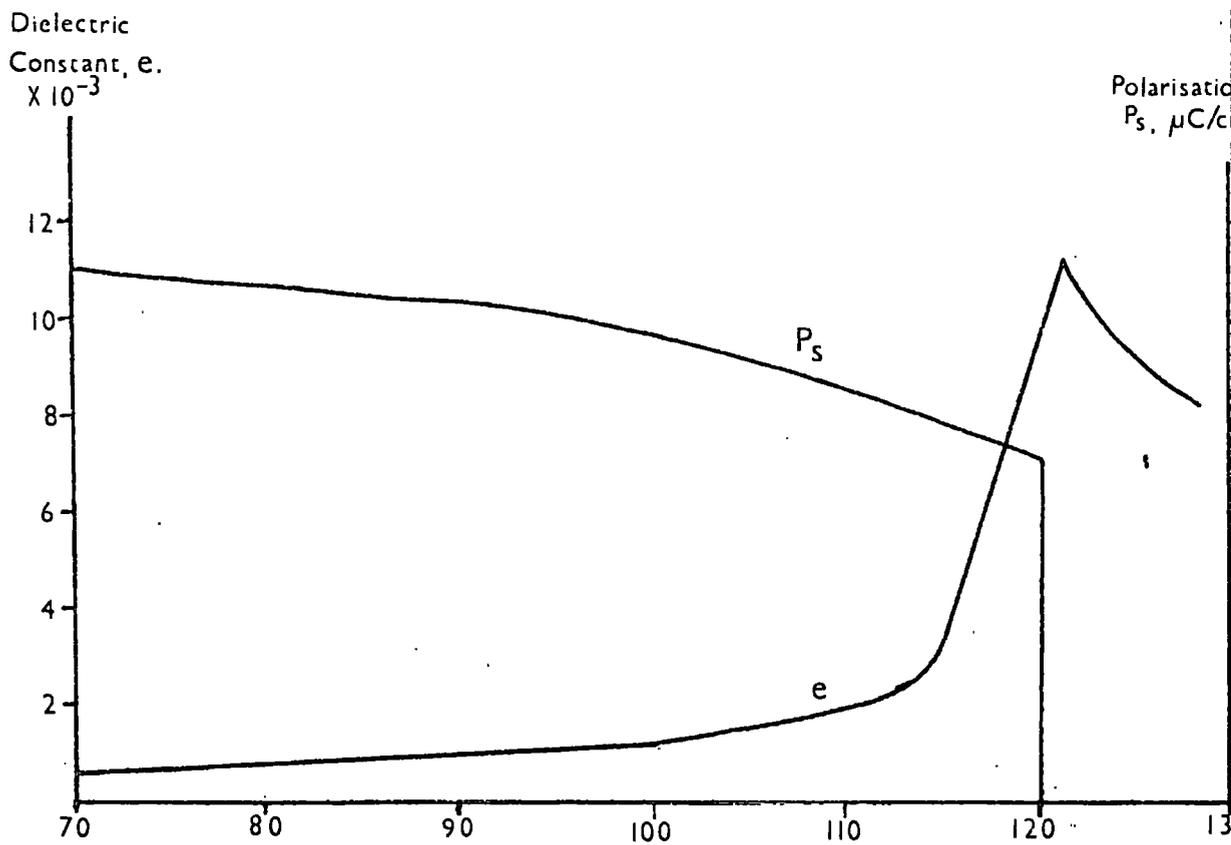
Fig. 2.h.   Dielectric constant and spontaneous polarisation
             in BaTiO₃.

6. Chemical processes involved in the reduction of flux grown
   barium titanate.

Arend and Coufova (2.11.) have used chemical methods (2.12)
to determine the processes which occur when single crystals grown
by the flux-melt process are heated in hydrogen. They show
that a simple model of oxygen being removed from the lattice to
form oxygen vacancies is insufficient. Their analyses show that
there are four processes which occur at different rates during
the reduction process. Of these four processes, however, only
three have a direct effect upon the electronic conductivity.

With the exception of the process of removal of oxygen
to form oxygen vacancies and water, the processes involved are
direct consequencies of the fluorine impurity incorporated into
the crystal during growth. The impure material (considering only
the potassium fluoride impurity) can be written

$$\left[Ba_{1-a}K_a \right] Ti \left[O_{3-a}F_a \right]$$

where equal numbers of potassium and fluorine ions form
substitutional defects on barium and oxygen sites respectively.

Arend et al. found that there were deposits of TiF_4 on the
surfaces of tubes in which heat treatment was performed. The
reaction of volatilization of TiF_4, however, does not liberate
conduction electron within the crystal. The reaction can be
written

$$[Ba_{1-a}K_a]Ti[O_{3-a}F_a] = xTiF_4 + [Ba_{1-a}K_a][Ti_{1-x}(TiV)_x][O_{3-a}F_{a-4x}(AV)_{4x}]$$
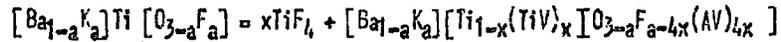
where (TiV) and (AV) represent titanium and anion vacancies respectively.

The fastest reaction which affects the electron concentration is the formation of HF. Hydrogen reacts readily with fluorine ions. One electron is liberated into the crystal for each molecule of HF formed. The reaction becomes

$$[Ba_{1-a}K_a]Ti[O_{3-a}F_a] + yH_2 = [Ba_{1-a}K_a][Ti_{1-x}(TiV)_x][O_{3-a}F_{a-4x-2y}(AV)_{4x+2y}] +$$
$$+ xTiF_4 + 2yHF + 2y\theta$$
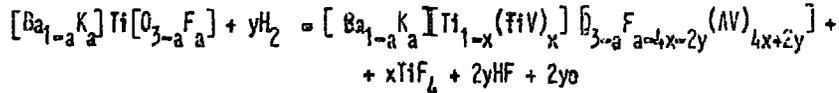
A second fluoride of titanium, TiF_3, is also volatilized and lowers the electron concentration. This process, however, is slower than that of the formation of HF. The initial increase in electron concentration due to the formation of HF is therefore followed by a decrease due to this process.

$$[Ba_{1-a}K_a]Ti[O_{3-a}F_a] + yH_2 = [Ba_{1-a}K_a][Ti_{1-x-z}(TiV)_{x+z}][O_{3-a}F_{a-4x-2y-3z}(AV)_{4x+2y+3z}]$$

$$+ xTiF_4 + 2yHF + zTiF_3 + (2y-z)\theta$$
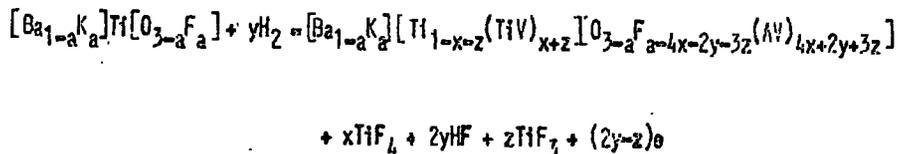
Finally, when all the fluorine ions are removed by one or other of these reactions, the process of removal of oxygen ions to form water becomes dominant. This is a slow process which results in additional conduction electrons. The final equation

involving all four reactions is as follows:

$$[Ba_{1-a}K_a] Ti[O_{3-a}F_a] + (y + u)H_2 = [Ba_{1-a}K_a][Ti_{1-x-z}(TiV)_{x-z}][O_{3-a-u}F_{a-4x-2y-3z}(AV)_{4x+2y+3z+u}]$$

$$+ xTiF_4 + 2yHF + uH_2O + zTiF_3 + (2y-z+2u)e$$
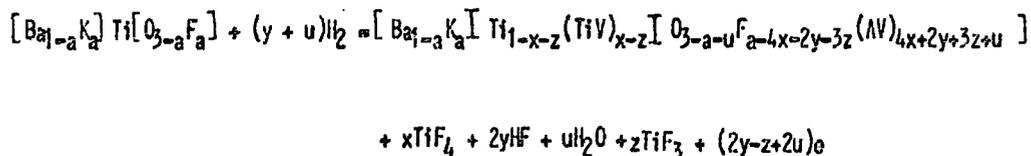
The experimentally determined electron concentrations due to these processes is shown in fig.2.i. The initial steep rise accompanies the formation of HF; the following decrease is due to the volatilization of TiF_3; the final slow increase indicates the removal of oxygen to form water.

Arend points out that since at no stage during this reaction has the lattice reached equilibrium with its surroundings, the impurity and vacancy concentrations and hence also the electron concentrations will vary through the thickness of the crystal.

The results of Arend et al. described above were obtained by chemical analysis. The variation of overall electron concentration is of relevance to the electrical properties. If the electron mobility remains substantially constant during the reduction process in flux grown crystals, it is to be expected that the measured resistivity would decrease rapidly during the first stage of the heat treatment in hydrogen but that it would rise again during the second stage and then finally decrease slowly again.

7.The positive temperature coefficient of resistivity.

One of the earliest properties of barium titanate ceramics to be noted was the region of temperature near the Curie point where the resistance was found to rise with increasing temperature. This positive temperature coefficient of resistivity, commonly referred to as the PTCR, was first explained by Heywang (2.12.). He assumes that at the surface of the crystallites of a barium titanate ceramic, there is a barrier layer which contributes to the resistivity of the ceramic.

Both the number of surface charges giving rise to the barrier and the dielectric constant vary rapidly in the region of the Curie point temperature. This gives rise to a rapid rise in the effective resistance of the barrier as the Curie point is approached and a falling off of this resistance at higher temperatures.

The theory has been modified by Jonker (2.11.) to consider certain small effects. A typical curve of resistance against temperature is shown in fig.2.j. after Heywang.

8.Conduction properties of single crystals.

There have been numerous reports of measurements of conduction properties in semiconducting barium titanate, both in reduced crystals and in doped crystals. These differ considerably from each other and are somewhat difficult to classify.

Early measurements differed in the extent to which the

ELECTRON

CONCENTRATION
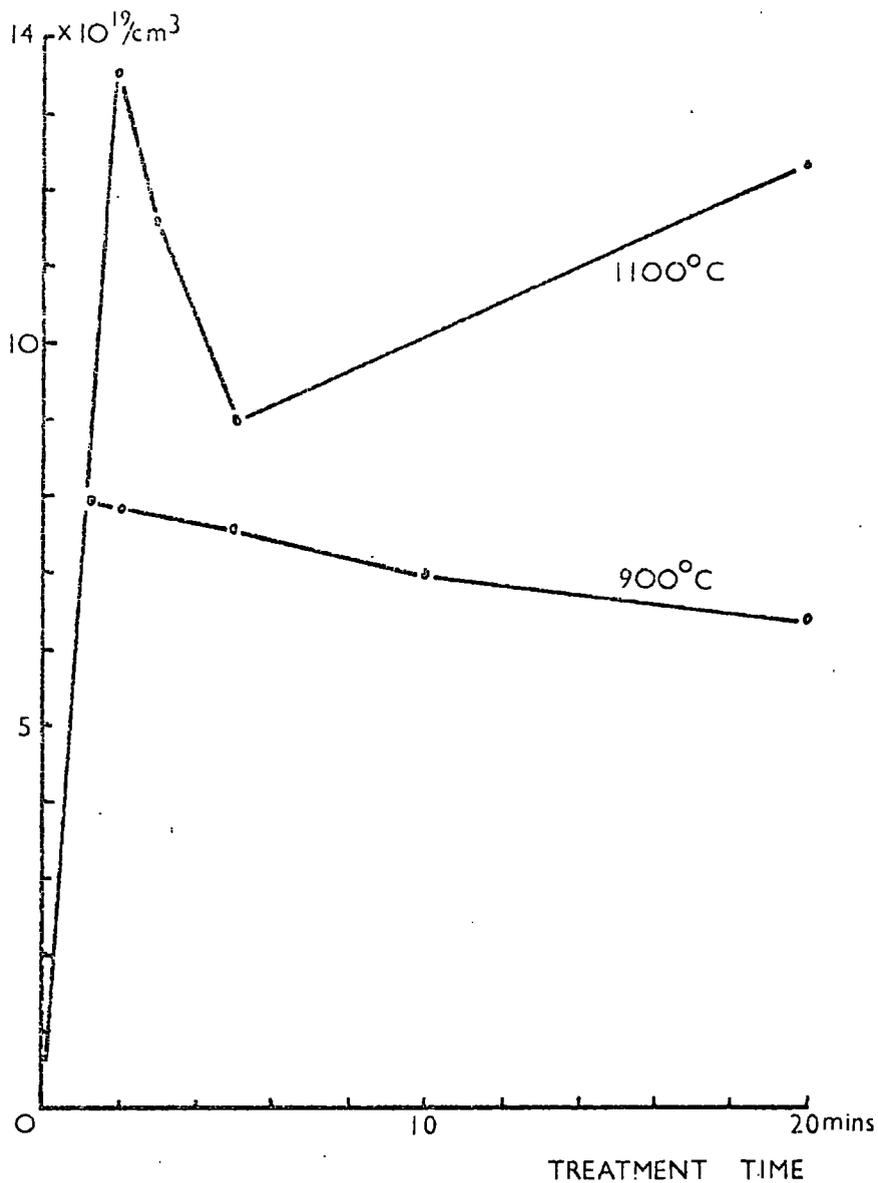
Fig. 2.1.   Electron concentration in reduced flux grown single
crystals.

PTCR effect was present. Fielding Brown and Taylor (2.15.)
working on flame fusion crystals (see chapter 3) doped with
niobium found very similar results to those of Ikegami and
Ueda (2.16.) who used flux melt grown crystals reduced in
hydrogen at 800°C. These workers used two probe methods and
observed strong discontinuities at the three transition temperatures,
120°C, 0°C and -90°C.

The measurements of Branwood and Tredgold (2.17.) working
on nominally pure crystals and of Kawabe and Inuishi (2.18.)
working on reduced crystals of unspecified growth process,
both show a PTCR similar in form to that obtained for ceramics.
Again the measuring technique used a two-probe geometry.

The question of a discontinuity or PTCR in single crystals
was resolved by Ueda and Ikegami (2.19.) who used three
geometries for their measurements; two probe across a plate;
two probe along a strip; four probe along a strip. These
experiments showed that the PTCR in single crystals was a result
of surface resistance of the type proposed by Heywang for
ceramics.

The conflicting nature of earlier measurements is exemplified
by three publications bearing the names Ikegami and Ueda (2.16,
2.19. and 2.20.) in which three different behaviours are
reported for reduced single crystals.

The work by Kawabe and Inuishi quoted above also attempted
to measure the Hall mobility. The doubt thrown on the resistivity

measurements from which the Hall mobility was calculated must, however, lead to some scepticism about the mobility results.

Very recent results by Berglund and Baer (2.21.), however, go far to rationalize the measurement of both the resistivity and Hall mobility of reduced single crystals. They use single domain ferroelectric, melt grown crystals very heavily reduced in hydrogen. Their results show a strong anisotropy in the mobility below the Curie point and an isotropic constant mobility in the region between the Curie point and 150°C. The value of n^* is continuous throughout the temperature range with a very low activation energy. Typical results are shown in fig.2.k. The Seebeck coefficient measurements of the same work are shown in the same figure.

9. Optical properties.

The optical properties of barium titanate have been well studied. The measurements which are perhaps the most relevant here are the measurements of band gap energy of Cox, Roberts and Tredgold (2.23.) and the optical absorption measurements in reduced crystals by Arend and Coufova (2.24.).

Cox et al. measured the optical absorption of flux-grown crystals in the region of the optical absorption edge. Measurements were made with crystals of varying thicknesses and the results were corrected by digital computer to obtain a best value of optical absorption coefficient, a, to fit the equation

* carrier density.

$\log_{10}$

resistivity
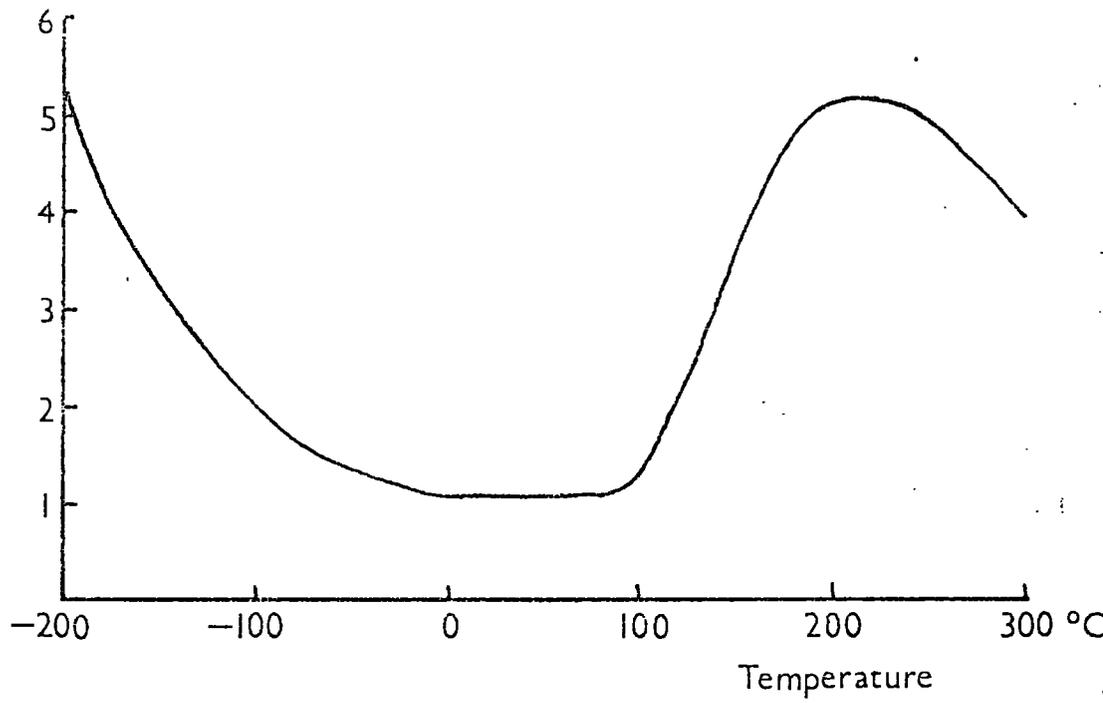
Fig. 2.j.   Positive temperature coefficient of resistance effect.
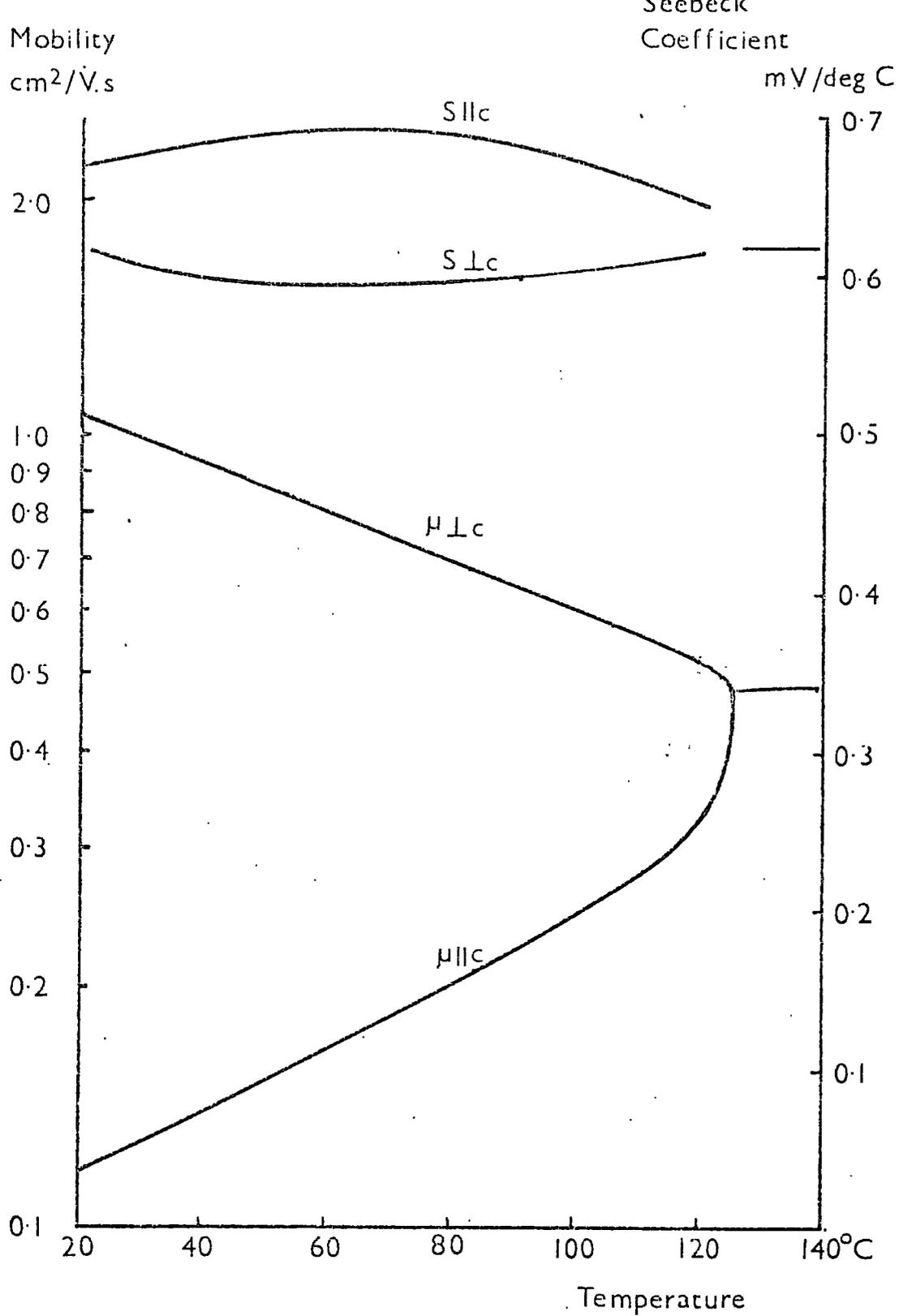
Fig. 2.k.Hall Mobility and Seebeck coefficient in reduced single crystals.

$$\frac{I_t}{I_i} = \frac{(1 - R)^2 \exp(-\alpha d)}{1 - R^2 \exp(-2\alpha d)}$$

Here, I_t and I_i are the transmitted and incident intensities respectively, R is the reflectivity and d is the thickness of the crystal. The results obtained were analysed and it was found that there is a direct gap of 3.05 eV and an indirect gap of 2.63 eV.

Arend and Coufova have measured the optical absorption of flux grown crystals in the region of the optical absorption edge with varying concentrations of iron impurity. All the crystals were reduced in hydrogen at 550°C for 10 minutes. The results are shown in fig.2.1. for reduced (upper curves) and unreduced (lower curves) specimens of various iron content.

The most notable features of these results are that
(i)the effect of reduction is negligible for small concentrations of iron,
(ii)for large concentrations of iron, reduction leads to absorption peaks at wavelengths of 0.58 and 0.65 µm.

Arend and Coufova have explained these results in terms of compensation of iron by oxygen vacancies and by fluorine ions incorporated during growth. No more will be added about these measurements here. They will be discussed further in chapter 5.
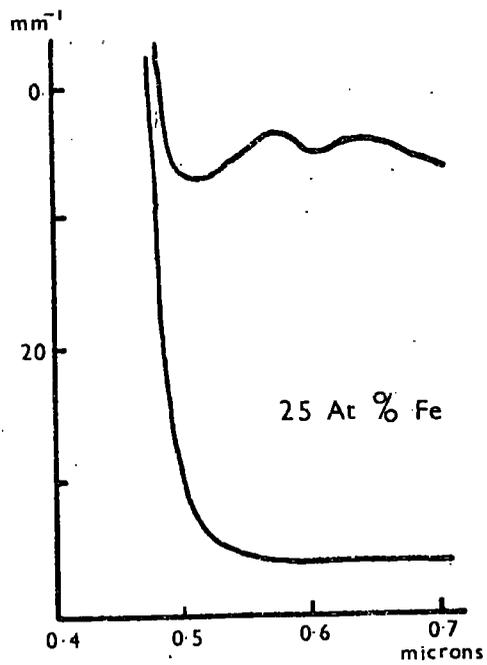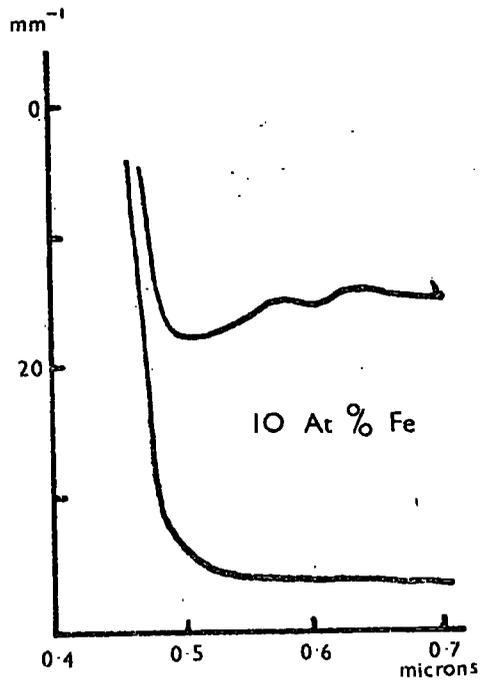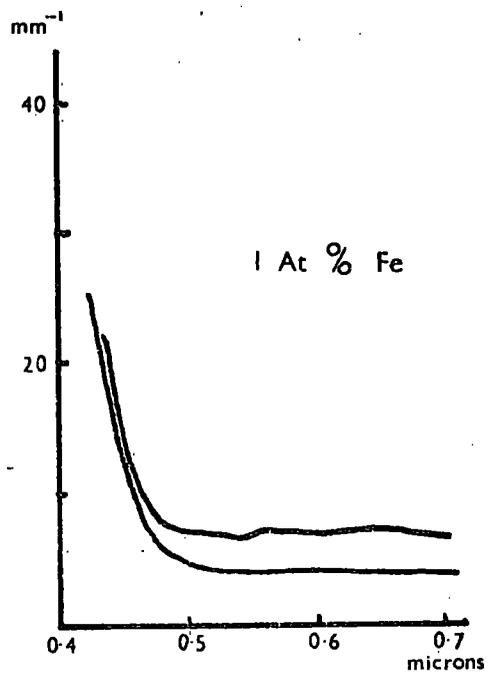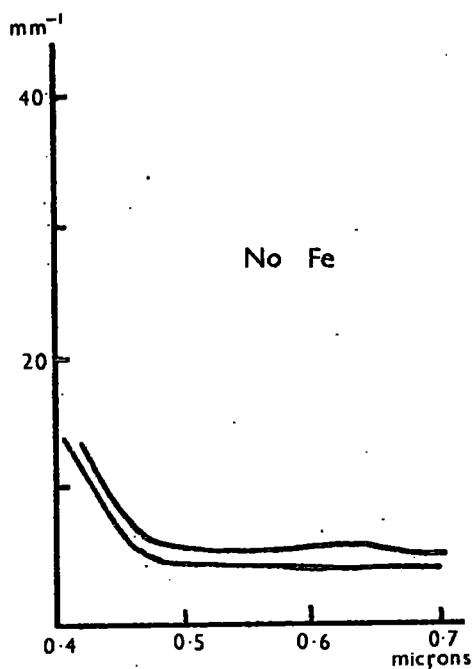
Fig. 2.1.   Optical absorption in single crystals.

Reik et al. (2.25. and 2.26.) have measured the infra-red reflectivity between 1 and 12µm wavelength. They find the form of the reflectivity is more consistent with a small polaron motion rather than a classical band motion of the electrons. This will be dealt with in more detail later (chapter 9) but the most important outcome of this work is that there is a broad maximum in the real part of the conductivity at about 4 µm. This maximum has also been noted by Ikegami and Ueda (2.16.) from their absorption measurements in this region.

10. Band structure in barium titanate.

In certain other perovskite materials, notably strontium titanate, the energy bands have been calculated and agree well with experiment (2.27.). It is agreed that, in these materials, conduction takes place in the bands formed from the transition metal 3d levels. In intrinsic material, the electrons are excited from the oxygen 2p levels.

It is doubtful, however, in view of the low mobilities quoted for barium titanate whether a Bloch type band model is appropriate. Optical reflectivity has been measured in the infra-red region by Riek et al. These measurements are correlated with reflectivities expected on a small polaron hopping model.

Bergland and Baer (2.21.) explain their results with the

band model, using the model proposed by Kahn and Leyendecker (2.27) for strontium titanate. This is a band model with a silicon-like band having six ellipsoidal minima along the 100 directions as shown in fig.2.m. Bergland and Baer do point out, however, that the shape of the constant energy surfaces could be as shown in the lower drawing of fig.2.m.

It can be said, then, that no direct evidence exists to promote any particular model for conduction in barium titanate. The main point for conjecture is whether a conventional band model is sufficient to explain the conduction processes in barium titanate or whether small polaron hopping processes are dominant.
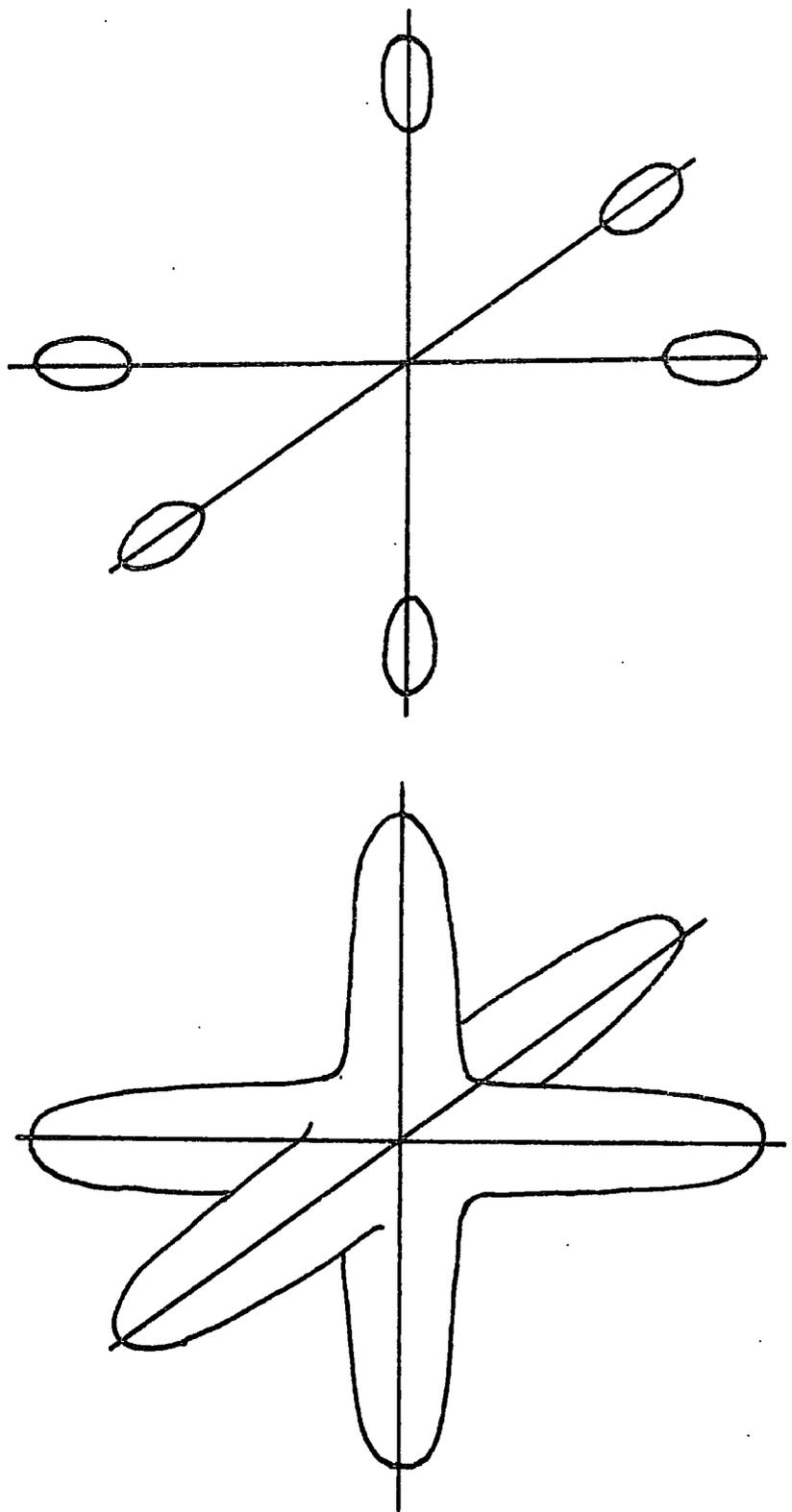
Fig.2.m. Possible electron constant energy surfaces in BaTiO$_3$.

Chapter 3.

Crystal Growth and Sample Preparation.

1. The $BaO - TiO_2$ System.

Nearly all the methods which have been used to prepare
barium titanate in either single crystal or ceramic form have
made use of the reaction

$$BaO + TiO_2 \rightleftharpoons BaTiO_3$$
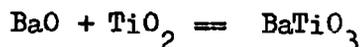
Slight modification can be made to this by replacing the
first reagent by simple barium compounds such as the hydroxide
or carbonate which decompose to the oxide on heating to the
temperatures involved in this reaction (around $1000^{o}C$).

Gallagher and Schrey (3.1.) however, made use of a reaction
involving the decomposition of barium titanyl oxalate to
produce ceramics, the reaction being described by a series
such as

$$BaTiO(C_2O_4)_2 \cdot 4H_2O \underset{230^{o}C}{\rightleftharpoons} BaTiO(C_2O_4)_2 + 4H_2O$$

$$BaTiO(C_2O_4)_2 \underset{350^{o}C}{\rightleftharpoons} BaTiO(C_2O_4) + 2CO_2$$

$$BaTiO(C_2O_4) \underset{520^{o}C}{\rightleftharpoons} BaTiO_3(CO)_2$$

$$BaTiO_3(CO)_2 \underset{670^{o}C}{\rightleftharpoons} BaTiO_3 + 2CO$$
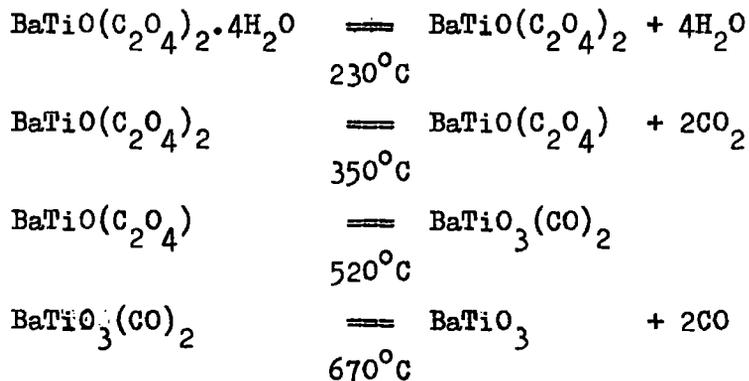
This method is somewhat cumbersome for single crystal growth although it has the advantages in ceramics preparation that a stoichiometric material is formed without weighing and that there is no need for a binder. Since the oxalate process has no application to the growth of single crystals, it will not be considered further.

The most detailed determination of the phase diagram of the barium oxide/ titanium dioxide system was carried out by Rase and Rustrum Roy (3.2.). A section of this diagram near the composition $BaO.TiO_2$ is shown in fig.3.a. The diagram shows that it is not possible to obtain cubic barium titanate from the barium oxide rich side of the equimolar composition. On the titanium dioxide rich side of this composition, however, it is possible to obtain the cubic modification at temperatures as low as $1322^{\circ}C$. It is in this region of the phase diagram that most attempts at melt growth have been made.

2.Growth of single crystals.

(a)Growth from the melt.

Single crystals of barium titanate have been made from titania rich melts by Horn (3.3.) and by Sasaki (3.4.). The former used a Czochralski type arrangement, the reagents being melted in an iridium crucible and the crystal boules being pulled from the melt on an iridium seed. A melt composition with 5% excess of TiO_2 gave boules 1 cm in diameter and $2\frac{1}{2}$ cm long.

Sasaki melted a 65% TiO_2/ 35% $BaCO_3$ mixture in a sealed platinum crucible and slowly cooled this at 5 - 10 deg. per
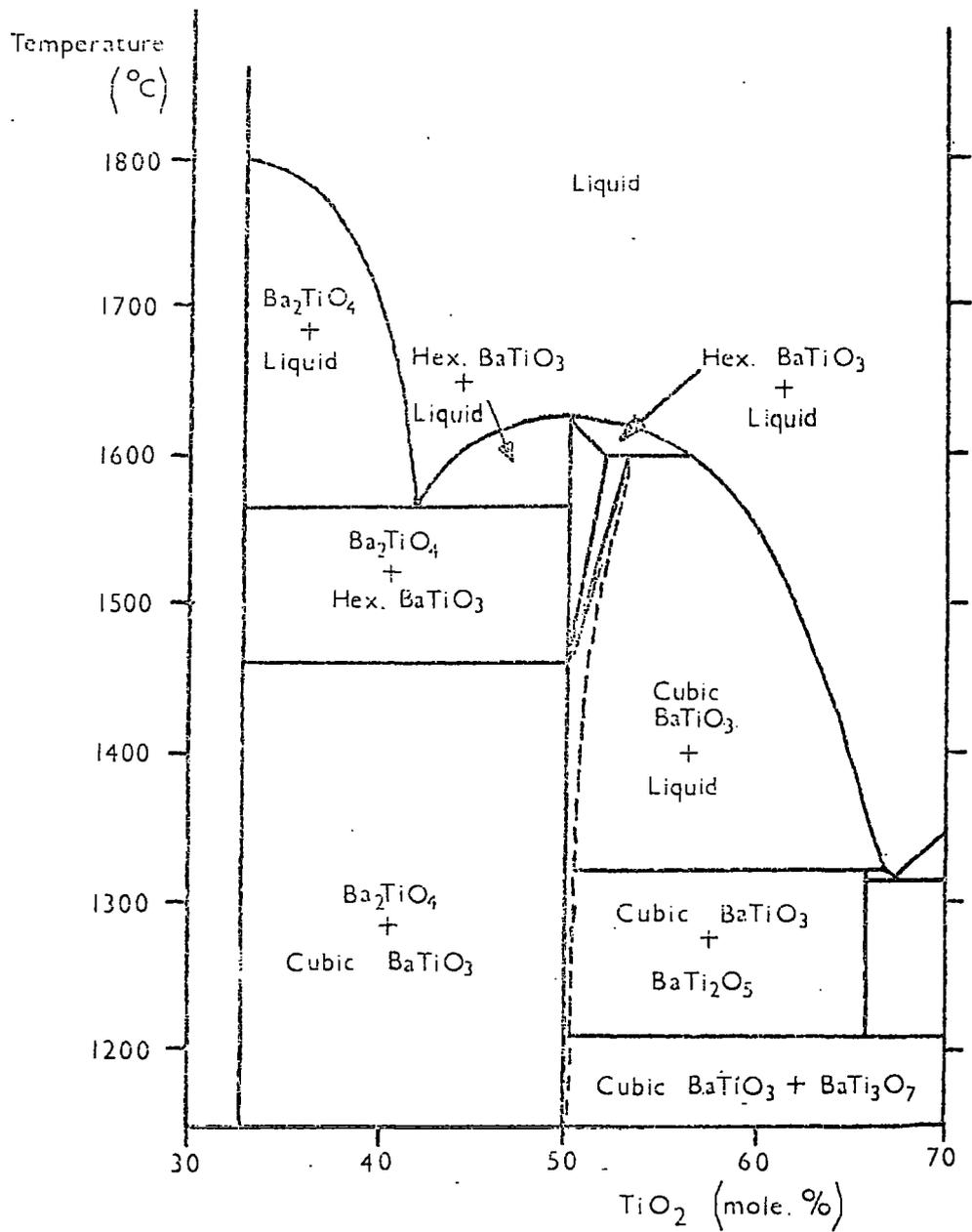
Fig. 3.a.   Phase diagram of the system BaO-TiO$_2$.

hour. Crystals about 3 m.m. across were retrieved from the
crucible after cooling.

(b)Floating zone growth.

Brown and Todt (3.5.) have produced boules of about the
same size as those grown by Horn by passing a ceramic barium
titanate rod through a gas flame ring at about 1600°C. It was
found, however, that 1.5% of strontium titanate had to be added
to the ceramic to suppress the formation of the hexagonal phase
relative to the cubic phase. In this method it is not possible
to add excess titanium dioxide, as this would produce non-
stoichiometric crystals. It was found necessary to anneal the
crystals very carefully when they emerged from the hot region
of the flame to prevent shattering but the crystals then
obtained were of very high quality.

(c)Flux melt process.

Remeika (3.6.) grew barium titanate crystals from solution
in molten potassium fluoride – a process which commonly bears
his name, and which will hereinafter be called the Remeika
method.

Preformed barium titanate or a stoichiometric mixture of
barium oxide and titanium dioxide is mixed with potassium
fluoride in a platinum crucible and heated to a temperature
in excess of 1100°C at which temperature the titanate is soluble
in the fluoride although a few hours are needed at this 'soak'
temperature before the equilibrium concentration is reached. The

melt is then slowly cooled to a temperature a little higher than
the melting point of potassium fluoride. During this period the
crystals of butterfly morphology described in chapter 2, section
3, grow up from the bottom of the crucible. The liquid fluoride
is then decanted off and the crucible is returned to the furnace
for slow cooling to room temperature.

Remeika found that, for the flat butterfly wing plates
to grow, it was necessary to add about 0.2 at. % of ferric
oxide to the melt. A further, more complete study of the
process by deVries (3.7.) shows that a necessary condition
for growth of the butterfly habit is the addition of the iron
oxide which stimulates a stacking fault in the initial formation
of the crystals leading to the formation of the butterfly twins.
This work also shows that the inclusion of rare earth oxides
(used in ceramics to make the material semiconducting) inhibits
growth of this habit.

3.Details of the Remeika method.

Remeika's method was used for crystal growth in the
present work for a number of reasons. Firstly, the two methods
employed by Horn and Sasaki require the addition of excess
titanium dioxide which could lead to non-stoichiometric crystals.
The method of Brown and Todt although leading to more perfect
crystals requires higher temperatures in what must be a neutral
flame. The difficulties in controlling the temperature and
oxygen content of the flame to within the required limits must
be prohibitive.

The method used in the present work for growing single
crystals was therefore essentially the same as that used by
Remeika although in some runs the composition of the charge was
varied. It has been noted by Cox (private communication) that
a dish of fairly shallow shape produces a better yield than the
crucibles used by Remeika and deVries. The charge usually
corresponded to the Remeika recipe;

$$BaTiO_3 \qquad 40 \text{ grams}$$
$$Fe_2O_3 \qquad 27 \text{ milligrams}$$
$$KF \text{ (anhydrous)} \quad 100 \text{ grams.}$$

It was placed in the platinum dish and then inserted into the
furnace.

The furnace is shown in fig.3.b. The construction is of
mineral insulating bricks such that the walls were 11.5 cm
thick. The furnace was lined with fireproof cement and had a
hearth of heavy firebrick. Heat was supplied by four silicon
carbide (Crusilite) elements of spiral tubular pattern. The
total resistance of these elements was 13 ohms enabling $4\frac{1}{2}$ kW
to be dissipated at full mains voltage. The insulating bricks
were contained in a jacket of sindanyo and the holes into which
the elements were fitted were filled with asbestos string in
order to reduce heat loss at the top of the furnace. Remeika
pointed out and the present work showed the necessity for the
temperature gradient in the furnace to be such that the bottom
of the furnace is always cooler than the top, especially during
the crystallising period. It seems that if this condition is not
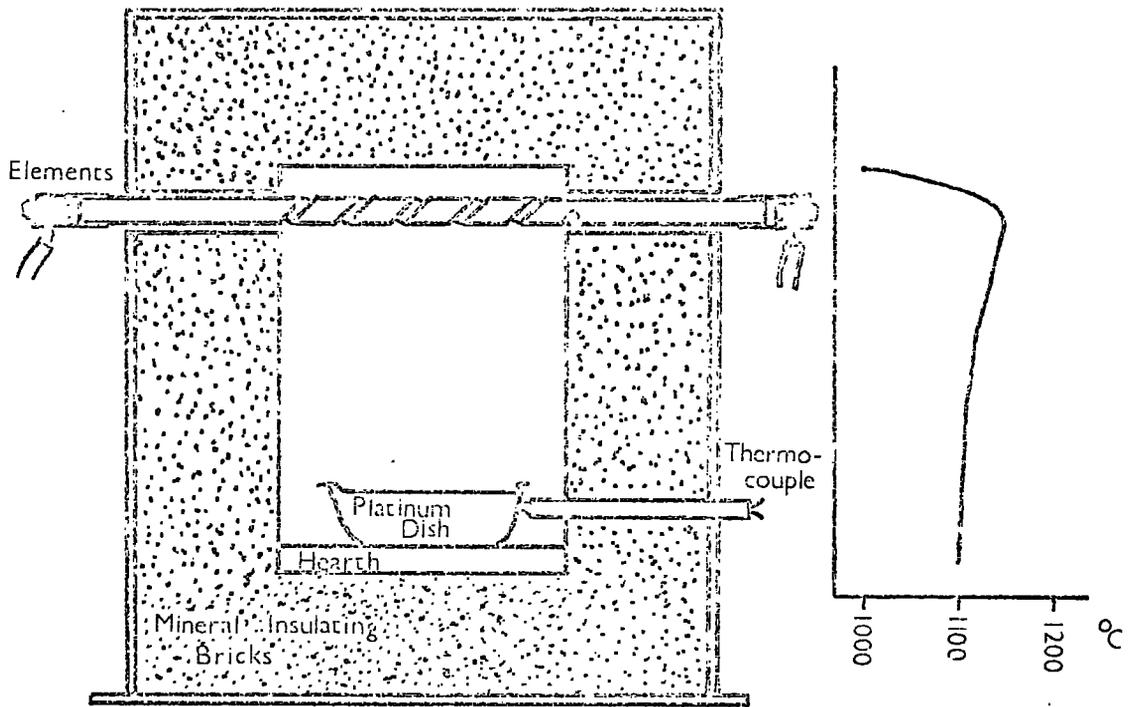
Fig. 3.6.   Crystal growing furnace showing typical temperature
profile during crystalisation.

fulfilled, the convection currents which are set up in the crucible prevent nucleation taking place. It was found, however, that the small equant crystals which form at the bottom of the crucible are larger under these turbulent conditions. Equant crystals of up to 2 m.m. cube were obtained in this way. The temperature profile in the furnace as used when non-turbulent conditions were required to produce butterfly wings is shown in fig.3.b.

The temperature in the furnace during the soak period must be kept constant and there must be a steady decrease in temperature during the crystallising period in order to obtain a maximum yield. In order to fulfil these conditions, the power dissipated in the furnace elements was controlled with a saturable reactor. This reactor was fed with the output from a voltage bridge which differentiated between a standard millivolt source and the output from a platinum - platinum/ 13% rhodium thermocouple. The complete control system is shown in fig.3.c. The output from the thermocouple is fed into the input unit, where the standard source is generated. The value of this standard source can be adjusted by means of a helical potentiometer and can be set at any value from zero to 15 mV. This enables the temperature to be set to the nearest degree centigrade at any temperature within the range required. A motor was geared to the potentiometer to enable the temperature to be lowered at 13 $^\circ$C per hour for crystallising and at about 50 $^\circ$C per hour for annealing. A time switch in the motor supply
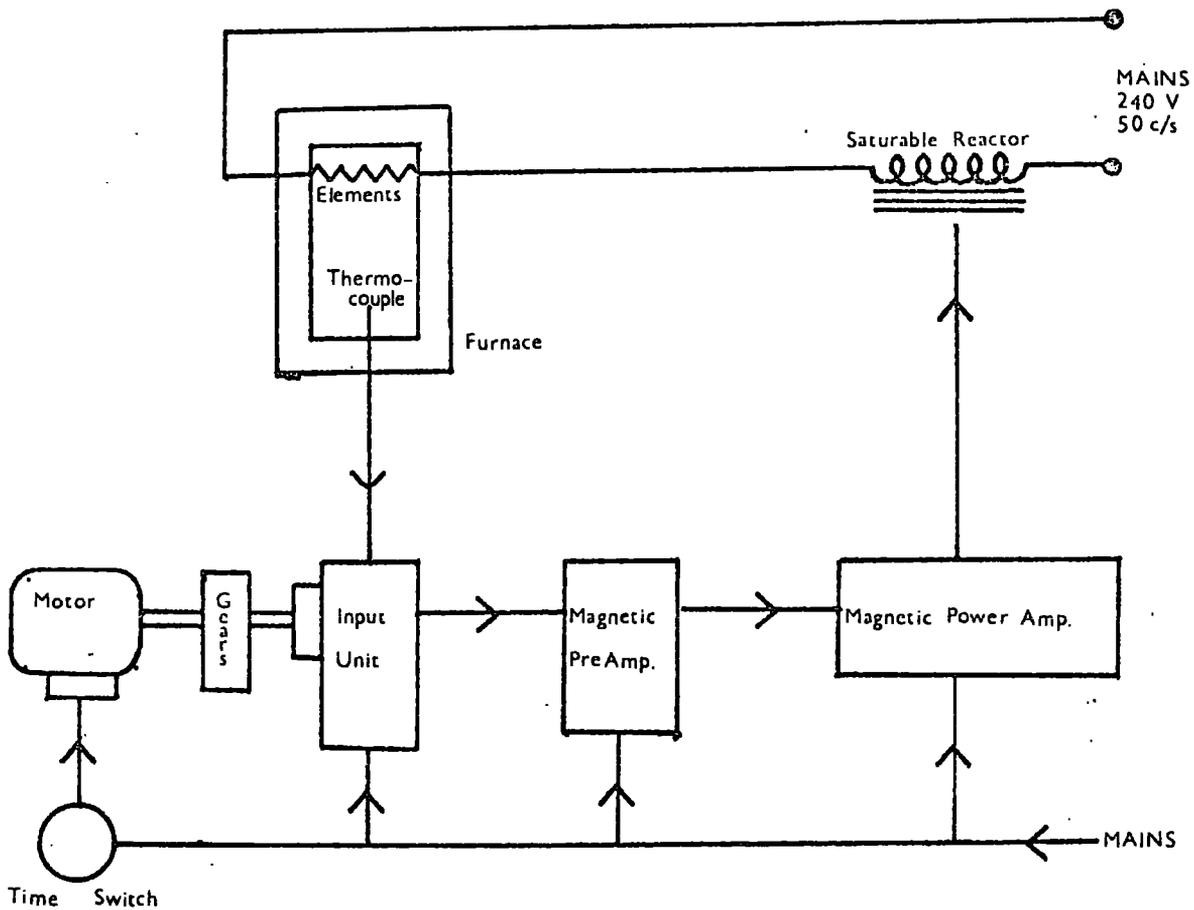
Fig. 3.c.   Control system of crystal growing furnace.

enabled the process to be partly automated. The output from the bridge unit was fed through a magnetic preamplifier and then through a magnetic power amplifier and then to the saturable reactor. The input unit, amplifiers and saturable reactor were from the range manufactured by Pheonix Telephone Co. and consisted of their input unit type T 5033, preamplifier type T 5102, magnetic amplifier type MA 420/200 and 3kW saturable reactor.

The soak temperature was not found to have much affect on the yield and a value of $1150^{\circ}C$ was usually employed and the soak extended for about 10 hours. The temperature was then lowered at $13^{\circ}C$ per hour until the temperature was about $950^{\circ}C$. The melting point of potassium fluoride being $850^{\circ}C$, there was just sufficient time on withdrawal to decant off the fluoride flux before it solidified.

4. Rare earth doped specimens.

Since the conduction anomaly in ceramic specimens is observed principally in material which has been doped with rare earths (usually introduced as oxides), it would be helpful in studying the bulk properties of this low resistivity material to use single crystals doped in the same way. Saburi (3.8.) reports that crystals grown by the flux melt method with 0.3 mol.% of lanthanum, antimony, neodymium and cerium were produced and that although there was some colour change, there was no significant change in resistivity. Brown et al. (3.5. and 3.9.)

report a considerable reduction in resistivity in niobium
doped crystals grown by the floating zone technique. The melt
grown crystals of Horn (3.3.) showed that any intake of cerium
which may have occurred was very inhomogeneous.

As part of the present programme, a series of growth runs
was performed to try to dope single crystals with lanthanum.
A proportion of lanthanum oxide equivalent to 0.3 atomic percent.
was added to melt, this being the amount which creates the
maximum PTCR effect in ceramic samples. The result was, as
found by deVries, that growth of the butterfly twin habit was
greatly inhibited. The crystals which were obtained measured only
about 3 m.m. along the hypotenuse. Furthermore, on investigation
under an optical microscope, it was found that the colour change
to blue caused by the intake of lanthanum was restricted to the
corner of the plate which had been at the bottom of the crucible.
Since all the crystals so obtained were small and non-uniformly
doped, no measurements were made on them.

5.Heat treated specimens.

Semiconducting barium titanate has been shown to be
produced when the material is heat treated in hydrogen. Ikegami
and Ueda have reduced barium titanate single crystals in hydrogen
at various temperatures (3.10.). They show that only at temperatures
of about $800^{\circ}C$ is the reduction homogeneous. At other temperatures,
the reduction is confined to a thin surface layer up to 0.1 m.m.
thick. In order to find how the resistivity of the material

varies with amount of reduction, samples were reduced by the author
in a furnace of small heat capacity. The furnace used is shown
in fig.3.d. The point of the low heat capacity was that the
duration of the reaction could be easily ascertained since the
furnace could be quickly heated and cooled, the power input to
the furnace being about 70 watts.

Specimens were placed in an alumina boat and inserted into
the furnace. The furnace was evacuated and flushed with hydrogen
several times. Then, with hydrogen still in the tube, the furnace
was quickly heated to $800^{\circ}C$. Reduction was timed from that time
at which the temperature controller began to control, usually
about two minutes after switching on. After the appropriate
reduction time, the furnace was switched off and allowed to cool.
The hydrogen was then pumped away and air admitted.

The electrical leads shown in fig.3.d. were used in two probe
resistance measurements described in chapter 8.

Some of the reductions (those on crystals used for optical
absorption measurements to be reported in chapter 5) were
performed in furnace tubes through which hydrogen was continuously
passing during the reduction process. In this case, the hydrogen
cooled the crystals to some extent below the temperature at which
the furnace was controlled. This had the effect of expanding the
time scale of the reduction process by a factor of six or so.

Heat treatments were also made in other atmospheres, notably
oxygen and argon. The apparatus was again that used for hydrogen
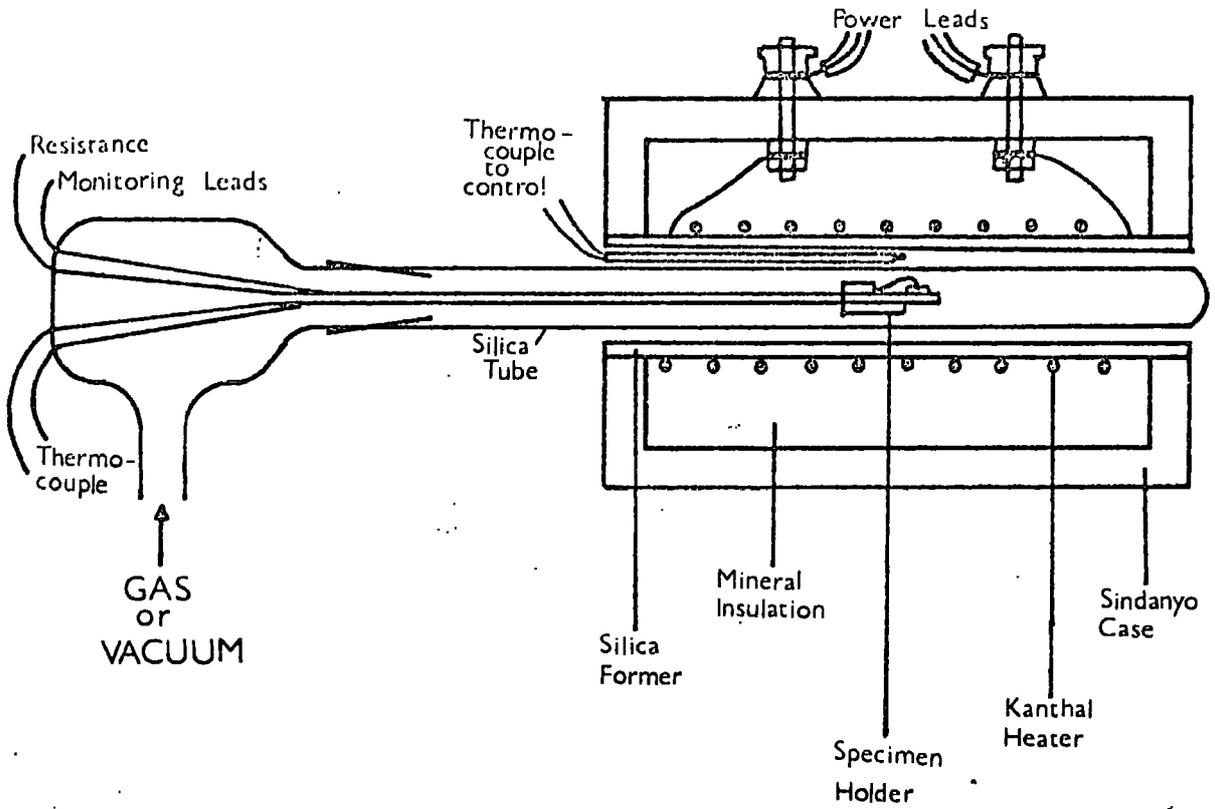
Fig. 3.d.   Heat treatment furnace.

reactions and the same procedure was adopted except that the different gas was used.

6.Contacts.

In the measurement of the electrical properties of semiconducting materials, the choice of contact material and the method of application of the contacts is of prime importance. The chief considerations in the choice of contacts are that the contacts should have ohmic current/voltage characteristics; that their resistance should be small compared with the resistance of the specimen (although a deficiency in this respect can be overcome to some extent with four-probe measuring techniques); that the contact should have adequate mechanical strength at all temperatures at which it is to be used and that the contact material should be chemically compatible with the sample material.

Several contact materials were tried for these barium titanate single crystals. It has been noted by Branwood et al. (3.11.) that certain noble metals, notably silver and gold, form injecting contacts on barium titanate.

Turner and Sauer (3.12.) have used electroless nickel to form ohmic contacts to barium titanate ceramics, using a process described by Pearlstein (3.13.). Landis (3.14.) compares the electrodes formed by this process on ceramic barium titanate with the contacts formed in other ways. The result of his survey showed that electroless nickel compares favourably with very low work function metals such as indium amalgam, which cannot be used

for the present work since the contacts are required for use at temperatures up to $200^{\circ}C$ for the four-probe measurements and up to $800^{\circ}C$ for the two-probe measurements.

The electroless nickel process was tried on the barium titanate single crystals used for the present work and it was found that a very good layer of nickel could easily be deposited on the surface. Turner and Sauer and Landis found that it was necessary to protect the nickel with a layer of common lead-tin solder which was also used to solder a wire to the surface of the ceramic. When this was tried with single crystals of barium titanate, it was found that the crystals could not stand the thermal shock of the soldering operation. Slow heating of the crystals to avoid this thermal shock resulted in a deterioration of the nickel layer so that the solder no longer wetted the surface.

Since it appeared that electroless nickel was not suitable for contacts to the single crystals, tests were made using various noble metal contact materials. When such materials as thermosetting silver (ex Johnson-Matthey Co., Ltd.) and platinum paste (also ex Johnson-Matthey) were used as directed, it was found that the resistance of the contact was very high. This may well have been due to a space charge mechanism of the sort described by Branwood. It has been reported by Morgan (3.15.), however, that the resistance of certain noble metal contacts can be reduced by applying a discharge from a condenser to the contacts. This technique was tried with both thermosetting silver and platinum paste contacts on barium titanate. It was found that the discharge

of a $0.1\,\mu\mathrm{F}$ condenser charged to 600 V for two-probe arrangements or to 800 V for four-probe arrangements was effective in reducing the resistance considerably and producing ohmic characteristics. The discharge was applied several times until the resistance did not change appreciably with successive sparking.

The results of these sparking tests were sufficient to enable these contacts to be used throughout the present work. Invariably, thermosetting silver preparation has been used where measurements have been made up to $200^{\circ}\mathrm{C}$ and platinum paste has been used where measurements have been made at higher temperatures.

The arrangement of these contacts in the two probe case is shown in fig.3.e. The platinum wires and the platinel thermocouple were clamped between silica slides and then the crystal was mounted on the middle slide and contact made to it using platinum paste. Clamping of the wires was achieved by heating the long edges of the silica slides until they fused. This arrangement is that used in the measurements made during reduction and shown in the drawing of the reduction furnace in fig.3.d.
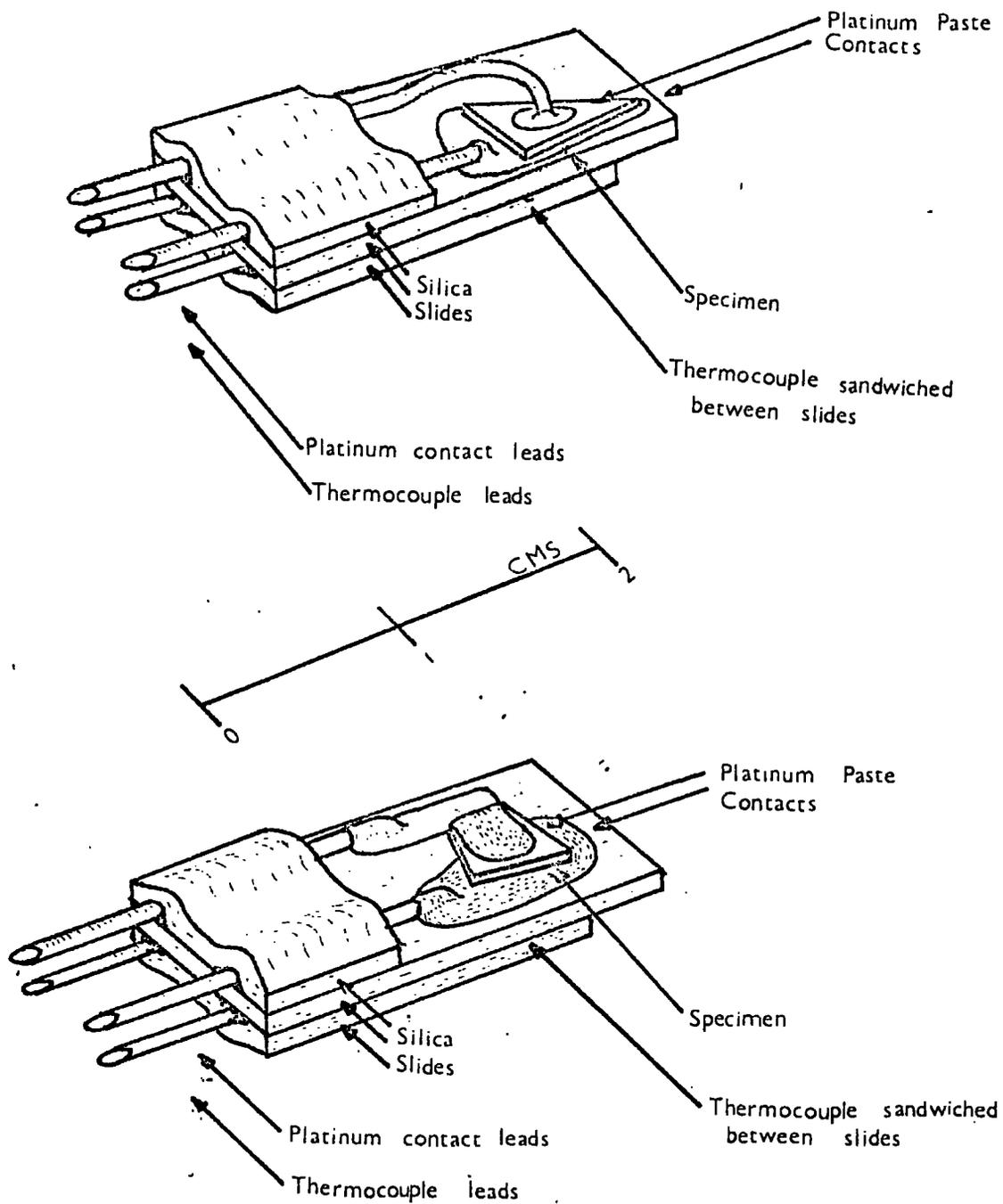
Fig. 3.e. Specimen holders for two-probe measurements.

Chapter 4
The Ferroelectric Curie Point.

1.General remarks.

Measurements of the temperature dependence of resistivity
in reduced single crystals indicated a transition between a
low slope which was sensibly zero and a higher slope equivalent
to an activation energy of about 0.12 eV. These results are
dealt with in detail in chapter 6. The temperature of this
transition varies with the degree of reduction, the value
calculated from the curves being about 50°C at 5 minutes reduction
and rising to about 100°C at 15 minutes reduction. The approach
of this transition to the Curie point at higher reduction times
suggested that perhaps there is a variation in the Curie point
with reduction and that this is responsible for the transition
observed in the resistivity measurements. In view of this it was
decided that a closer look at the variation of the Curie point
with reduction might be useful. Several methods were used to
attempt to measure the variation in the Curie point. These are
discussed here with an assessment of the results.

2.Measurement of the Curie point.

Three methods were used to try to assess the effect of the
reduction process on the Curie point temperature. Firstly, the
temperature variation of the dielectric constant of the material
was measured using an a.c. bridge. Secondly, hysteresis loops
were observed in the reduced crystals and the temperature noted

when the loop disappeared at the Curie point. Both these methods failed essentially because the resistive current in the reduced crystals swamped the capacitative current so that dielectric effects were blurred. Measurements were finally made by observing the ferroelectric domains as they disappeared on heating through the Curie point.

(a)Dielectric constant measurements.

The specimens were mounted in the same way as those used for measurements of the resistance of the crystals during reduction (see fig.3.e.). That is, two contacts, here of thermosetting silver were applied to opposite faces of a plate crystal mounted on a silica slide. The two contacts were connected to a pair of platinum leads which in turn were connected to a Wayne Kerr Component Bridge, Type B 522. The applied signal was at 50 Hz. The temperature of the crystal was measured with a copper/constantan thermocouple using a Phillips Type GM 6020 microvoltmeter. The specimen holder was placed inside a furnace and the capacitance was measured as a function of temperature from room temperature up to 200°C. In an as grown crystal, the characteristic was similar to that shown in fig.2.h. after Cross. There was a sharp peak in the capacitance at the Curie point which was at 115°C as expected in a crystal containing about 5 milligrams per mol. of iron. When reduced crystals were measured, however, it was found impossible to measure the capacitance. The resistive current through the crystals was so high that a balance could not be obtained.

(b) Hysteresis loops.

Ferroelectric crystals show an electric hysteresis in the
same way that ferromagnetic materials show a magnetic hysteresis.
If an alternating field is applied to the crystal, the current
through the crystal is not linear with applied field as in a
paraelectric material. The hysteresis loop can be displayed
on an oscilloscope in the same way as a magnetic hysteresis loop.
Two contacts are again applied to the crystal in the same way
as in the previous experiment and an a.c. field is applied to
the crystal. Voltages proportional to the a.c. current and
voltage applied to the crystal are displayed on perpendicular
axes on an oscilloscope. The circuit used to do this is shown in
fig.4.a. In this circuit, the 50 Hz signal applied to the crystal
is applied to the x-plates of the oscilloscope and the voltage
across the condenser, C, which is proportional to the current
through the crystal, is applied to the y-plates. The potentiometer,
R_4, is used to bleed a signal proportional to that applied to the
crystal into the circuit at the point between the specimen and the
condenser. The current bled into the circuit in this way is in
phase with the resistive current through the crystal and so,
by careful adjustment of R_4, the resistive component can be
balanced so that the oscilloscope sees only the capacitative
component through the crystal.

This circuit was used to measure the Curie point of an
'as grown' crystal and of a crystal reduced for 3 minutes. It
was found that the resistive component could not be satisfactorily
balanced for more conducting crystals than this but the results
obtained for these two specimens agree with those obtained by the
next method.
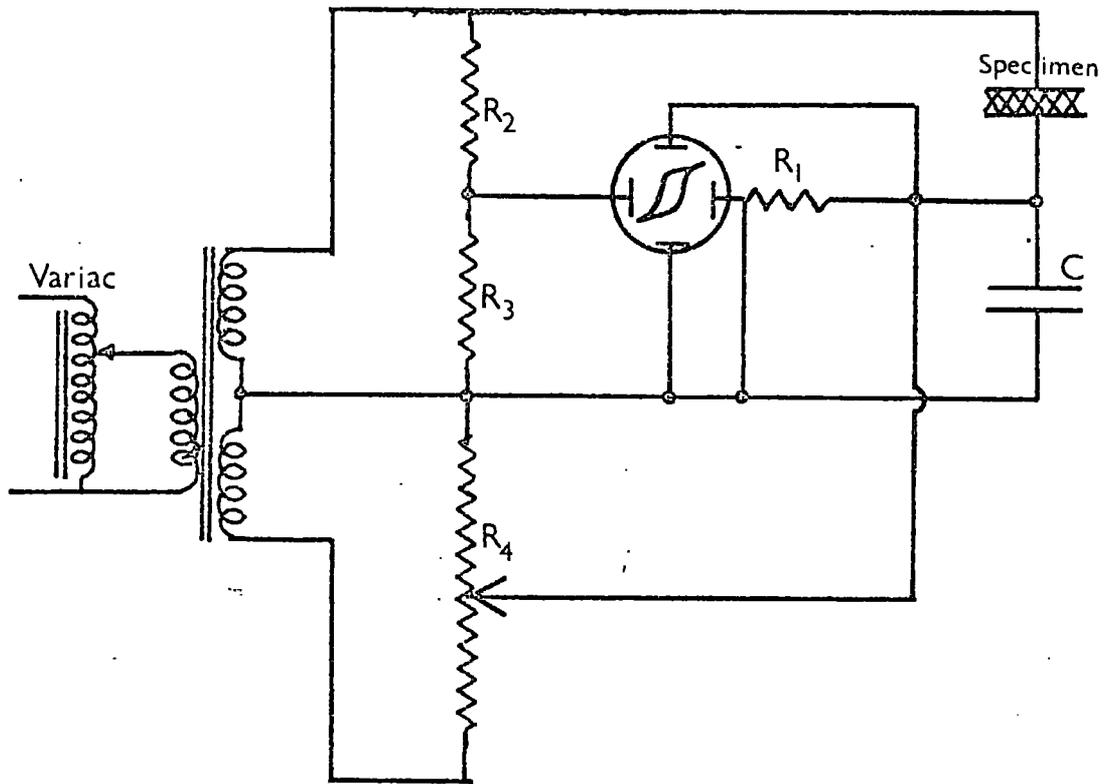
Fig. 4.a.   Circuit for displaying hysteresis loops.

(c)Ferroelectric domains.

In ferroelectric crystals, domains are formed within the crystal such that the directions of polarisation in adjacent domains are different. Since the direction of polarisation must be derived from one of the 'a' axes in barium titanate, the change in the direction of polarisation between one domain and the next is a multiple of 90°. Most of the domain walls in flux grown barium titanate crystals are 90° boundaries since this type of boundary represents a lower energy than the less common 180° boundaries. The position of the domain walls can be observed by observation in a polarizing microscope. Since the ferroelectric phase is tetragonal, the material is birefringent and if viewed between crossed polarizers, a series of coloured interference fringes are observed. Since the direction of polarisation of the crystal is nearly always in the plane of the plate, a light beam perpendicular to the plate between crossed polarizers will always appear to be coloured with these interference fringes. The rotation of the direction of polarization of the light is different on each side

---

The author has made use of the alternative spellings of the word 'polarisation' in section 2 (c). There are two different meanings of the word in this section and to the words 'direction of polarisation'. In order to distinguish the properties of a light beam from those of ferroelectric materials, the 'z' spelling has been used for the former and the 's' spelling has been used for the latter.

of a domain boundary, however, resulting in a line of colour contrast along the domain edges.

When the material is heated through the Curie point, the ferroelectric structure, and with it the domain structure, is destroyed. The crystal is no longer birefringent and crossed polarizers yield a black field. This is, therefore, a very sensitive test for the Curie point. It was found that this method of detecting the Curie point is insensitive to the conductivity of the crystal although it was noticed that the domain widths are substantially reduced in the highly conducting crystals, indicating a reduction in the polarisation energy.

The technique adopted was to mount the crystal on a heated microscope slide. The construction of this slide is shown in fig.4.b. A copper/constantan thermocouple was attached to the crystal with a small blob of thermosetting silver and the voltage developed was measured on a Phillips microvoltmeter as before. The hot slide was placed on the stage of a Swift polarizing microscope.

When the microscope was adjusted until the thermocouple was partly in the field of view, it was found that the thermocouple slightly cooled that region of the crystal under it. This region, therefore, was the last to lose its ferroelectric properties on heating and the first to regain them on cooling. This made measurement of the Curie point temperature very sensitive since the exact temperature at which the material

objective

specimen

microscope
slides

spacer

heater

microscope stage

illumination
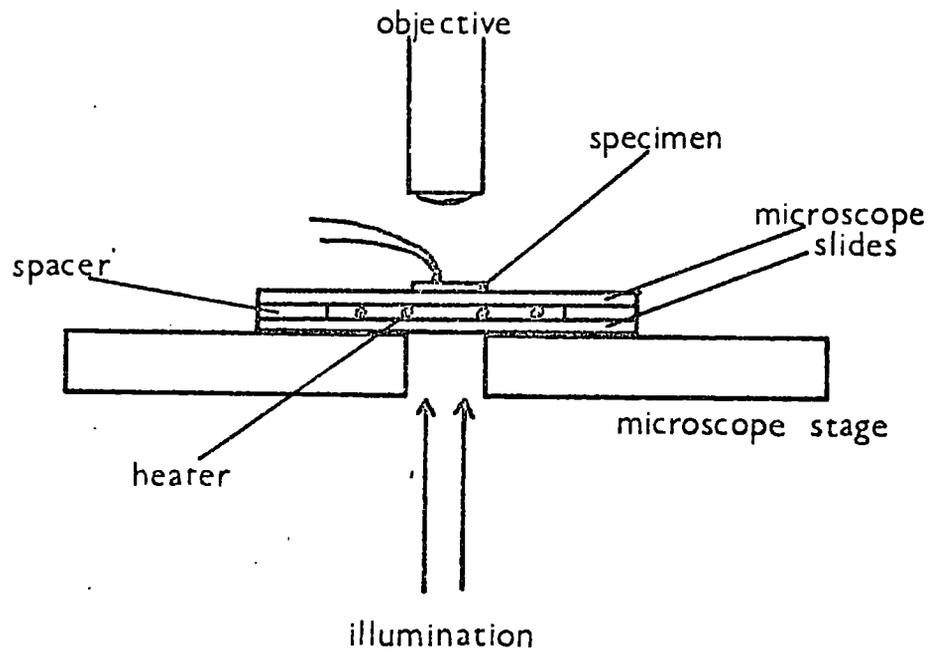
Fig. 4.b.   Heated microscope slide.

around the thermocouple changed phase could be determined.

This method, then, allowed the Curie point to be measured
at all reduction levels. The results are shown in fig.4.c.
The reduction in the Curie temperature is too small to account
for the transition observed in the resistivity.

The shape of the curve of fig.4.c. does, however, show
certain interesting features. The Curie point drops on reduction
for the first five minutes and then rises again. It will be
shown in chapter 8 (fig.8.a.) that the resistance of a hydrogen
heat treated specimen also drops for the first five minutes of
treatment and then rises again. In chapter 6, (fig.6.h.) a similar
result is obtained for four probe resistivity measurements.
A correlation would appear to exist here, and it will be shown
in chapter 9 that both these effects, that on the Curie point
and that on the resistance, are functions of the conduction
electron concentration.

3.Jaynes' theory and the Curie point.

In his electronic theory of barium titanate, Jaynes (4.1.)
considers not only the polarisations of the ions, P_i, and
of lattice displacements, P_d, but also considers the polarisation
of the electronic structure of the oxygen octahedra, P_e. He
assumes that the six oxygen atoms associated with each unit cell
contribute on average one valence electron per unit cell.

The effective field in the octahedron is given by

$$F = E + \beta(P_e + P_i + P_d) \qquad\qquad 4.A.$$

where F is the effective field and E is the applied external field. β is the Lorentz factor which is treated as an unknown constant. Jaynes says further that $(P_i + P_d) = \nu F$ where ν is the polarisability of the ion cores and the lattice displacements. Elimination of $(P_i + P_d)$ from these gives

$$F = \frac{E + \beta P_e}{1 - \beta\nu} \qquad\qquad 4.B.$$

Jaynes then shows that the first excited state of the electronic structure of the octahedron will be split under the F. The unperturbed and perturbed energy levels are shown in fig.4.d. The quantity b is given by

$$b = (1 + \mu^2 F^2/\varepsilon)^{\frac{1}{2}} \qquad\qquad 4.C.$$

where μ is the maximum dipole moment due to the mixing states.

The energy of the first excited state in the unperturbed case is 2ε and the zero of energy is taken for convenience to be midway between the ground state and the excited state.

The perturbed unit cell now has a partition function
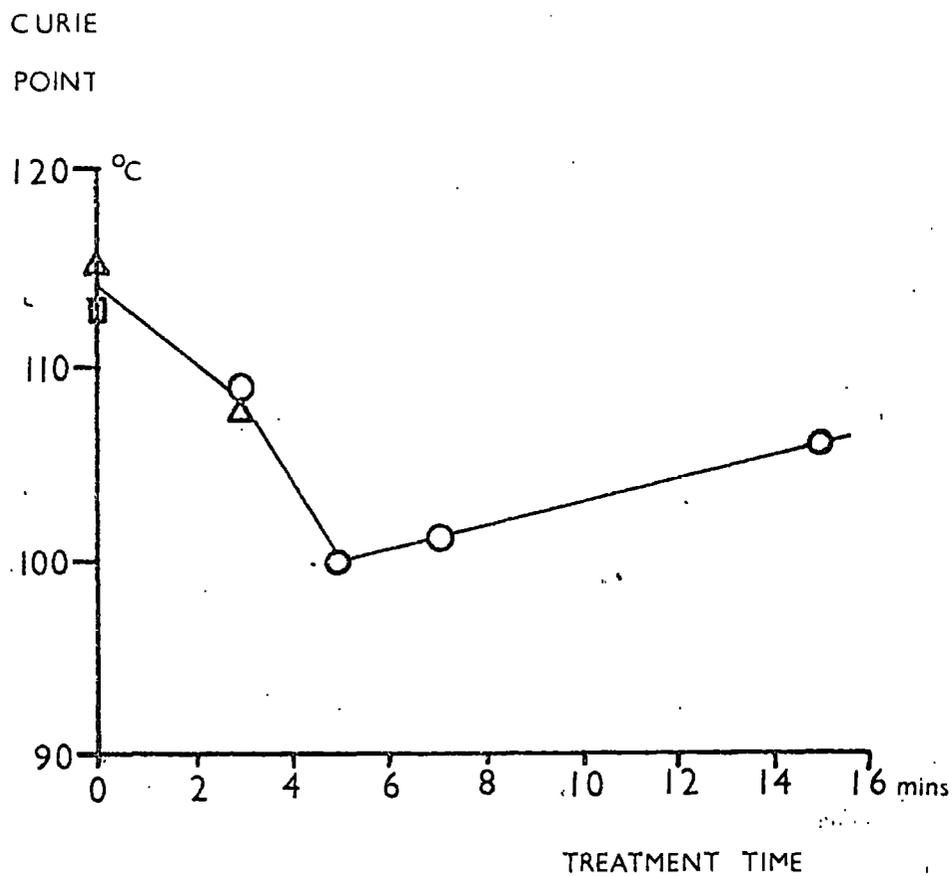
CURIE

POINT

Legend:
- ▯ from dielectric constant
- △ from hysteresis loops
- ○ from domains

Fig. 4.c.   Ferroelectric Curie point.

$$Z = \exp(b\varepsilon/kT) + \exp(-b\varepsilon/kT) + 2\exp(-\varepsilon/kT)$$

$$= 2\left(\cosh(bx) + \exp(-x)\right) \quad \text{where } x = \varepsilon/kT \qquad 4.C.$$

The 2 appears because the level at $+\varepsilon$ is twofold degenerate. The free energy of the cell is $A = -kT\log_e Z$ and the mean dipole moment is

$$D = -\frac{\partial A}{\partial F} = \frac{kT}{Z}\frac{db}{dF}\frac{\partial Z}{\partial b} = \mu\frac{(b^2 - 1)^{\frac{1}{2}}}{b} \cdot \frac{\sinh(bx)}{(\cosh(bx) + \exp(-x))} \qquad 4.D.$$

The polarisation is then

$$P_e = \frac{\mu}{v} \cdot \frac{(b^2 - 1)^{\frac{1}{2}}}{b} \cdot \frac{\sinh(bx)}{(\cosh(bx) + \exp(-x))} \qquad 4.E.$$

where v is the volume of the unit cell.

The equation 4.B. can now be rewritten incorporating equation 4.C.

$$P_e = \frac{\varepsilon}{\beta\mu}(b^2 - 1)^{\frac{1}{2}}(1 - \beta v) - \frac{E}{\beta} \qquad 4.F.$$

Equations 4.E. and 4.F. can now be equated to give the fundamental relationship for the polarised state in barium titanate.

$$\frac{(b^2 - 1)^{\frac{1}{2}}}{b} \cdot \left\{ Kb - \frac{\sinh(bx)}{\cosh(bx) + \exp(-x)} \right\} = \frac{vE}{\mu\beta} \qquad 4.G.$$

where $\quad K = \dfrac{\varepsilon v(1 - \beta v)}{\mu^2 \beta}$ \hfill 4.H.

For spontaneous polarisation, we put $E = 0$ in equation 4.G.
Then

$$Kb = \frac{\sinh(bx)}{\cosh(bx) + \exp(-x)} \qquad 4.I.$$

The Curie point is the temperature at which the internal
field F just disappears so that it can be seen from equation
4.C. that the Curie point is given by putting b = 1. Making
this substitution in equation 4.I. gives

$$\tanh x_c = \frac{2K}{1 + K} \qquad \text{where } x_c = \varepsilon/kT_c \qquad 4.J.$$

Jaynes goes on to calculate the value of x_c for normal
barium titanate. He obtains the value 2.0 so that ε is about
0.067 eV. If we put this value into equation 4.J. we find
that $\tanh x_c$ is 0.964. In this region of x_c, $\tanh x_c$ is close
to 1 and is varying much less quickly than x_c. The value of T_c
is therefore very sensitive to small changes in K. The maximum
shift observed in T_c as shown in fig.4.o. is a drop of 15°C.
This shift can be accounted for in the theory outlined above
by a change of only 1% in K.

The energy levels in fig.4.d. are completely non-localised
in the perfect crystal and there must be a broadening of the
levels due to the interaction between neighbouring octahedra.
Since K is directly proportional to ε(equation 4.H.) there

$\in +$ ——— $+\in$

$\in -$

$+b\in$

$+\in$

$-b\in$

UNPERTURBED

PERTURBED
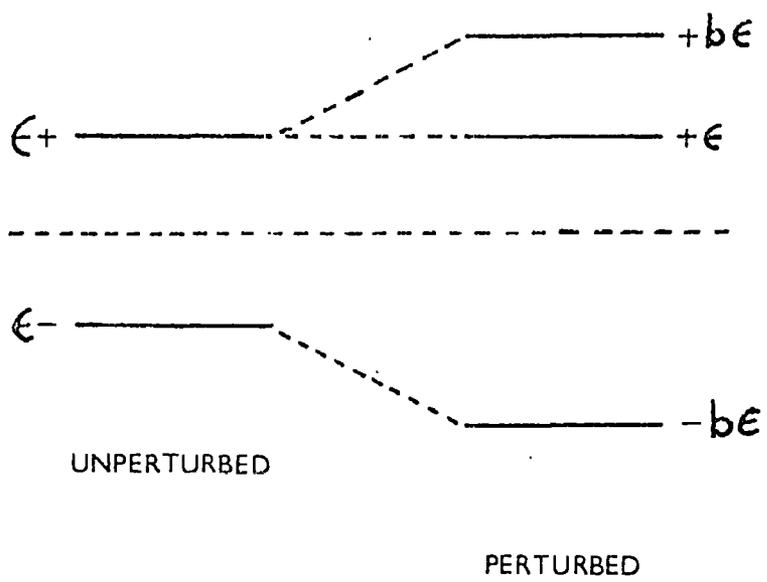
Fig. 4.d.   Energy levels of oxygen octahedra showing field splitting.

must also be an effective broadening in K. The value of K will
not be precisely defined and a broadening of T_c is to be
expected.

This dependence of T_c on K must lead to a dependence of
T_c on the crystalline properties. It has been shown that a
change of only 0.0007 eV in ε is sufficient to account for
the observed change in T_c. This, one imagines, could easily
be accounted for by the removal of oxygen ions from the lattice.

Jaynes maintains that the ferroelectric properties of the
crystal are dependent on the oxygen valence electrons. These
non-localised valence levels in fact constitute the valence
band in the semiconducting state so it may be expected that
if valence electrons are excited to the conduction band, then
the Curie point will be affected. This is because the valence
electron polarisation will be decreased by removal of the
electrons.

The number of electrons released from the oxygen
octahedra into the conduction band after, say, a reduction
time of five minutes is known. At this point, the resistivity
is 20 ohm.cm. (see chapter 6) and if we assume the mobility
of Bergland and Baer (~ 1 cm^2/V·s.) we arrive at an electron
concentration of 6×10^{17} per c.c. These electrons are
removed from the structure described by Jaynes so that the
distribution of electrons within the octahedra will be
multiplied by a factor $(1 - n/N)$ where n is the number

of electrons released from a total of N. The expression
in 4.F., however, remains the same. On making this adjustment
it is found that equation 4.J. still stands if K is multiplied
by $(1 - n/N)$.

The density of valence electrons in the octahedral
structure of an unreduced crystal is 4.5×10^{22} cm^{-3}.
The value of K is therefore only increased by a factor of
1 part in 10^5 when the crystal is reduced for five minutes.
The observed change in Curie point, therefore, cannot be
explained in terms of numbers of electrons. We deduce,
therefore, that the major effect of reducing the crystals
in the present context is that it leads to a change in the
mean energy difference between the first two excited states

4. The Mason-Matthias Theory and others.

The theory developed by Mason and Matthias (4.2.)
considers the effect of an external field on the titanium
ions within the oxygen octahedra. Mason considers that the
titanium ion has six stable positions as suggested in
chapter 2, section 4. An effective field, F, acting in the
[001] direction acts on this ion. The partition function is

$$Z = 2(\cosh \mu F/kT + 2) \qquad\qquad 4.K.$$

where μ is again the maximum dipole moment per unit cell.
The polarisation due to the displacement is again designated

P_d and the field is given by

$$F = E + \beta P = E + \beta(P_d + \nu F) = \frac{E + \beta P_d}{1 - \beta\nu} \qquad\qquad 4.L.$$

where ν is the total polarisability due to all mechanisms other than titanium ion displacements per unit cell. The total observed polarisation will then be

$$P = P_d + \nu F = \frac{P_d + \nu E}{1 - \beta\nu} \qquad\qquad 4.M.$$

The mean polarisation is given by

$$P_d = NkT \frac{\partial}{\partial F} (\log Z) \qquad\qquad 4.O.$$

or $\quad P_d/_{N\mu} = \dfrac{\sinh(\mu F/kT)}{\cosh(\mu F/kT) + 2} \qquad\qquad 4.P.$

where $N = 1/v$ is the number of unit cells per c.c. Combining equations 4.L. and 4.P. we see that spontaneous polarisation occurs only below T_c given by

$$\frac{N\mu^2}{3kT_c} = \frac{1 - \beta\nu}{\beta} \qquad\qquad 4.Q.$$

It can be seen here that under this theory, the Curie point is directly proportional to the number of unit cells

contributing to the polarisation. Even if we take the extreme
view that every unit cell in which an oxygen ion is removed
has its polarisation completely destroyed, the effect of
6×10^{17} vacancies (calculated to exist at the five minute
reduction) would lead to a change in the Curie point temperature
of one part in 10^5 i.e. a change of about $0.004^{\circ}C$. It is
evident that theories which rely on displacements of ions
will not account for the large drop in Curie point temperature
observed in the present experiments. Theories such as those
of Devonshire (4.3.) and of Slater (4.4.) which rely on
polarisabilities of ions are less likely to explain the
current results since the total number of polarisable ions
is even greater than the number of titanium ions so the effect
will be even smaller.

In conclusion it may be said that the observed change
in the Curie point indicates that it is not directly connected
with the transition observed in the resistivity. The electronic
theory of Jaynes is likely to be the most effective in
explaining the large drop in the Curie point. Even here,
without calculation of the change in energy introduced by
oxygen vacancies, there is no direct proof at this stage
that the theory is correct. It will be shown in the final
chapter, however, that small polaron hopping mechanisms for
transport in barium titanate lead to lower mobilities than
those quoted by Bergland and Baer. This in turn leads to
higher electron concentrations which are compatible with the
observed change in Curie point.

Chapter 5

Optical effects in reduced crystals

In order to determine more about the energy levels concerned in the conduction processes in barium titanate, measurements of optical absorption were made. An attempt was also made to measure a photoconductive effect in order to determine which transitions resulted in an electron being in the conduction band.

1.Optical absorption.

A number of crystals were reduced for different lengths of time. The times used were somewhat longer than those used in other measurements since an older reducing furnace was employed. This furnace operated at a pressure somewhat lower than that at which the later furnace was used, involving the use of longer reduction times in accordance with the Law of Mass Action equation. ` . ` . The times used were, however, equivalent to those used for other measurements.

The experimental arrangement is shown in fig.5.a. Light from a tungsten source S was focused by means of the concave mirror M_1 and plane mirror M_2 onto the slits of a Barr and Stroud Type Monochromator. A photomultiplier was used to measure the intensity of the radiation emerging from the monochromator.

The specimen under test was placed in the holder H and the intensity of the transmitted radiation was measured as a function of wavelength. The specimen was then removed and the intensity of the incident radiation was measured as a function of wavelength.
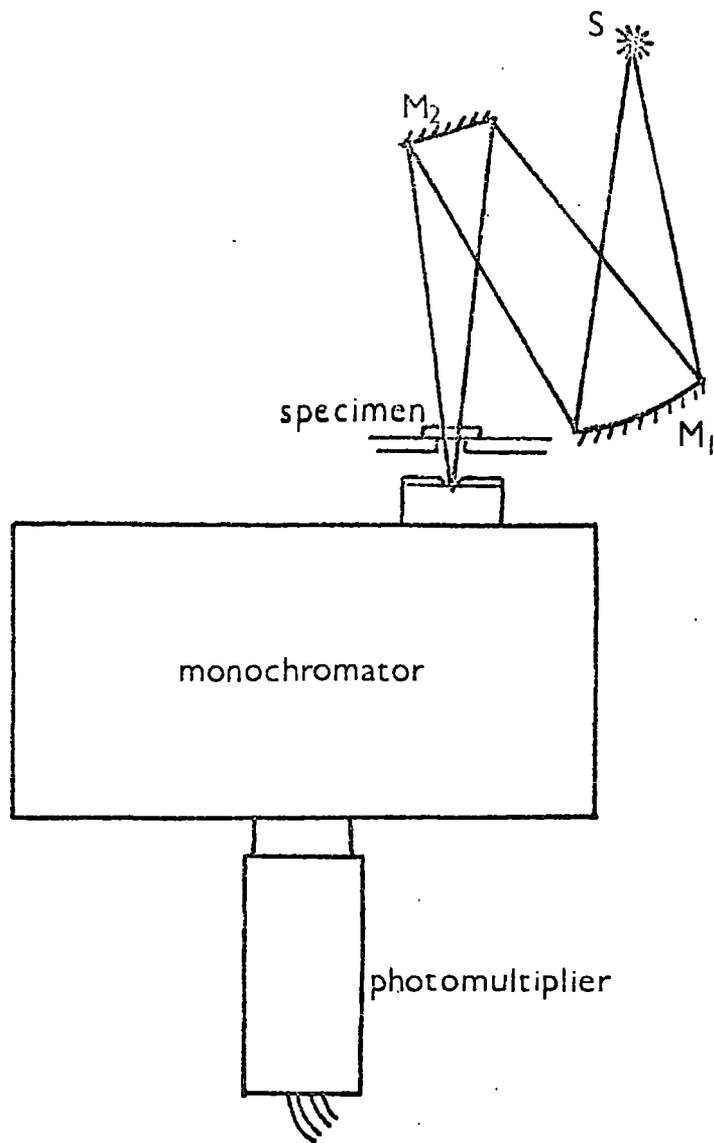
Fig. 5.a.   Apparatus for measurement of optical absorption.

In order to ensure that the incident radiation was unchanged
during the period of measurement, a constant voltage source
was used to supply the tungsten lamp and the lamp was allowed to
warm up for about 15 min. before use.

Having obtained the incident and transmitted intensities,
the thickness was measured with a microscope and the absorption
coefficient was calculated from the equation

$$I_t/I_i = \exp(-\alpha d) \qquad\qquad 5.A.$$

where the symbols have the same significance as in equation 2.P.
The thicknesses of the samples were insufficient to allow
polishing down so that the correction for thickness made by
Cox et al. could not be made in this case. In assessing the
results, therefore, it must be remembered that the measured
absorption includes the reflection at the surfaces.

The results for crystals grown by the author are shown in
fig.5.b. and for those grown by the Harshaw Chemical Co. in
fig.5.c. The general form of these curves is in good agreement
with those of Arend and Coufova (2.23.), if one takes the iron
content of the crystals grown by the author to be about 10 to
15 milliatoms per mol. and that of the Harshaw crystals to be
less than 5 milliatoms per mol. The Harshaw crystals are brown
in colour when reduced due to the edge absorption in the blue.
The author's crystals, however, were blue when reduced due to
the absorption peak at about 2.1 eV., which is supposed to be
due to f centres caused by oxygen vacancies as suggested by
Dvorak (5.1.). ~~The present work has shown, however, that the~~

Absorption coefficient
mm⁻¹

A as grown
B reduced ¹/₆ h
C reduced ¹/₂ h
D reduced 1 h
E reduced 2 h

Wavelength (microns)
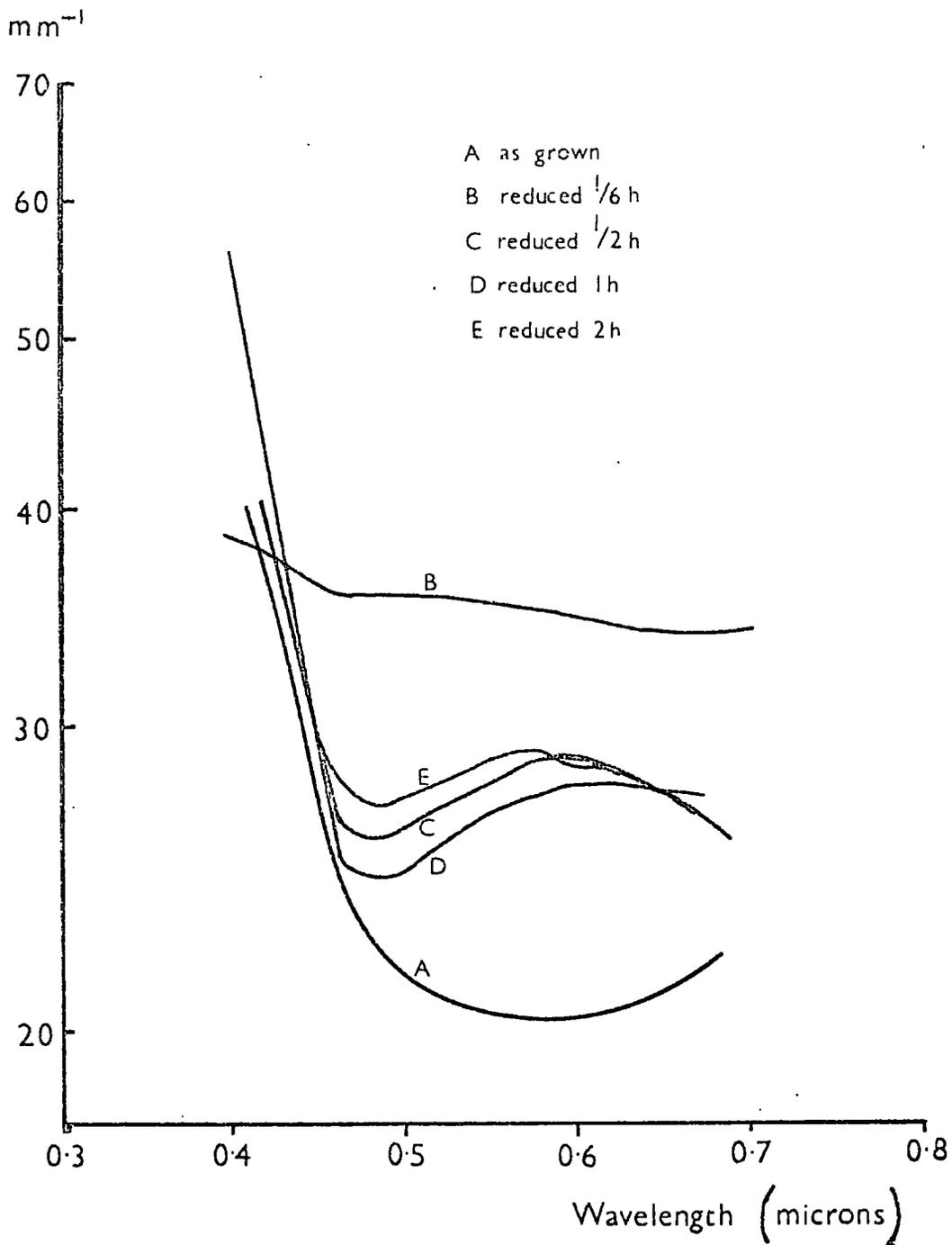
Fig. 5.b.   Optical absorption in crystals grown by the author.
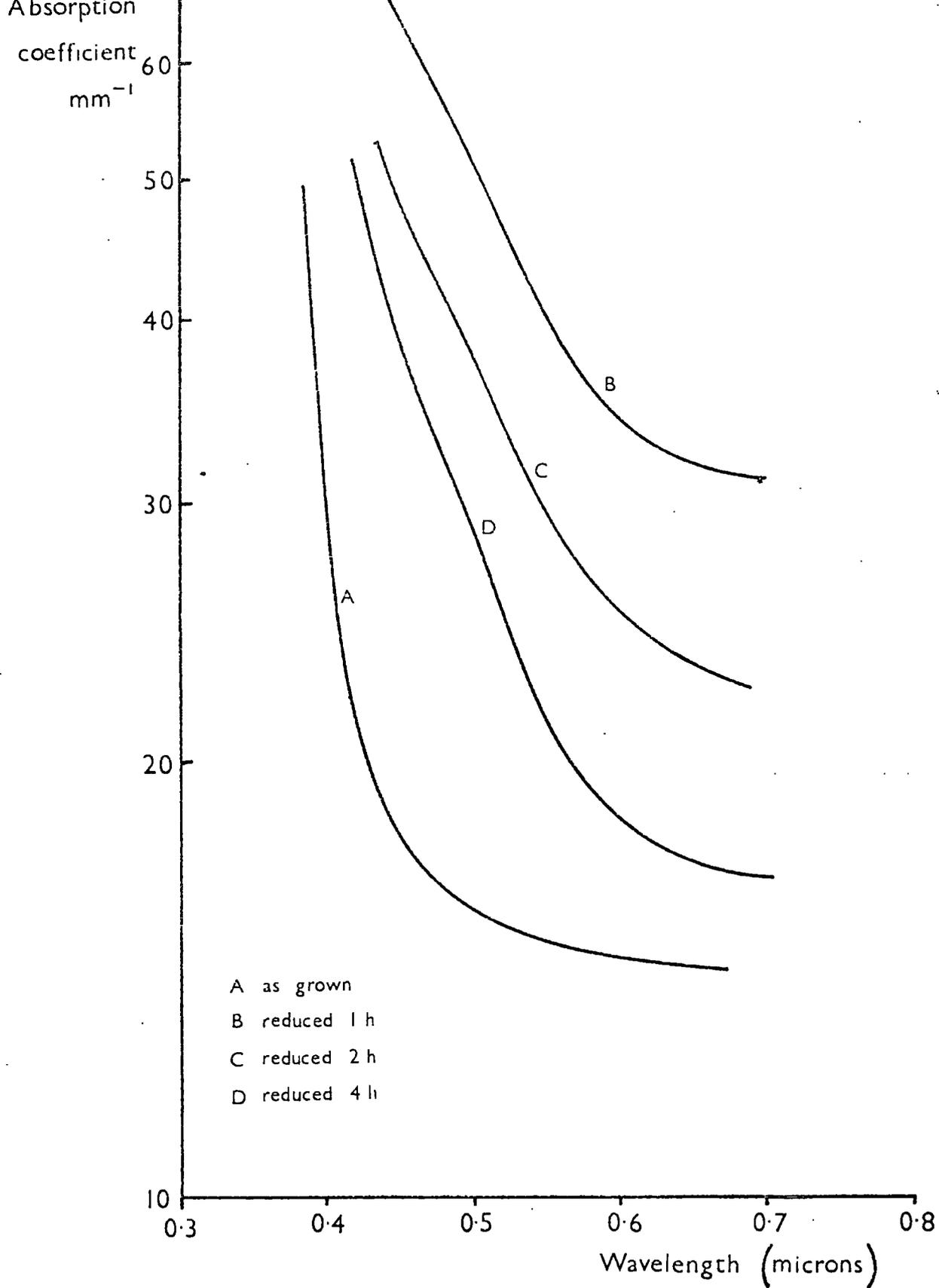
Fig. 5.c.   Optical absorption in crystals grown by the Harshaw
             Chemical Co.

~~iron even in the crystals with little iron impurity is not compensated since the resistivity change on reduction shows that it is not until the crystal is reduced that the iron is completely compensated.~~ The lack of a peak in the optical absorption of crystals of low iron content would seem ~~then~~ to be unexplained.

2.Photoconductivity.

In order to determine whether the peak found in the last section is indeed a freeing of electrons into the conduction band or whether the transition concerned is from one bound state to another, experiments were performed to detect a photocurrent. The experimental arrangement is shown in fig.5.d. Light from a tungsten source S is focused through the lens L and the infra red filter F onto the crystal. Two thermosetting silver electrodes on the specimen allowed a current from a battery to be passed through the crystal and through a standard resistance R. The voltage across this standard was monitored on a pen recorder. On switching on the lamp, a slow current response was detected which reached a maximum of about 30% of the initial current. In order to ensure that the response was not due to heating of the crystal, the specimen was placed in a holder on a cold finger cooled with mains water. It was found that no change in photocurrent resulted whether or not the crystal was so cooled.

In order to ascertain the spectral response of this photoconductive effect, the crystal was placed in a holder on the output side of a monochromator. It was found that the
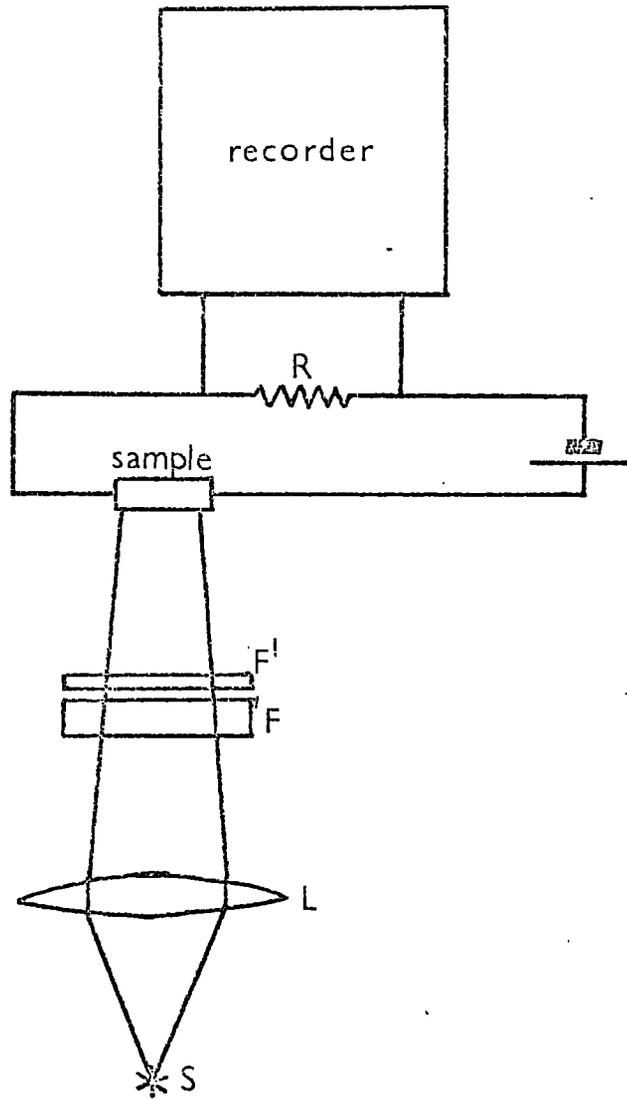
Fig. 5.d.   Apparatus for detection of photoconductivity.

intensity was not sufficient to produce a response with the lamp available.

In the absence of a spectral response, it was decided to return to the arrangement shown in fig.5.d. but various optical filters F_2 were used to filter out various parts of the visible spectrum. The absorption spectra of the filters are shown in fig.5.e. They are standard Chance-Pilkington filters and the standard letter codes are continued here.

It was not possible to detect any current with the present apparatus for an 'as grown' crystal. Measurements were therefore made on crystals which had been reduced for 7 min. and 15 min. On each crystal, the photoresponse was measured, firstly with no filter F_2 and then successively with each of the coloured filters. The current was allowed to return to the dark current between each measurement. The relative responses expressed as a fraction of the unfiltered response are tabulated below.

Filter. No.	Crystal reduced 7 min.	Crystal reduced 15 min.
OX7	27	77
OB10	55	50
OY2	71	65
OY1	68	42

It is difficult to draw any very concrete conclusions from these results but it would appear, since a photoresponse is
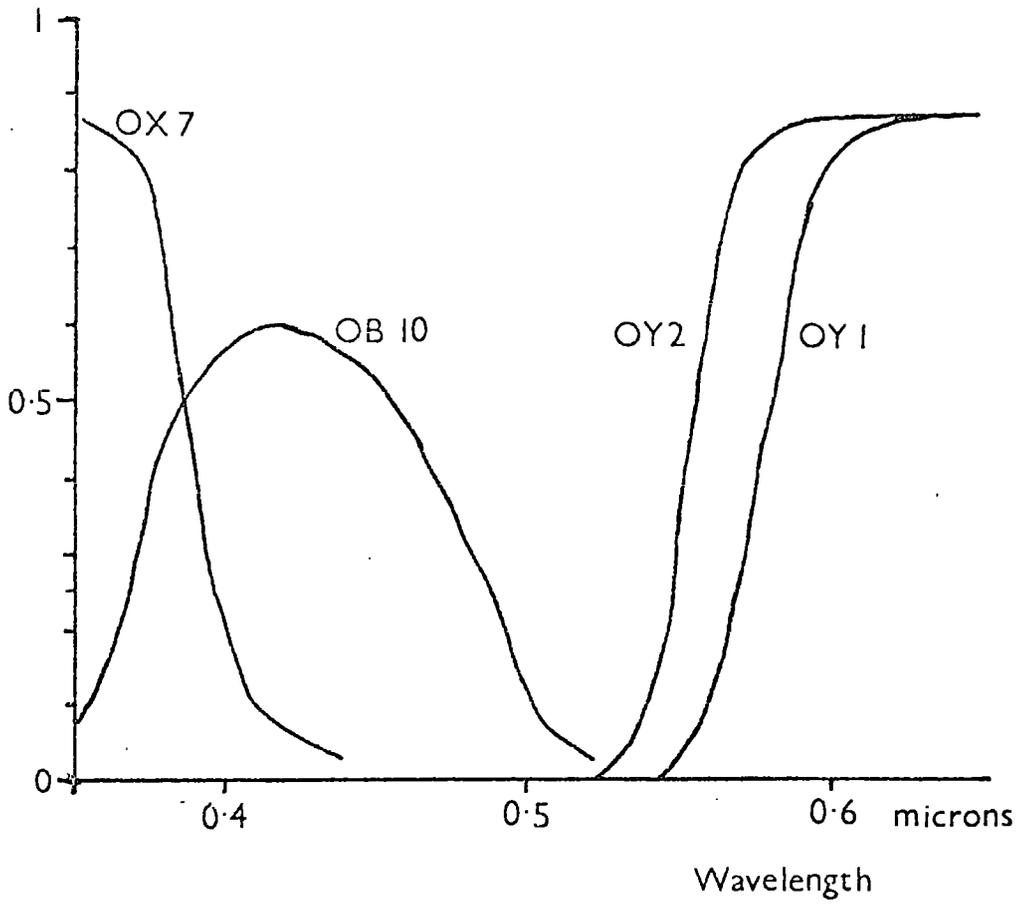
Fig. 5.e. Absorption spectra of filters used in photoconductivity experiments.

obtained in the red end of the visible spectrum, that the peak
at 2 ~~microns~~ eV could well be explained by f centres caused by
oxygen vacancies.

During the measurements outlined above, it was found that
the decay of the photocurrent was very slow. During one such
decay, the current was measured as a function of time and was
found to be an exponential decay. The time constant associated
with this decay was 20 min. This long time constant must be
associated with a complex process since on standard diffusion
theory, a single process with such a time constant and with
such a mobility, would have a diffusion length of a few centimetres.
Such a long path could not be associated with such a low mobility.

Generally, then, one can say that the optical absorption
processes involved in these reduced specimens are complex. The
edge absorption is, however, unchanged and there is a peak in
the optical absorption at about 2 eV which could well be due to
excitation of electrons from oxygen vacancies.

3.The Absorption Edge.

As described in chapter 2, section 9, Cox et al. have
measured accurately the direct and indirect band edge energies
in unreduced barium titanate, assuming allowed transitions.
In these two cases and in the corresponding forbidden transition
cases, simple power laws relate the absorption coefficient and
wavelength. These power laws can be masked, however, by exciton

peaks (5.2. and 5.3.) or by polaron effects (5.4.). The problem
of distinguishing between these edge absorption effects is a
complex one. The results shown in fig.5.f. are inadequate for
analysis since no correction can be made for the reflectivity.
It can, however, be said that the position of the edge is in
general agreement with Cox et al. It will be shown in chapter 9
that conduction in these crystals is most likely in the small
polaron hopping mode. This is corroborated by the reflection
measurements in the infra-red region made by Riek and Heese
described in chapter 2, section 9. If this mechanism is correct,
considerable doubt would be thrown on the analysis of Cox et al.
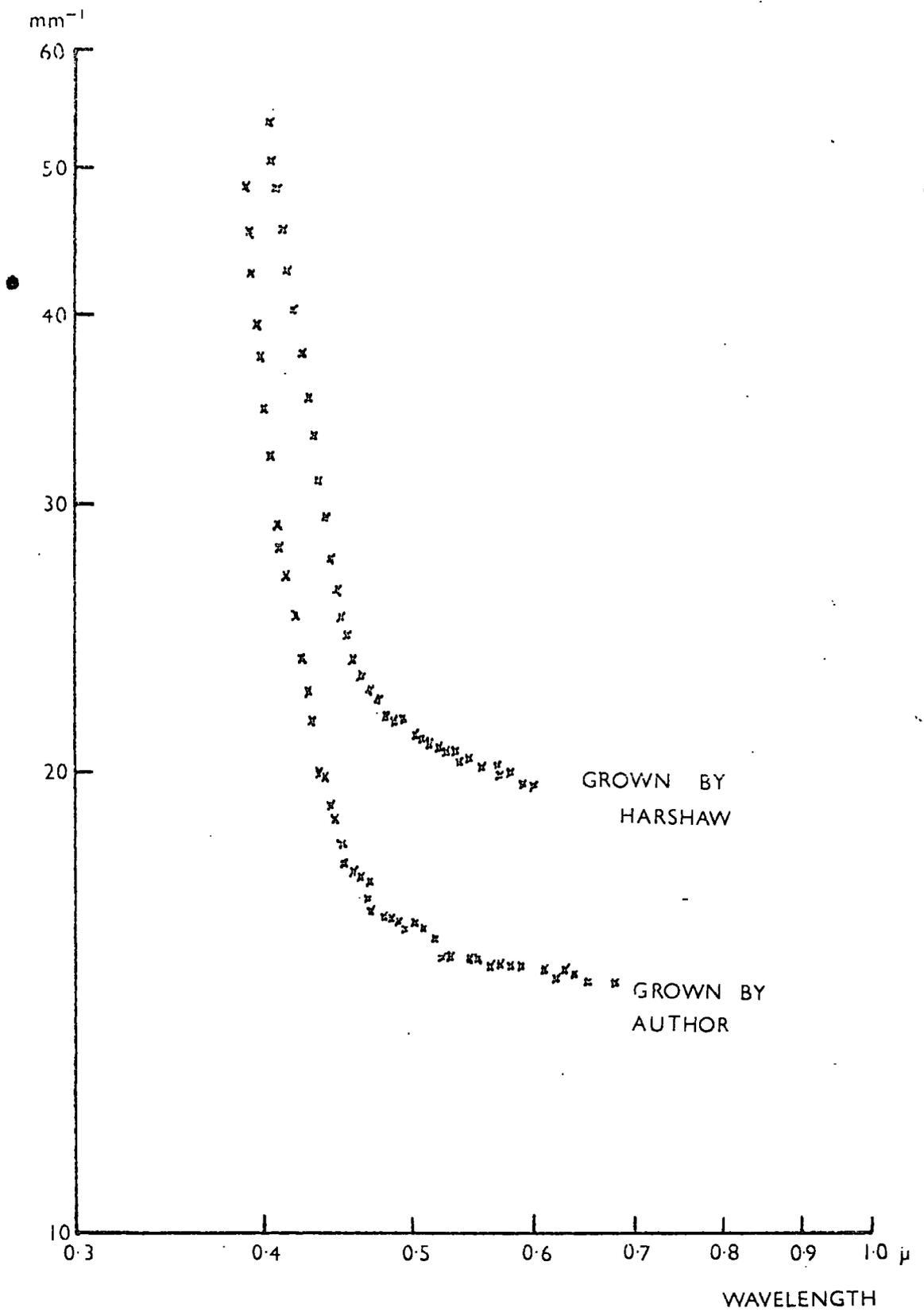
Fig. 5.f. Band edge in barium titanate.

Chapter 6.

Resistivity and Hall mobility

1.General remarks.

It will be assumed here that the reader is acquainted
with the elementary definitions of electrical resistivity,
mobility and Hall coefficient. The simple semiconductor
expressions for these quantities will be used without proof
since these are readily found in standard texts on semiconductor
physics (e.g. Smith (6.1.); Putley (6.2.). The results of
Berglund and Baer (chapter 2, section 8) show that reduced
barium titanate crystals are n-type. It will be assumed,
therefore, since all the results obtained by the author were
from quite heavily reduced crystals that they too are n-type
(this was confirmed by the sign of the Seebeck coefficient
obtained from the author's crystals). The expressions which
occur in semiconductor expressions for resistivity and mobility
involve $(n\mu_n + p\mu_p)$ and $(n + p)$ only and so in the present
instance the quantities $p\mu_p$ and p can be neglected.

These considerations leave us with the expressions:
$$\rho = 1/ne\,\mu \qquad\qquad 6.A.$$
and
$$R_h = 1/ne \text{ x } \text{constant} \qquad\qquad 6.B.$$

The suffix $_n$ has now been omitted since there is no need to
distinguish from $\mu_p p$. The constant in equation 6.B. is a
function of the scattering parameter. It is given by the
expression

$$\frac{3\pi^{\frac{1}{2}}}{4} \frac{\Gamma(2s + 5/2)}{\Gamma(s + 5/2)}$$

where s is the scattering parameter defined by the relaxation time, τ, for a carrier of energy E by $\tau = kE^s$. The expression $\frac{3\pi^{\frac{1}{2}}}{4} \frac{\Gamma(2s + 5/2)}{\Gamma(s + 5/2)}$ always has a value between 1 and 2 depending on the scattering mechanism. In chapter 9, it will be shown that optical mode scattering yields the most self consistent explanation of the results of Seebeck coefficient measurements. The value of $s=-\frac{1}{2}$ in this case gives a constant in equation 6.B. of approximately 2.

Simple division gives immediately,

$$R_h = \rho \mu \text{ x constant.} \qquad\qquad 6.C.$$
$$= \sim 2\chi \, \rho\mu \text{ for optical mode scattering.}$$

So, with certain reservations, measurement of resistivity and Hall mobility give directly, the concentration of electrons and their mobility.

2.Hall effect in the conventional geometry.

It is usual to measure the Hall mobility and resistivity using a rectangular specimen with contacts as shown in fig.6.a. A current is passed through the sample from end to end, a magnetic field is applied in a direction perpendicular to the current and a voltage is observed across the specimen in the third mutually perpendicular direction. If the dimensions of the crystal are as shown, the Hall coefficient is given by

$$R_h = V \, b/i \, B \qquad\qquad 6.D.$$
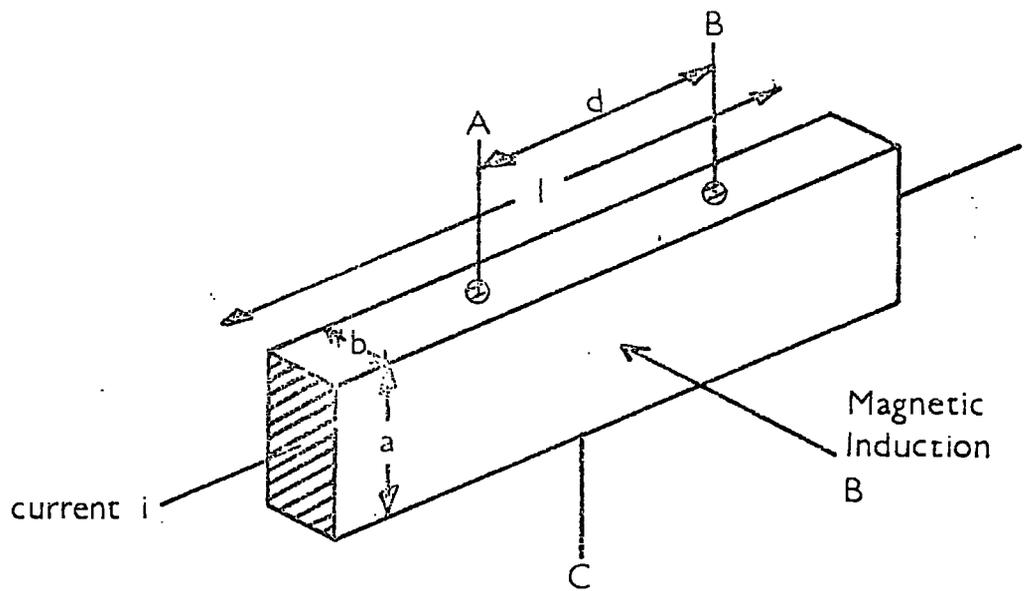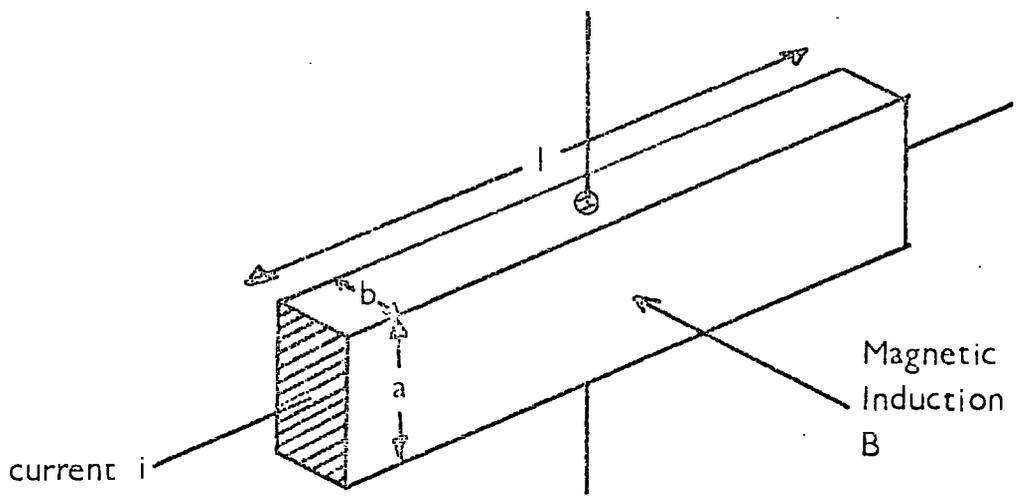
Fig. 6.a. Conventional four and five probe geometries for measurement of Hall mobility.

Here, V is the voltage generated, i is the current flowing
and B is the magnetic induction all in e.m.u.

In order to be able to measure the resistivity at the
same time, it is usual to use a five terminal method as shown
in the lower part of fig.6.a. Here, the voltage drop across
the two contacts A and B is used to measure the resistivity and
a potential divider can be connected between A and B such that
the voltage between its centre tap and the contact C is zero
when there is no magnetic field. On application of a magnetic
field, the Hall voltage is measured between the centre tap of
the potentiometer and the contact C.

In the first geometry, care must be taken that the Hall
voltage is not shorted by the current contacts. The condition
that the shorting effect is negligible is that $1/a$ should be
greater than or equal to 4. In the five probe case, this
condition becomes $(1-d)/a \gt 4$.

If this condition is satisfied, the expressions for
and R_h become;

$$R_h = bV_h /iB \quad \text{and} \quad \rho = abV_d/di \qquad 6.E.$$

now, V_h is the hall voltage measured at the potentiometer and
V_d is the voltage drop across the length d.

In using this method, errors are easily introduced by
finite contact size which cause errors in measuring the distances

a,b,d and l. Furthermore, it is important that the potentiometer which is used to balance the voltages at either side of the crystal has a resistance large compared with the crystal resistance between A and B. This in turn means that the instrument used to measure the voltages has to have an even higher input impedance than would be necessary to measure the crystal directly. In this way, for 1% accuracy, the potentiometer will need a resistance of 100 times the impedance of the crystal across A and B and the instrument will need an impedance of 10^4 times that of the crystal. When dealing with samples which have high impedances, this can be something of a problem.

There is a further practical difficulty with the conventional method in the present instance. The largest sample which could be cut from a typical specimen such that the condition $(1-d)/a > 4$ holds with a suitably measureable distance d would be a strip about 5 m.m. long by about 0.4 mm wide. Such a specimen would be very fragile, would have a resistance which would be high and would require very small contacts to prevent errors due to inaccuracies in measuring distances.

In view of these difficulties, a geometry was sought which would lead to more satisfactory measurements. It is felt that the method described in the next section is more promising.

3. The van der Pauw arrangement.

Van der Pauw (6.3.) describes how four contacts placed in

any positions around the perimeter of a lamina of arbitrary
shape can be used to measure the resistivity and Hall mobility.
If the four contacts applied to the edges of the slice are
labelled cyclically round the crystal A, B, C and D, and if
we define the resistance R_{abcd}, to be the potential drop across
AB per unit current through CD, the resistivity is given by

$$\rho = \frac{d(R_{abcd} + R_{bcda})}{\ln 2 \quad 2} f\left\{ \frac{R_{abcd}}{R_{bcda}} \right\} \qquad 6.F.$$

where d is the thickness of the slice, and where the correction
function is defined by the equation

$$\frac{R_{abcd} - R_{bcda}}{R_{abcd} + R_{bcda}} = \frac{f}{\ln 2} \quad \text{arc cosh } \left(\frac{\exp(\ln 2/f)}{2} \right) \qquad 6.G.$$

The correction function f is shown in fig.6.b. It has been
shown by Allen (6.4.) that the approximate formula for f, vis,

$$f \approx 1 - \left\{ \frac{R_{abcd} - R_{bcda}}{R_{abcd} + R_{bcda}} \right\}^2 \ln 2 - \left\{ \frac{R_{abcd} - R_{bcda}}{R_{abcd} + R_{bcda}} \right\}^4 \left(\frac{(\ln 2)^2}{4} - \frac{(\ln 2)^3}{12} \right)$$

$$\dots \, 6.H.$$

is correct to 4 significant figures to values of R_{abcd}/R_{bcda}
of 1.6 while the present author has shown that at $R_{abcd}/R_{bcda} = 10$,
the approximate formula is correct to 5%. For a specimen of
roughly uniform shape with contacts uniformly spaced around it,
R_{abcd}/R_{bcda} is expected to be close to unity and certainly less
than 10. Van der Pauw goes on to show that the Hall mobility
is given by
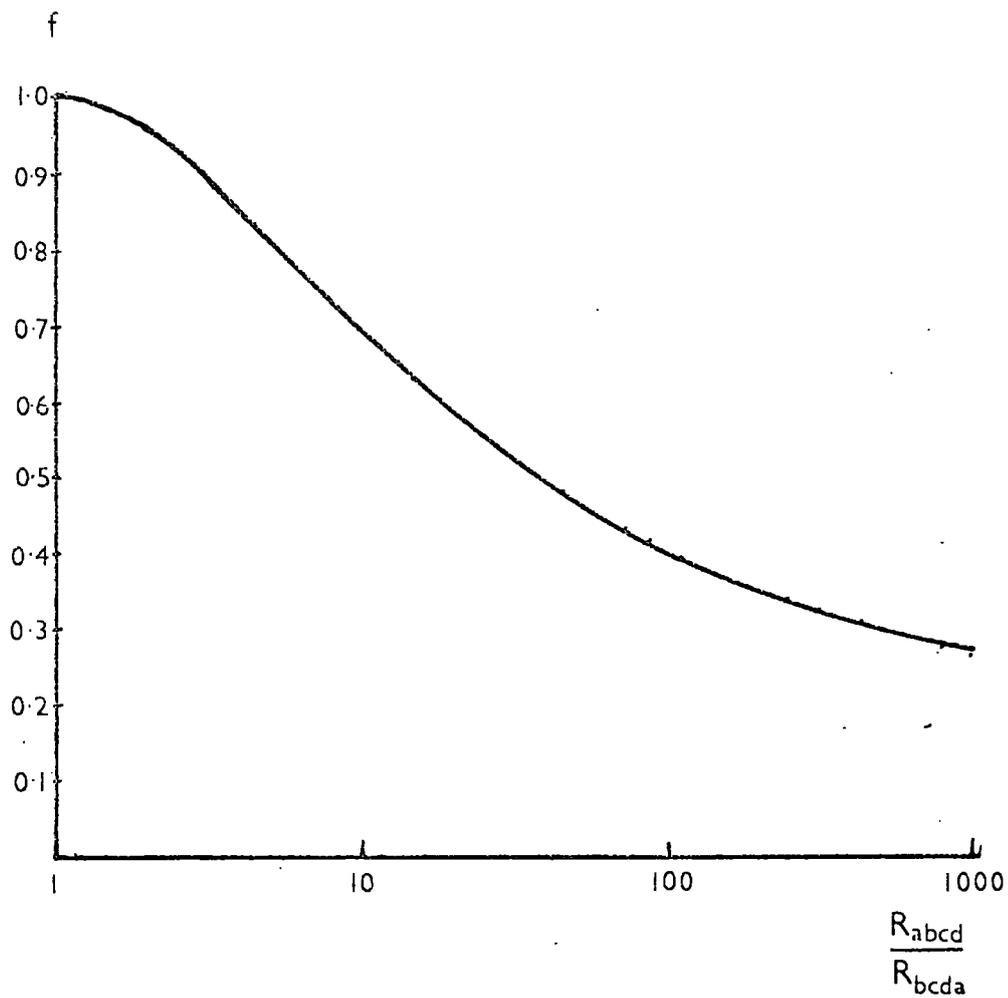
Fig. 6.b.   Correction function used in calculation of
             resistivity in van der Pauw arrangement.

$$\mu = \frac{d}{B} \cdot \frac{\Delta R_{bdac}}{\rho} \qquad\qquad 6.I.$$

where the change in resistance R_{bdac} on application of a
magnetic induction B is ΔR_{bdac}.

This method has the immediate advantage over the conventional
five probe method that only one crystal dimension is required.
This being the thickness, it can be measured quite accurately
using a microscope. In practice, for plate type crystals, a
larger crystal can be used and the current which can be passed
through the crystal is greater. Furthermore, the crystal
resistances between contacts can be smaller so that an
instrument of lower input impedance can be used.

The major difficulty with this method, is that the
expressions 6.F. and 6.I. are only valid for point contacts.
The use of finite sized contacts can lead to quite large
systematic errors in the results. Van der Pauw suggests that
a 'clover leaf' as shown at the top of fig.6.c. is most effective
in reducing these errors. This geometry ensures that the
important parts of the crystal where the current density is
greatest are separated from the contacts.

Attempts were made by the present author to cut clover
leaf shapes from flux grown plates using an Airbrasive cutter.
A miniature lathe was constructed to cut circles from the
crystals and the four slits were then cut with the aid of a
micromanipulator. Although this technique was found to work
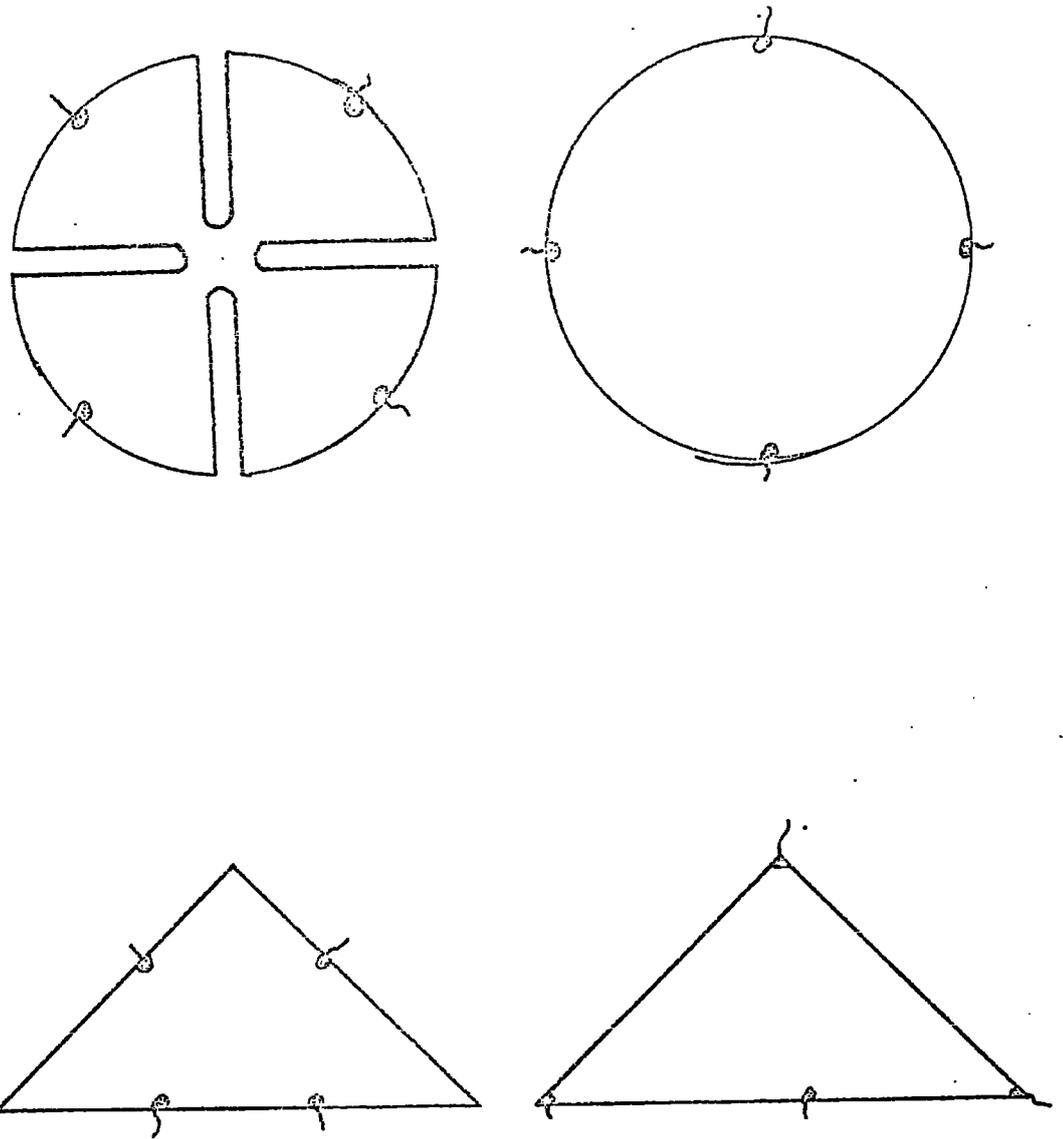
Fig. 6.c.   Various geometries used for appraisal in van der Pauw
              arrangement.

well with other materials, it was found that the barium titanate
crystals were too brittle, the necks between the slits being
the weak points.

In order to ascertain a suitable sample shape, which would
not lead to unmanageable errors due to finite contact size,
a series of tests was made using graphited paper with silver
dag electrodes painted on. In each shape used, a very small
contact size was used first and then it was enlarged to be
of dimensions about 10% of the dimensions of the paper shape.
The change in measured resistivity was noted. As expected, the
clover leaf sample showed the least error due to the finite
contacts. Of all the other shapes tried (illustrated in fig.6.c.)
the triangular specimen shown at the bottom showed the least
change in resistance with increased contact size. In order to
verify that this sample shape would be suitable for van der Pauw
type measurements, a further series of tests was made on the
graphited paper to determine the effect of finite contact size
from each contact. Each contact was increased in size individually
and the effect on measured resistance was plotted. It was found
that the contact at the centre of the hypotenuse of the triangle
was the worst at producing contact size errors.

A rough calculation of the voltage change which produces
the resistance change R_{bdac} in the measurement of Hall mobility
showed that the signal voltages which could be expected in
this geometry would be about four times as great as in the
conventional five probe method.

The question of shorting of the Hall voltage by the current contacts was also resolved using the graphited paper. A set of equipotential lines were plotted on the paper for each of the two possible Hall configurations i.e. with current between apex and hypotenuse and between acute angled corners. The results of these plots are shown in fig.6.d. It can be seen that in the case when the current flows from 45° corner to 45° corner, the current is disturbed by the contact at the centre of the hypotenuse. In this configuration, therefore, the Hall mobility will not be correctly measured. The other possible direction for current flow, however, appears to be satisfactory.

It was decided, then, to use this geometry to measure the resistivity and Hall mobility in the flux grown crystals since no cutting of the crystals was necessary.

4.Experimental arrangements.

Preliminary estimates showed that the impedance of samples to be measured would be possibly as high as 10^9 ohm. Furthermore, the smallest signals which were likely to be measured would be between 10 and 100 microvolts. It was decided to measure the voltages concerned with an electrometer amplifier of the type manufactured by H. Tinsley. This amplifier is essentially an electrometer triode bridge. Control of the balance is obtained by adjustment of the grid bias on one valve while the grid of the other valve is used as a high impedance detector.
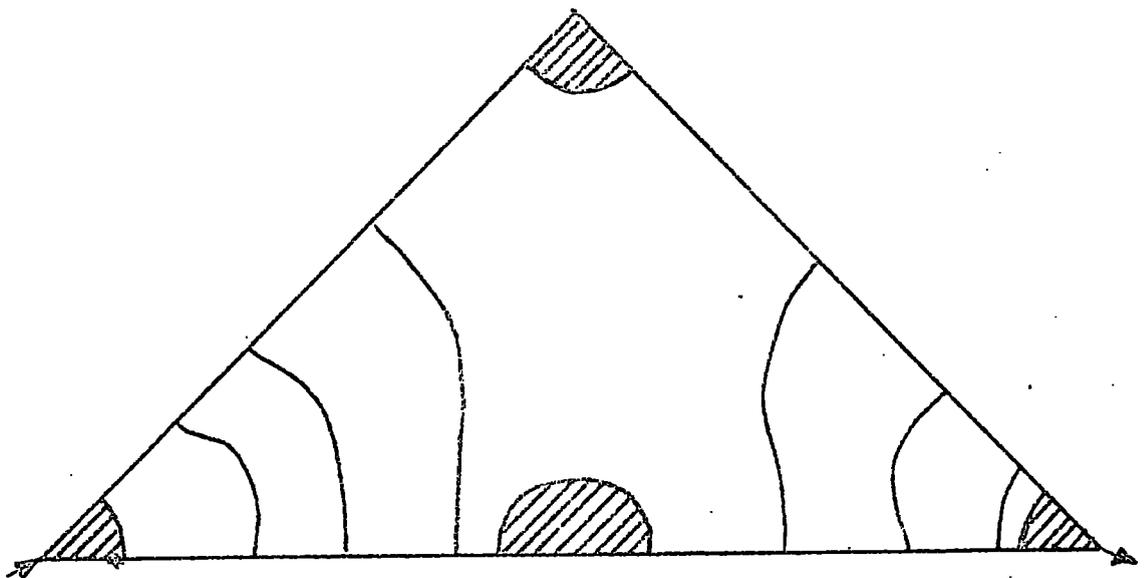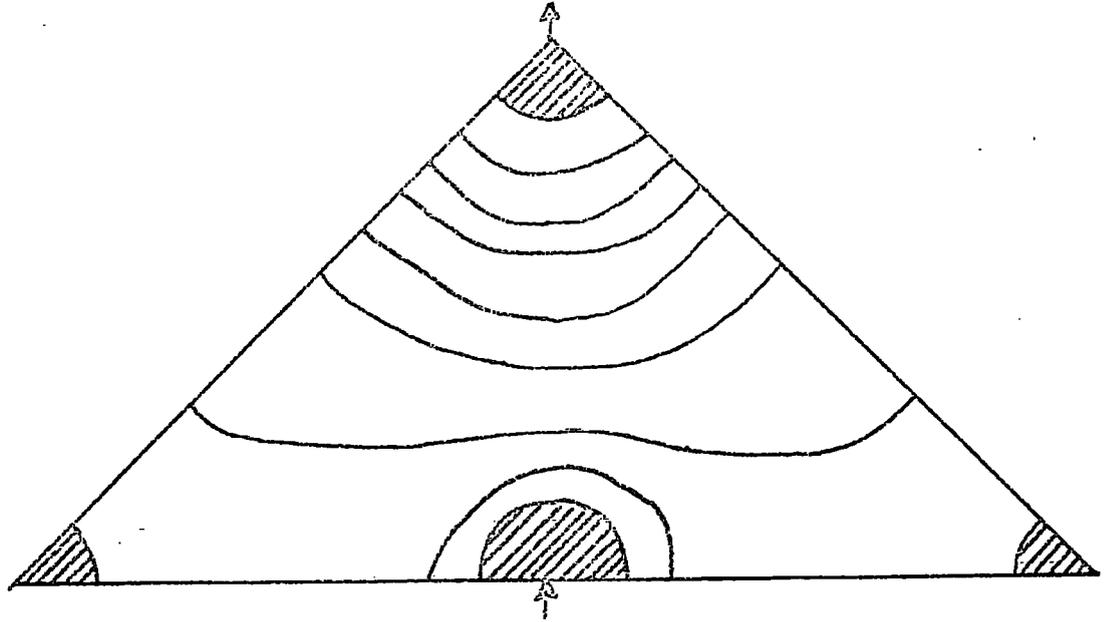
Fig. 6.d.   Equipotentials in triangular lamella.

The out of balance current of the bridge is measured between the anodes with a galvanometer. This detection system is used, then, to measure out of balance voltages between the source and a normal potentiometer. The limit of measurement of this apparatus is then 100 microvolts in 10^{10} ohms. At lower impedances, it is expected that the values will be more stable and that an improvement to 10 microvolts will be obtained.

The complete measuring apparatus is shown in fig.6.e. A current is driven by a battery through the stabiliser to the specimen and to a standard resistance. In order to be able to apply the current to any pair of contacts on the crystal, a switching unit was arranged to apply the current to any pair of contacts and to measure the voltage across any pair of contacts or across the standard resistance (this is shown in detail in fig.6.f.). The voltage output from the switching unit was fed directly to the electrometer amplifier.

The technique of using the system was to standardise the potentiometer using the galvanometer 2 as a detecting instrument. The grid bias on the electrometer triode was then adjusted to give zero deflection on the galvanometer 1. The appropriate current and voltage contacts were selected with the switching unit and the unknown voltage connected to the electrometer amplifier. The output from the potentiometer was then adjusted until the galvanometer 1 again showed no deflection. The output voltage from the potentiometer then gave the unknown voltage.
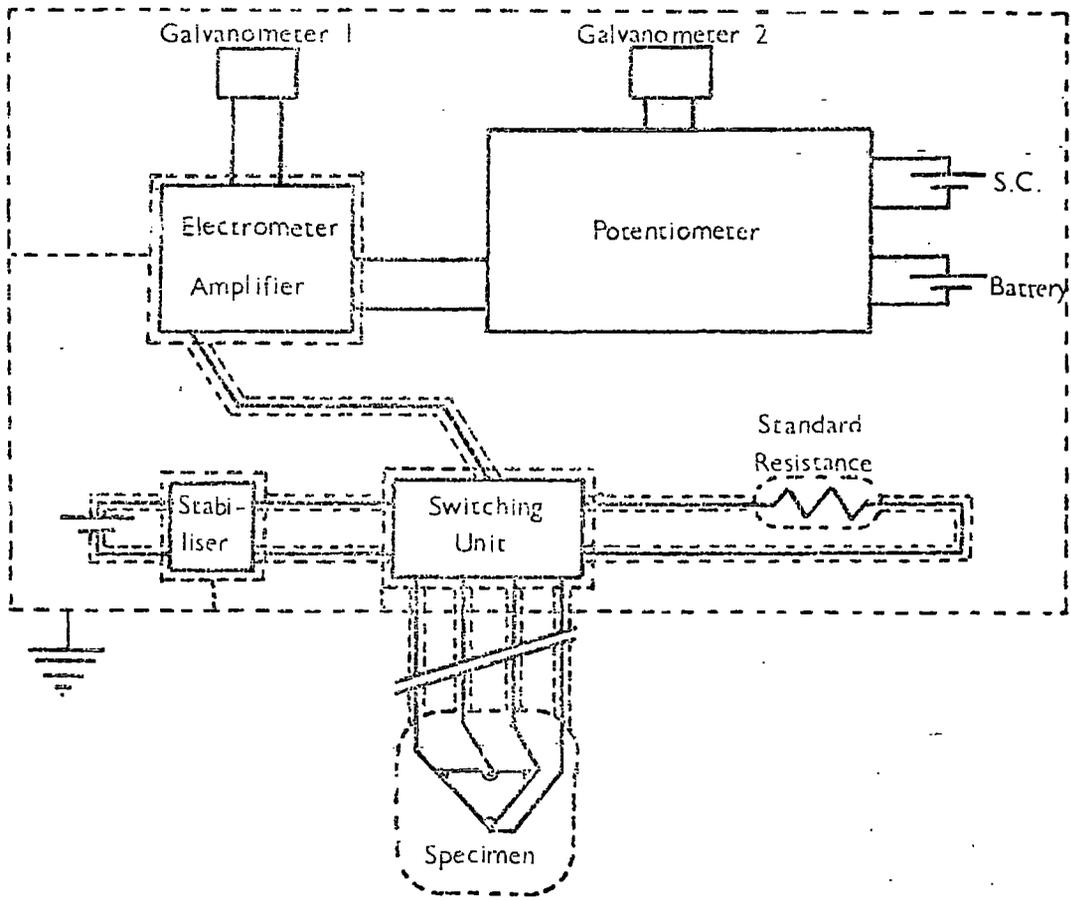
Fig. 6.e.   Measuring apparatus used for resistivity and Hall
            mobility measurements.
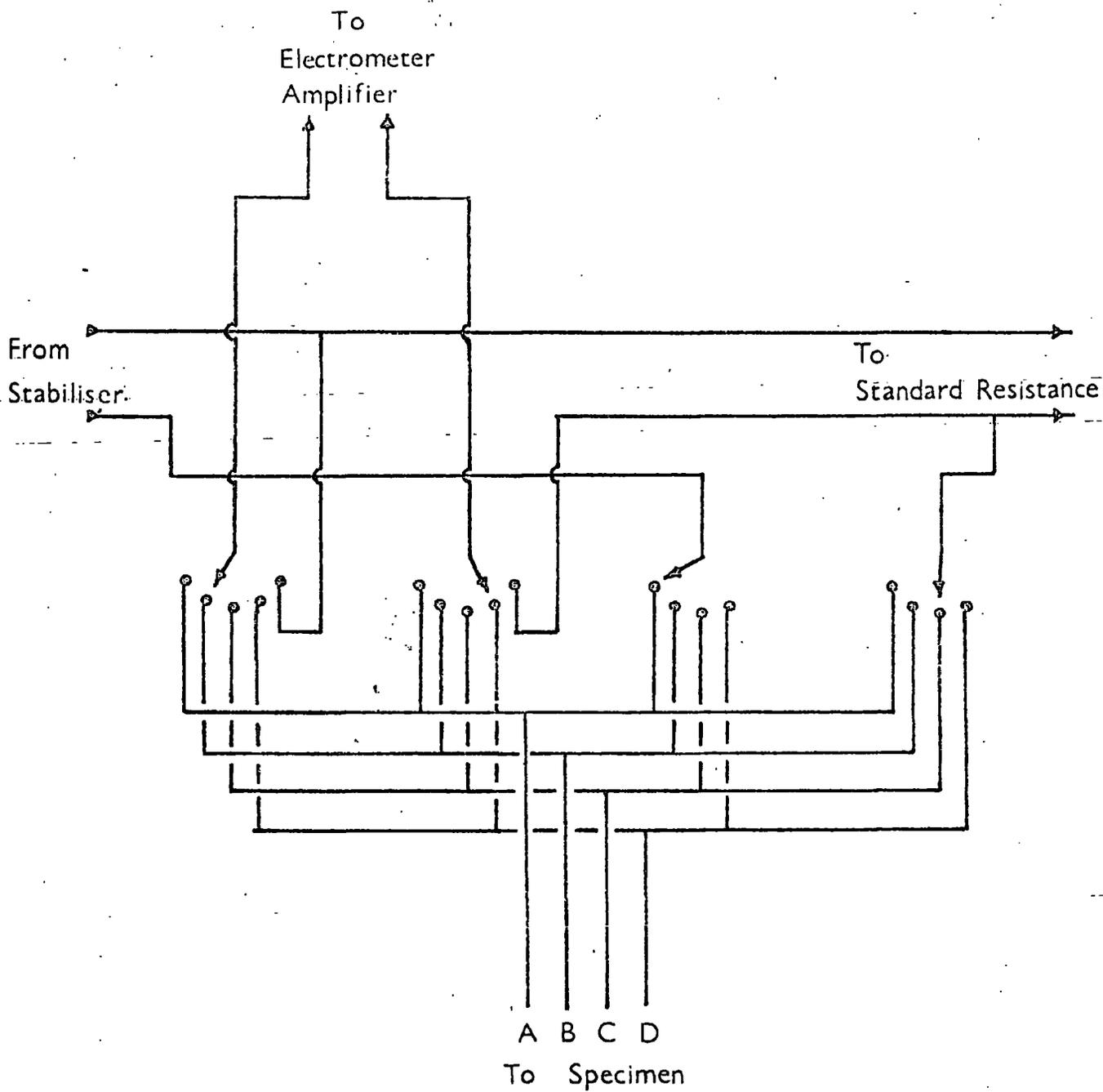
Fig. 6.f.   Switching unit used in resistivity and mobility
            measurements.

In use, it was found that the system was very sensitive
to external a.c. fields, notably mains pick-up. It was
therefore found necessary to provide adequate screening from
these fields. In the circuit diagram in fig.6.e. the broken
lines indicate screening. The broken lines adjacent to wires
indicate that a low noise screened cable was used. Other
broken lines indicate aluminium or brass enclosures.

The specimen holder is shown in detail in fig.6.g.
This consisted of four 1.5 m.m. diameter brass rods which
served as leads to the specimen as well as a mechanical support.
On the end of the rods, the specimen was mounted on a silica
slide with four platinum wires connecting the four thermosetting
silver contacts with the brass rods. A pair of thermocouple
leads of copper and constantan were threaded through small
holes in the insulating spacers and joined to form a thermocouple
very close to the crystal. The leads at the top were connected
to coaxial sockets on a hexagonal head. The screen connections
on the sockets were connected to the brass head which in turn
made contact with the brass jacket surrounding the specimen.
A kanthal wire heater was wound around the jacket so that the
temperature of the interior could be raised to 200°C. The
overall diameter of the jacket with the heater was small enough
to insert into a 5 cm. magnet gap.

In order to measure the resistivity, with this arrangement,
the four cyclic resistances, R_{abcd}, R_{bcda}, R_{cdab}, R_{dabc} were
measured and these were taken in cyclic pairs and the resistivity
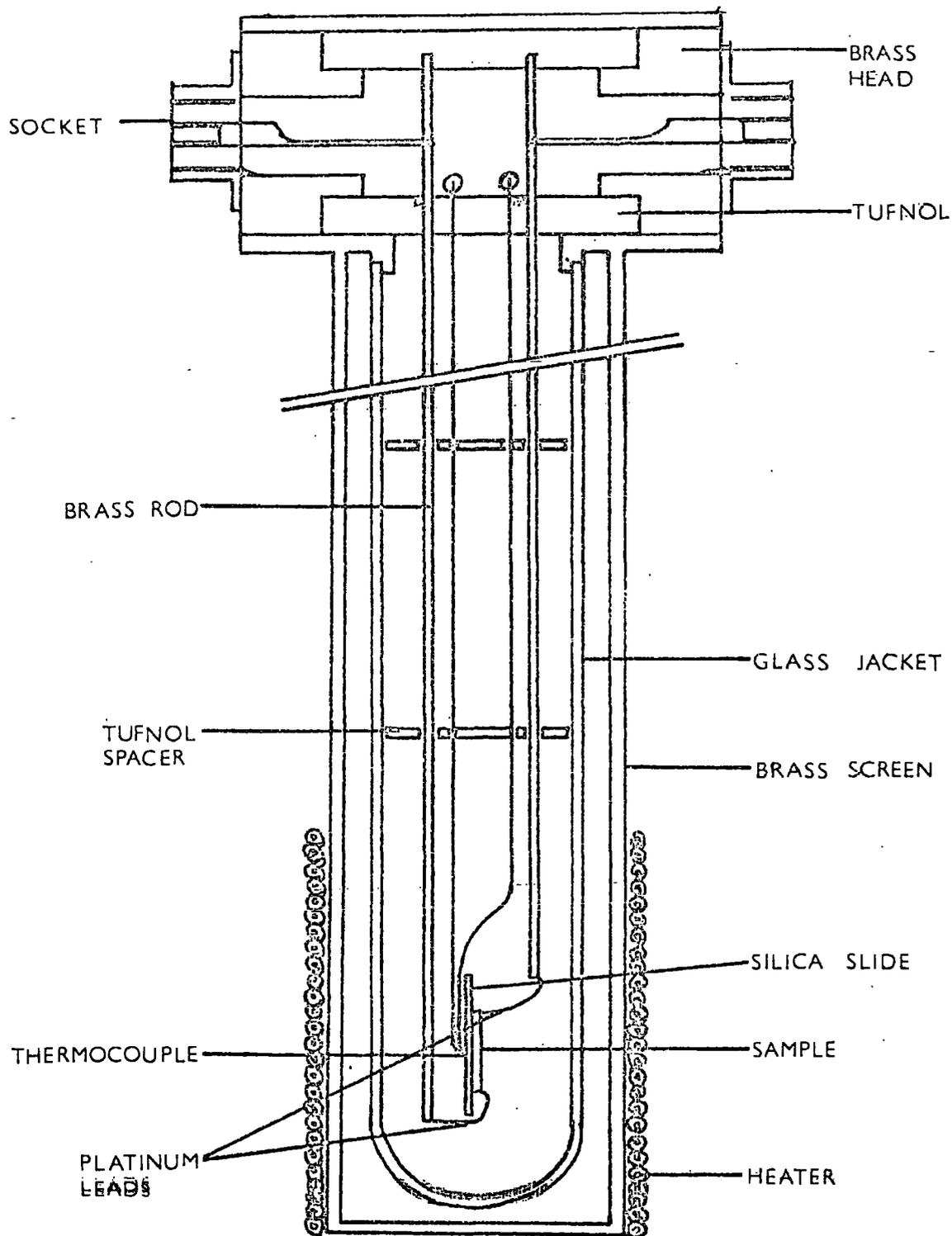
Fig. 6.g.   Specimen holder for resistivity and mobility
measurements.

calculated from equation 6.F. The mean value of these four
results was then taken to be the correct resistivity. In
practice, the scatter between the four resistivity values
obtained was of the order of $\pm$ 5%. The van der Pauw method,
it should be pointed out, assumes isotropic specimens. This
averaging of the four resistivity values will be equivalent
to an averaging of any anisotropy which may be present.

5. Results.

An attempt was made to measure the resistivity of an
'as grown' crystal using the above techniques. It would seem
that the resistivity at room temperature is too high to be
measured with this arrangement. The resistivity at 200°C was
measured to be 10^9 ohm.cm. The results for reduced crystals
are shown in fig.6.h. These results were not all taken on the
same crystal. The first crystal was reduced for 3 min.,
measured, reduced for further 2 min., measured and reduced for
another 2 min. On measuring the resistivity at a reduction of
7 min., the crystal cracked, presumably as a result of continued
thermal cycling. A new crystal was reduced for 7 min. and
measured. Its resistivity was the same as that of the first
crystal to within the experimental error. The successive reductions
and measurements were made on this second crystal. The coincidence
of the result for the crystal which had been reduced for 3 min.,
2 min., 2 min. respectively with that for the crystal reduced
directly for 7 mins. indicates that the results are reproducible
and that successive reductions on the same crystal are additive
in effect.
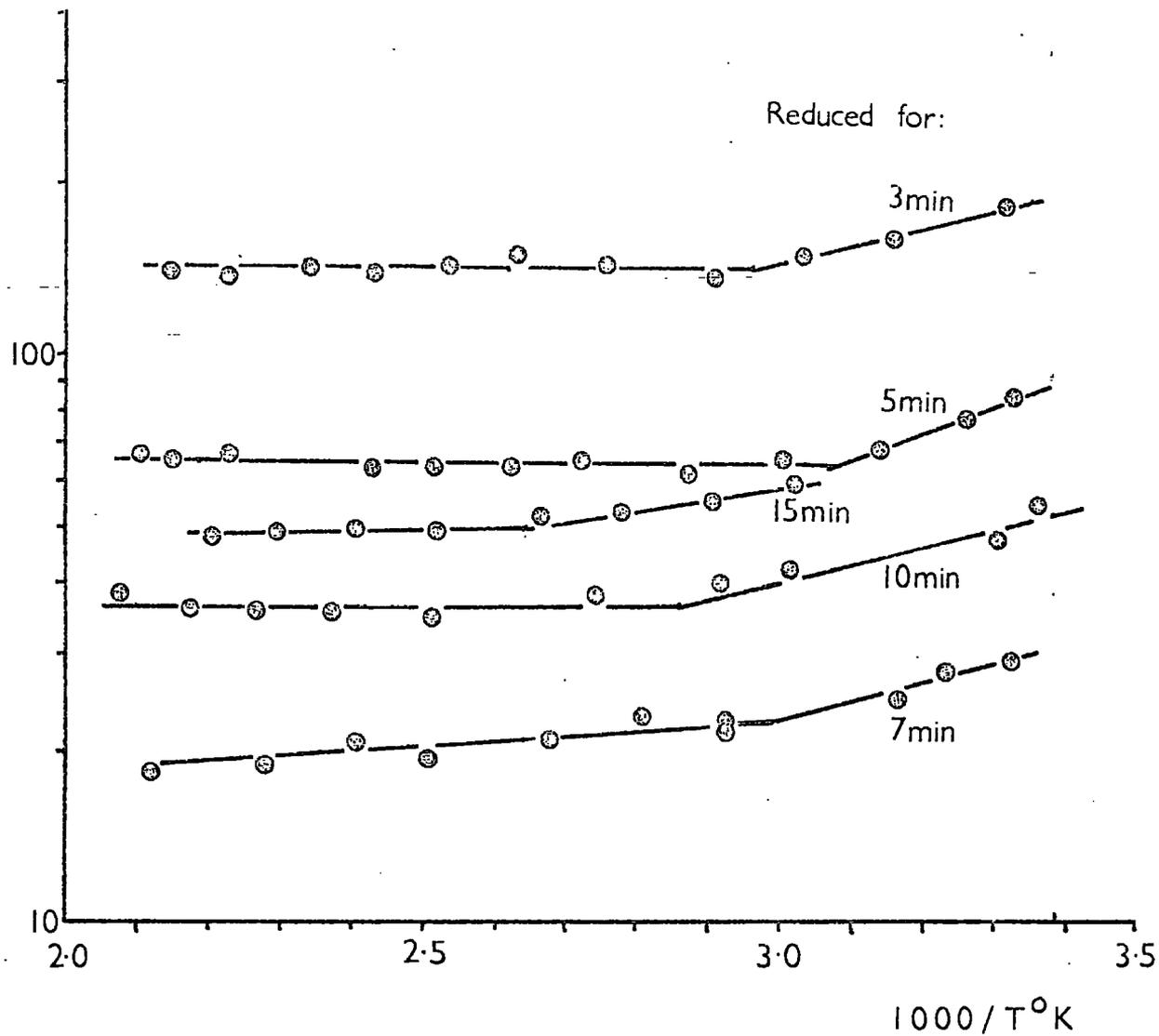
Fig. 6.h.   Resistivity of reduced crystals.

The main features of the results are that the resistivity behaves in the same way as the two-probe resistance on successive reduction. That is the resistivity decreases with reduction to a minimum value. Further reduction leads to an increasing resistivity to a steady value.

The form of each temperature curve shows a level section on decreasing the temperature from $200^{o}C$. At a particular temperature which varies from specimen to specimen, the resistivity begins to increase with an activation energy of about 0.1 eV although the exact slope also changes from one reduction level to another.

The activation energies of the five reduction levels in the cold region are shown in the following table together with the temperature at which the conductivity saturates.

Reduction Time	Activation Energy	Saturation Temperature
3 min	0.12 eV	$69^{o}C$
5 min	0.15 eV	$21^{o}C$
7 min	0.12 eV	$60^{o}C$
10 min	0.11 eV	$82^{o}C$
15 min	0.08 eV	$106^{o}C$

These results will not be discussed further here, since they will be dealt with in some detail in chapter 9.

At every reduction level, an attempt to measure the Hall
mobility was made. The apparatus was sufficiently sensitive
to measure any Hall mobility greater than 0.1 cm^2 V^{-1}sec^{-1}.
At every reduction level, however, it was found that the
fluctuations in the resistance R$_{bdac}$ were so great that the
small changes which were required to be measured were obscured.
The voltage across the voltage probes was in this case about
1 volt and the voltage changes which were expected were of the
order of 100 microvolts.* Even with a current stabiliser in the
current circuit, no reproducible signal voltage could be
detected. The signal voltages obtained were in fact of the
order of hundreds of microvolts but were highly unstable,
varying both in magnitude and sign as a function of time. It
is suspected that the contacts were responsible for the wild
behaviour at these small signal levels. Bergland and Baer in
their conventional geometry measurements used liquid gallium
electrodes.

* If the Hall mobility is similar to that obtained by
Berglund and Baer.

Chapter 7.

The Seebeck coefficient

1.General remarks.

On a normal semiconductor band model, the Seebeck
coefficient enables one to find the effective masses of the
carriers. If it is assumed that only one carrier species
(in this case, electrons) is responsible for the conduction
in the material, then the general expression for the Seebeck
coefficient is

$$S = k/e \left\{ E_F/kT - \frac{(5/2 + s) \, F_{(3/2 + s)}}{(3/2 + s) \, F_{(1/2 + s)}} \right\} \qquad 7.A.$$

where S is the Seebeck coefficient, E_F is the fermi energy
measured from the bottom of the conduction band, the functions
F are the fermi functions* and the scattering parameter s is
determined from the energy distribution of scattering relaxation
time as defined by the equation

$$\tau = \tau_o \, E^s \qquad\qquad 7.B.$$

When the semiconductor is completely non-degenerate, the
equation 7.A. reduces to

$$S = [(5/2 + s) - \log_e(N_o/n)] \, k/e \qquad 7.C.$$

Here, N_c is the density of states at the bottom of the conduction
band and is given by

$$N_o = 2(2\pi m_e^* \, kT/h^2)^{3/2} \qquad 7.D.$$

* A function of the electron energy distibution.
  For definition and tables see Semiconductor Statistics,
  J. Blakemore, (Pergamon, 1962).

In equation 7.C., n is related to N_c by the expression

$$n = N_c \, F_{\frac{1}{2}}(\eta) \, / \, T_{3/2} \qquad\qquad 7.E.$$

which becomes for non-degenerate case

$$n = N_o \, \exp(\eta) \qquad\qquad 7.F.$$

2.Experimental arrangement.

The measurements were carried out in the same specimen holder used for the resistivity and Hall measurements and shown in fig.6.g. The only adaptations necessary were the mounting of a small 1 watt kanthal wire heater at the bottom end of the support rods. The heater drew its power supply through these rods. The inclusion of a further thermocouple, still of copper and constantan, allowed the temperature of each end of the specimen to be measured. The copper branches of the two thermocouples were used to measure the potential difference set up along the specimen. In other respects, the specimen holder was the same as used for the earlier experiments.

In order conveniently to measure the small temperature differences involved in making Seebeck measurements, the switching device in fig.7.a. was used. This switch consisted of a 3 gang, single pole, 4 way switch wired in such a way that the output from the unit in position 1 was the voltage from thermocouple 1; in position 2 was the voltage from thermocouple 2;

TO VOLTMETER

3·GANG
I POLE
4 WAY
SWITCH

Cu
Con
Cu
Con

COLD
JUNCTIC
ENCLOSL

Cu Con Cu Con

SPECIMEN
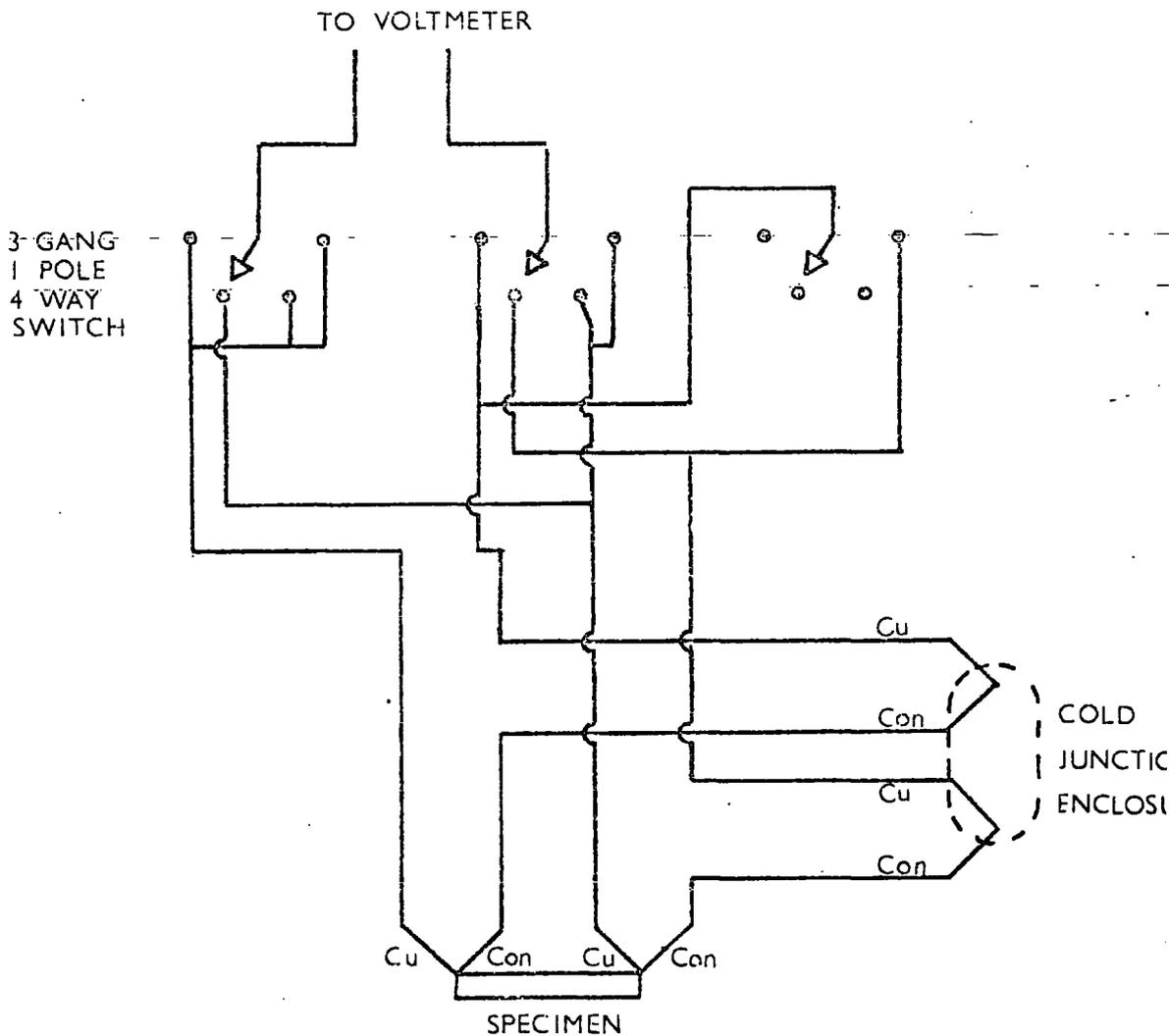
Fig. 7.a.   Switching device used in the Seebeck coefficient
measurements.

in position 3 was the Seebeck voltage and in position 4 was
the voltage derived from the two thermocouples by backing
one off against the other. The way in which this was done
is clearly seen in the diagram.

A preliminary measurement was made on an as grown crystal
using the electrometer amplifier circuit described in chapter 6.
It was found that the resistance of the crystal was somewhat
too high to be able to measure with any certainty. It was
possible, however, to make a very rough estimate of the Seebeck
coefficient which was about 10 mV/deg K.

Since all the crystals which were finally measured had
resistances of a few kilohms, they were measured using not the
electrometer amplifier but a Phillips type GM 6020 microvoltmeter.
This was sufficiently sensitive to measure all the voltages
concerned, even the voltage derived from the backed off
thermocouples, to an accuracy of 5%. Since the calibration of
the thermocouples and of the differential thermocouple were
known accurately, the Seebeck coefficients should carry an error
of 10%.

Tests were performed to determine whether the thermoelectric
voltages were linear with temperature difference in the case of
each crystal measured. In each case, it was found that, initially,
the thermoelectric voltage was wildly non-linear with temperature
difference and even non-reproducible. In all cases, however, it
was found that the use of the sparking technique described in

chapter 3, section 6, applied through the copper leads to the thermosetting silver contacts was sufficient to correct these faults. A typical curve of thermoelectric voltage against temperature difference is shown in fig 7.b. The intercept on the temperature axis is a systematic error introduced by the zero on the microvoltmeter. The slope of the line gives the Seebeck coefficient.

3. Results.

The results of the experiments are shown in fig.7.c. The crystals used had been reduced for 3 m, 7 m, 15 m respectively. The experimental points have been drawn without any attempt at drawing a line through them, since the scatter involved is so great that it is difficult to determine where such a line should be drawn. It should be pointed out, however, that the experimental error quoted in the last section covers this scatter.

Seebeck Voltage
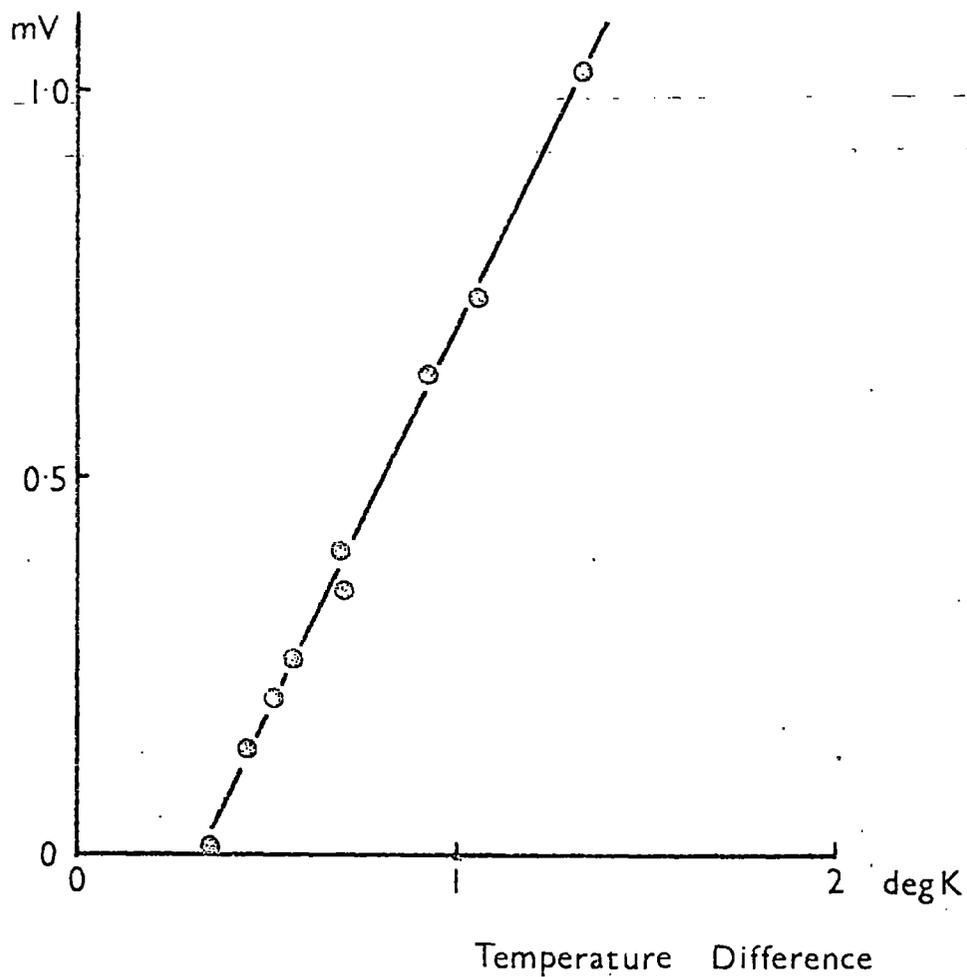
Fig. 7.b.   Thermoelectric voltage against temperature difference.

Fig. 7.c.   Seebeck coefficient of reduced crystals.
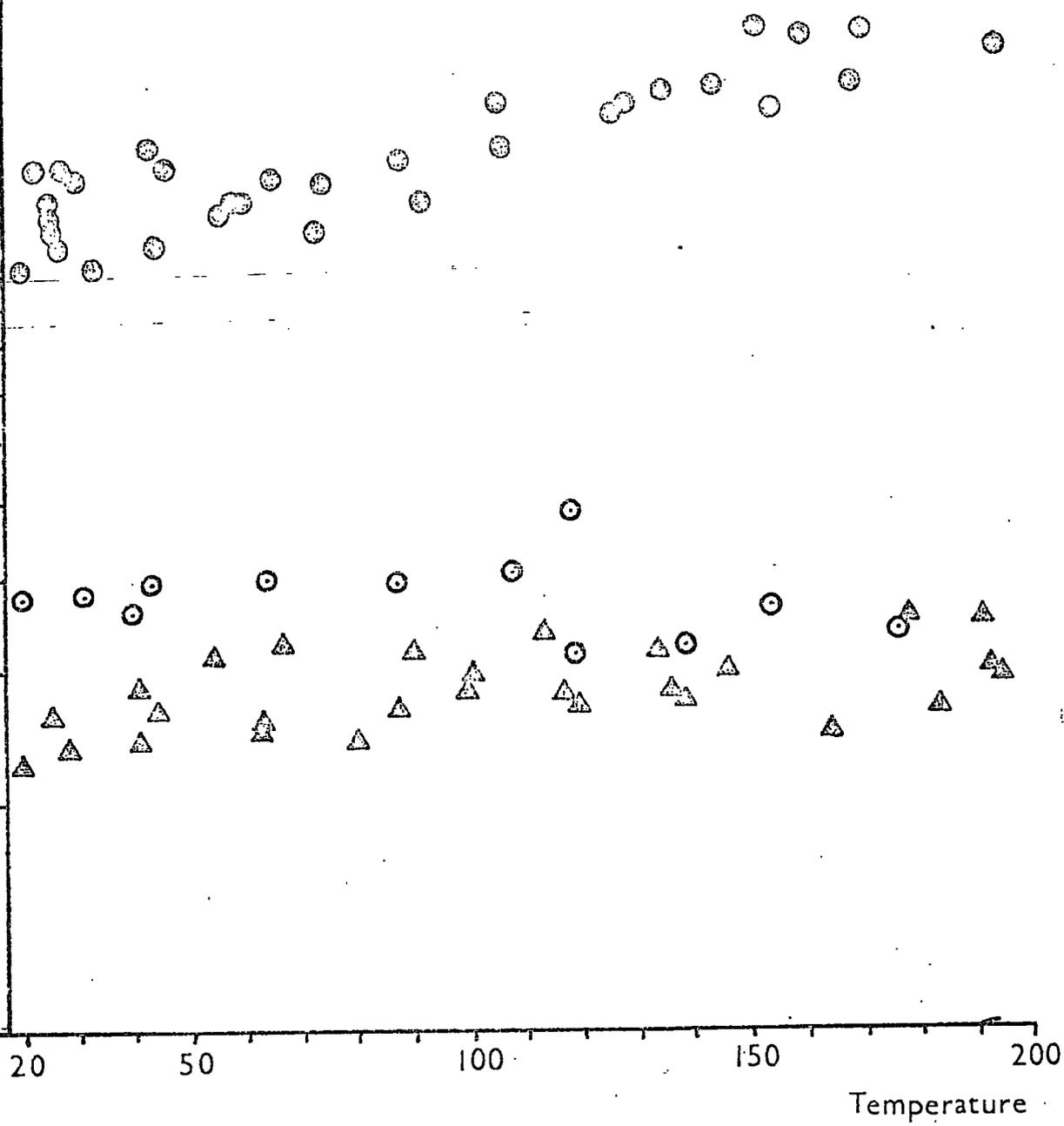
Chapter 8

Two-probe measurements

1.General.

The experiments of Ueda and Ikegami previously mentioned
in chapter 2, section 8 showed how a PTCR effect could be
observed in single crystals if a two-probe measuring technique
is used but is eliminated in the four-probe geometry.

Two-probe geometries were used in the present work in two
instances. Firstly to determine whether the PTCR effect was
detectable in the crystals heat treated in hydrogen and secondly
it was considered a more convenient method of measuring the
resistance of crystal slices at elevated temperatures during the
heat treatment processes.

2.Resistance measurements during heat treatments.

The changes in resistivity and optical absorption have
shown that the initial processes involved in the heat treatments
of the single crystals are rapid. The resistivity minimum occurs
after about five minutes heat treatment in hydrogen. If four
probe resistivity measurements were to be made during this process,
the necessary voltage measurements would take too long. The
resistivity would change appreciably during a particular
measurement. Resistance measurements made during heat treatments
were therefore made on samples set up for two-probe measurements

as described in chapter 3. The specimens were mounted with
platinum paste contacts in one of the configurations shown
in fig.3.e. and heat treated in the furnace shown in fig.3.d.
Resistance measurements were made with a Mk 8 Avometer.

Measurements of this kind were made on specimens during
heat treatments in hydrogen, oxygen and argon atmospheres.
The results are shown in figs.8.a. and 8.b. In fig.8.a., the
left-hand vertical axis and bottom horizontal axis refer to
the hydrogen treated crystal while the right-hand vertical
axis and top horizontal axis refer to the oxygen treated crystal.
Differences in sample shape and thickness lead to the different
resistance scales. All these results correspond to crystals
grown by the author. The hydrogen treated crystal shows the
initial decrease in resistance during the first five minutes
followed by an increasing resistance up to twenty minutes as
in the four probe measurements made at lower temperatures (fig.8.c.).
This is a good indication that the electronic properties of the
hydrogen process can be frozen into the crystals by fast cooling.

The heat treatment in the inert argon atmosphere is of
particular interest. Here the resistance increases from the
beginning of the heat treatment until it reaches a steady value
after thirty minutes or so. The time scale of this process is
about the same as the second stage of the hydrogen heat treatment
which also entails an increased resistance. In chapter 9, it
will be shown how this correlates with the results of Arend et
al. described in chapter 2, section 6.
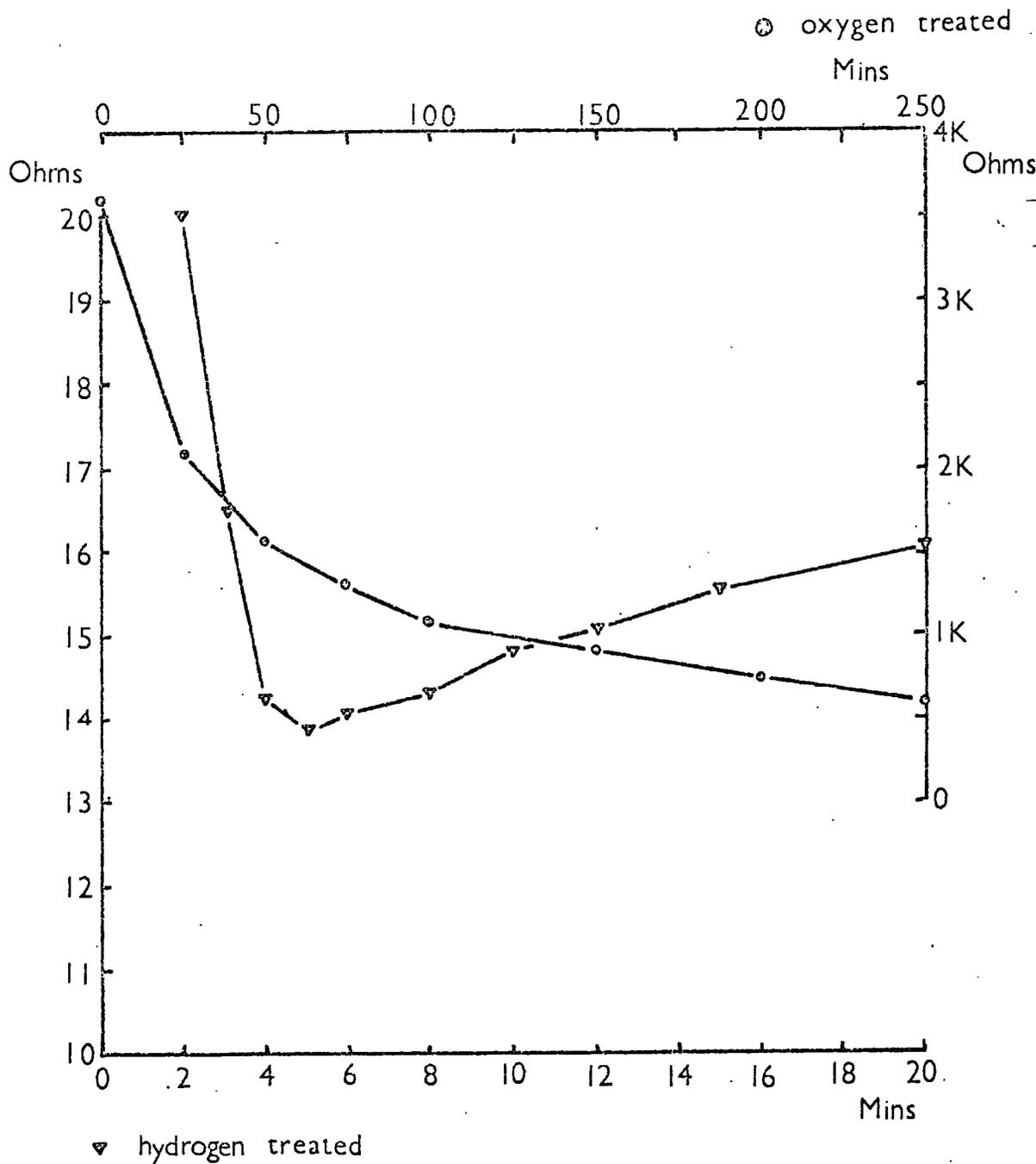
Fig. 8.a. Resistances of crystals during heat treatment in
hydrogen and oxygen.
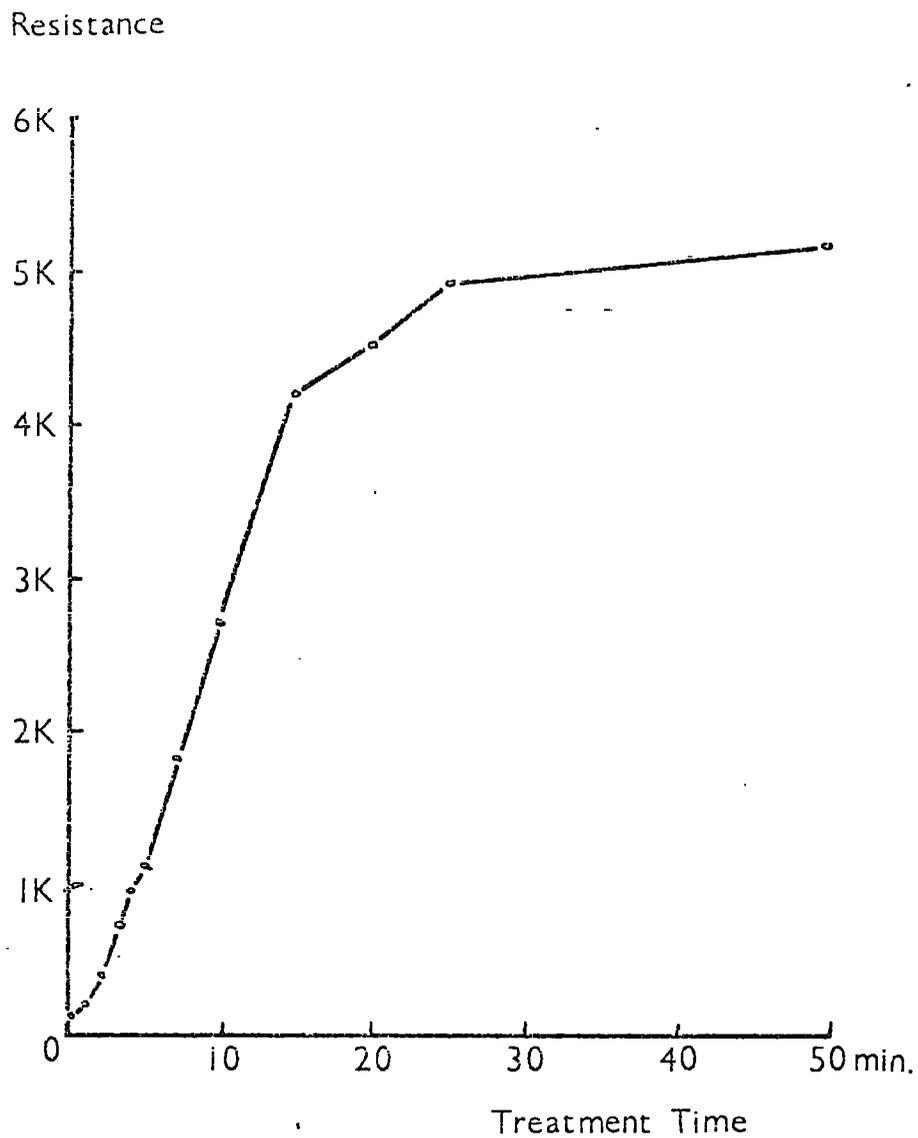
Fig. 8.b.   Resistance of crystal during heat treatment in argon.
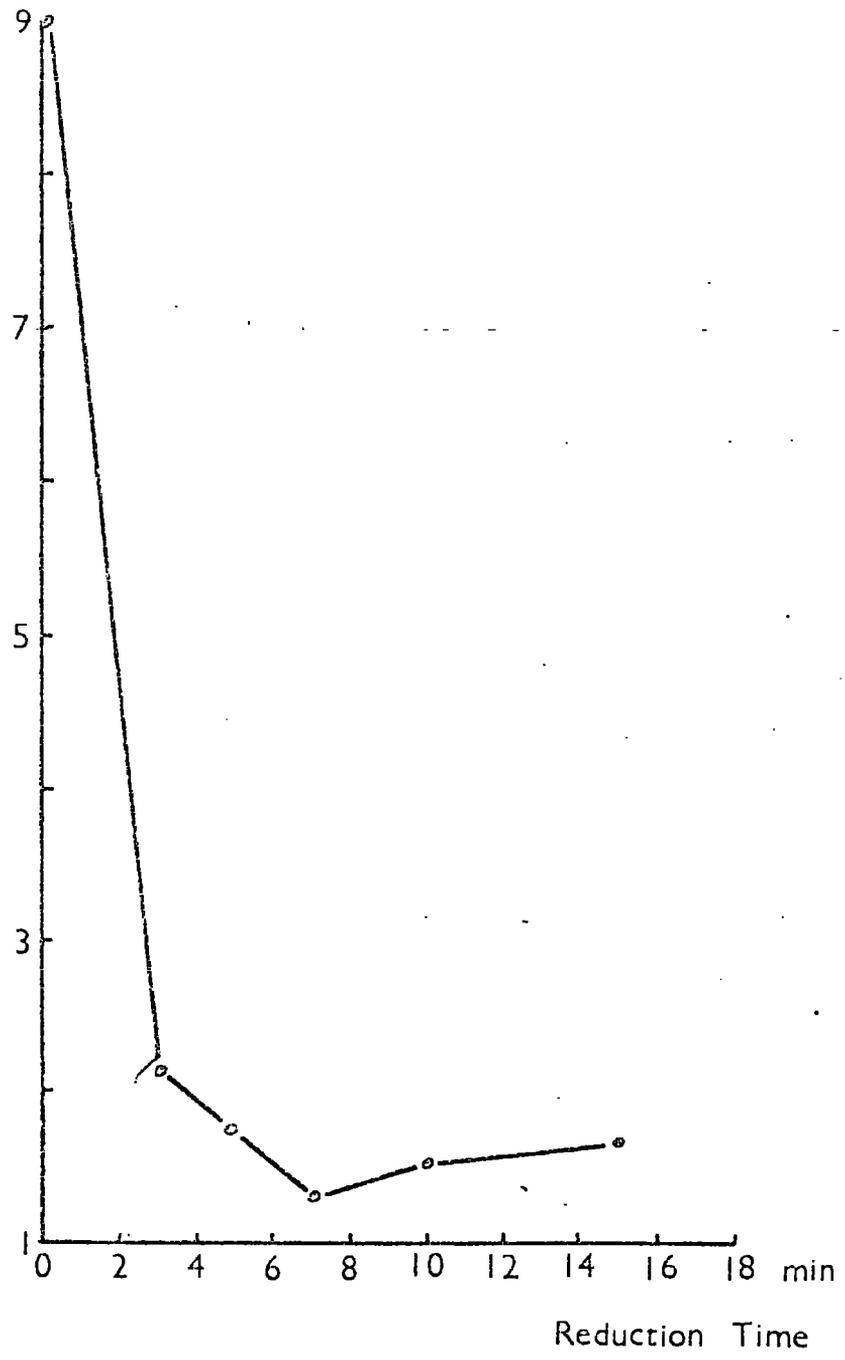
Fig. 8.c.   Resistivity at room temperature of crystal heat
treated in hydrogen at 800°C.

3.Resistive effect.

a. PTCR.

Two probe specimens were again set up in the same way
as was described in chapter 3, section 5 in order to measure
their resistance as a function of temperature up to 200°C.
In order to verify the Heywang type of space charge model,
specimens of varying reduction states were used. In general,
the results showed a similar peak to those found by Heywang
(fig.2.j.) in ceramics except that the effect was not as
strong. This is what one would expect for a sample which has
only one space charge surface, as is the case with a single
crystal.

b. Oxidation of unreduced crystal.

In the case of an unreduced crystal however, it was found
that at high temperatures, above about 600°C, and in an air
atmosphere the resistance varied with time as shown in fig.8.d.
At various intermediate stages, the crystal was allowed to cool
in order to find whether there was any change in activation
energy. The results of such measurements, made with an Avometer
Mk 8, are shown in fig.8.d. The activation energy defined by
the equation

$$\rho_T/\rho_0 = \exp(E_a/kT) \qquad\qquad 8.A.$$

which is initially 0.76 eV, is found to decrease slightly to
0.51 eV on oxidation. There is, however, a further interesting
feature. A shoulder appears on the curve at about 450°C. This
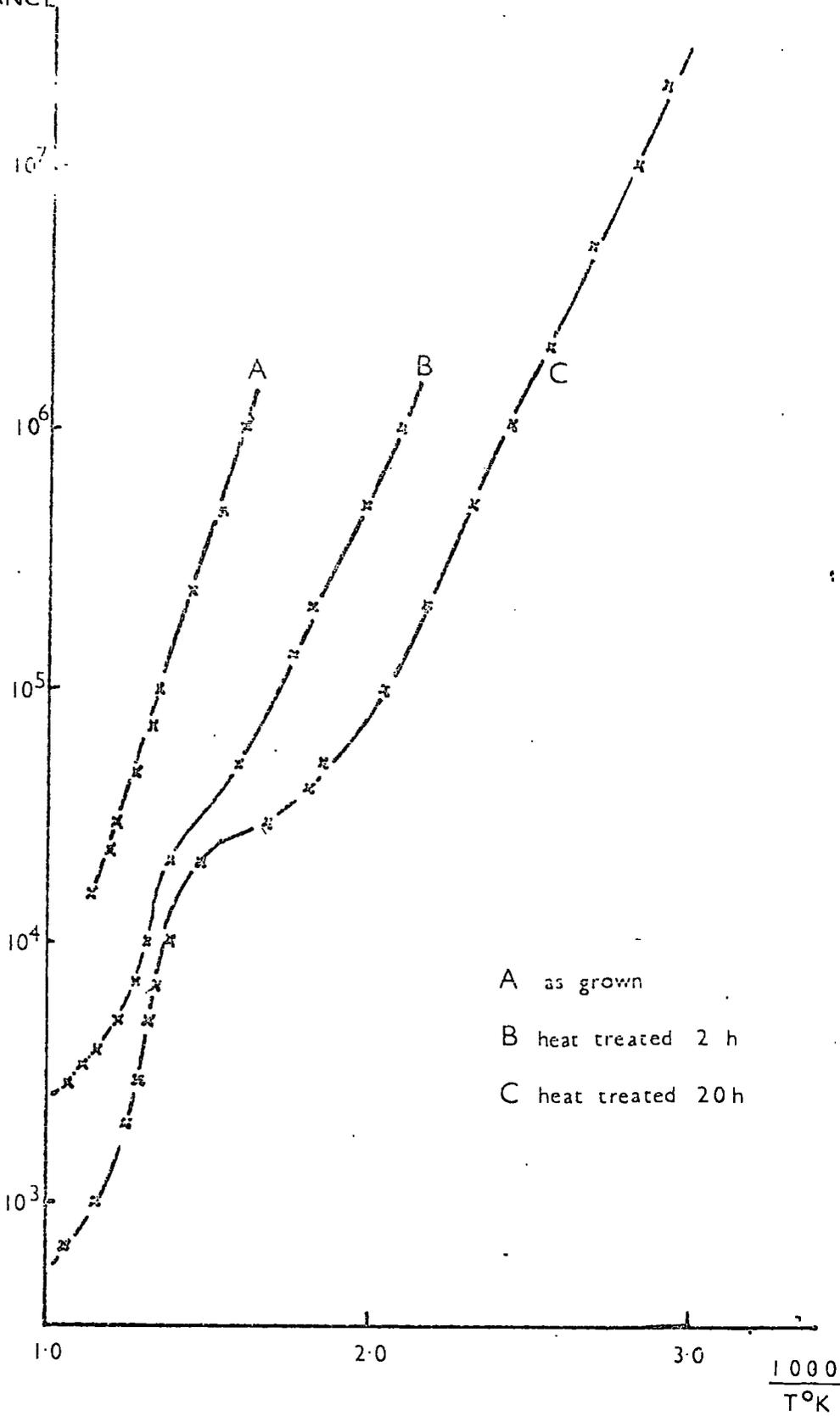
Fig. 8.d.   Resistance of crystal heat treated in air at 800°C.

shoulder increases in size as the heat treatment progresses.
The possibility of a.c. effects from the surrounding furnace
was eliminated by checking with an oscilloscope that there
was no pick-up in the crystals. A transistor curve display
apparatus was also used to check that non-linear effects were
not responsible for this peak. The specimens were found to
have linear v-i-curves up to temperatures of 550°C. In order
to obtain more information about this peak, the a.c. measurements
described in the next section were performed.

4.Capacitative effect.

The fully oxidised specimen whose d.c. temperature variation
of resistance is shown in the lower curve of fig.8.d. was
remeasured using a Wayne Kerr Component Bridge as the resistance
measuring apparatus. The capacitance was measured simultaneously,
to determine whether there was an associated capacitative effect.
The results of the resistance measurements are shown in fig.8.e.
Here, the solid line indicates the measurements made at 50 Hz
and the broken line is the d.c. curve (curve C of 8.d.). Fig.8.f.
shows the capacitance of the specimen measured simultaneously
with the a.c. resistance measurements. It can be seen that the
peak at the Curie point is present. In addition, however, there
is another peak at higher temperatures. This is higher than the
Curie point peak and coincides approximately with the resistance
anomaly. The absolute values of the dielectric constant in this
region are difficult to ascertain since the crystal thickness
was not measured and the effective contact area on the sample
is difficult to assess. If one estimates the dielectric constant
from the geometry of the crystal, one obtains rather low values,

LOG$_{10}$ RESISTANCE in ohm ·

50 Hz

d.c.

10^3/T °K
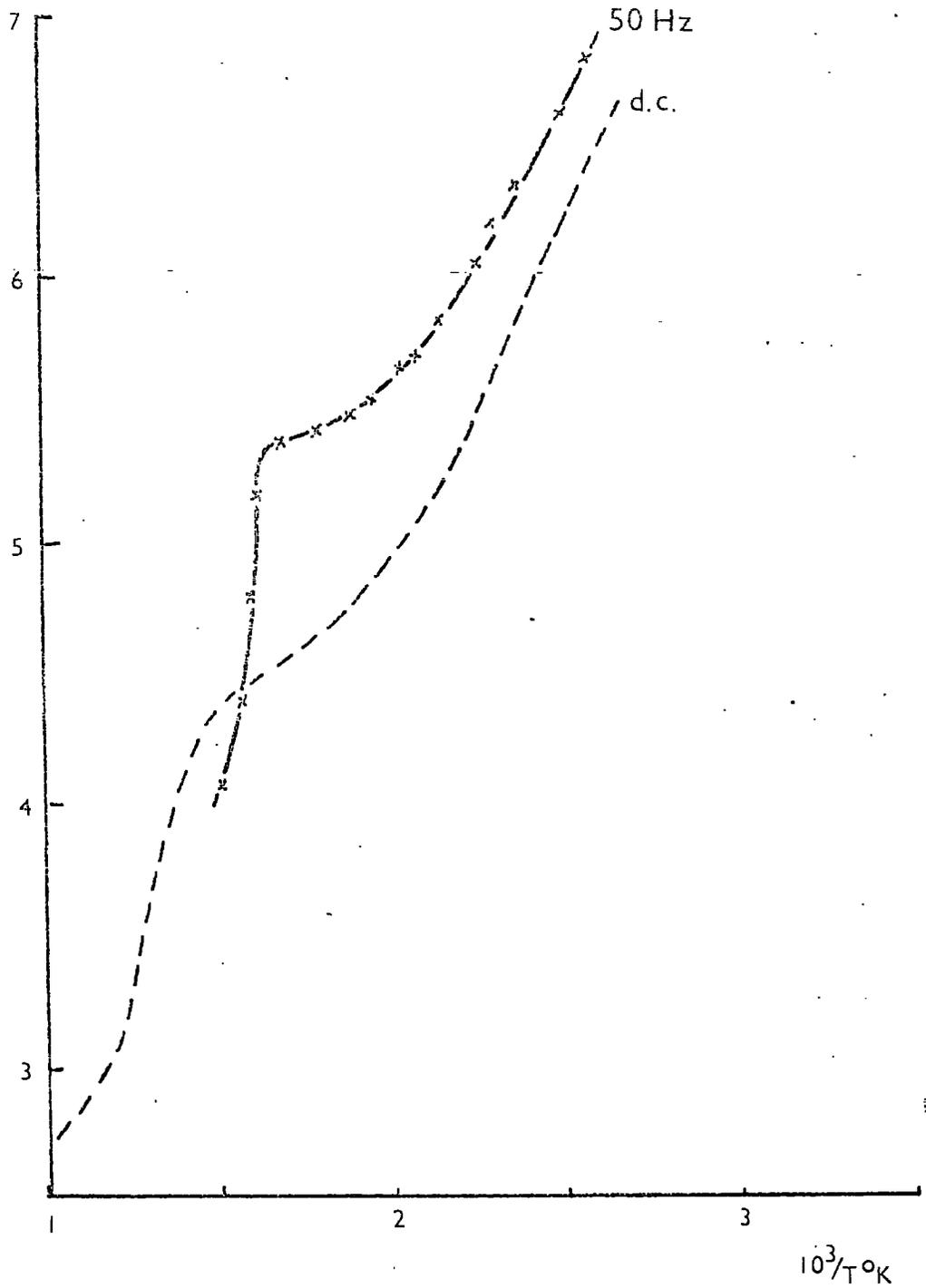
Fig. 8.e.   A.C. resistance of specimen heat treated in air.
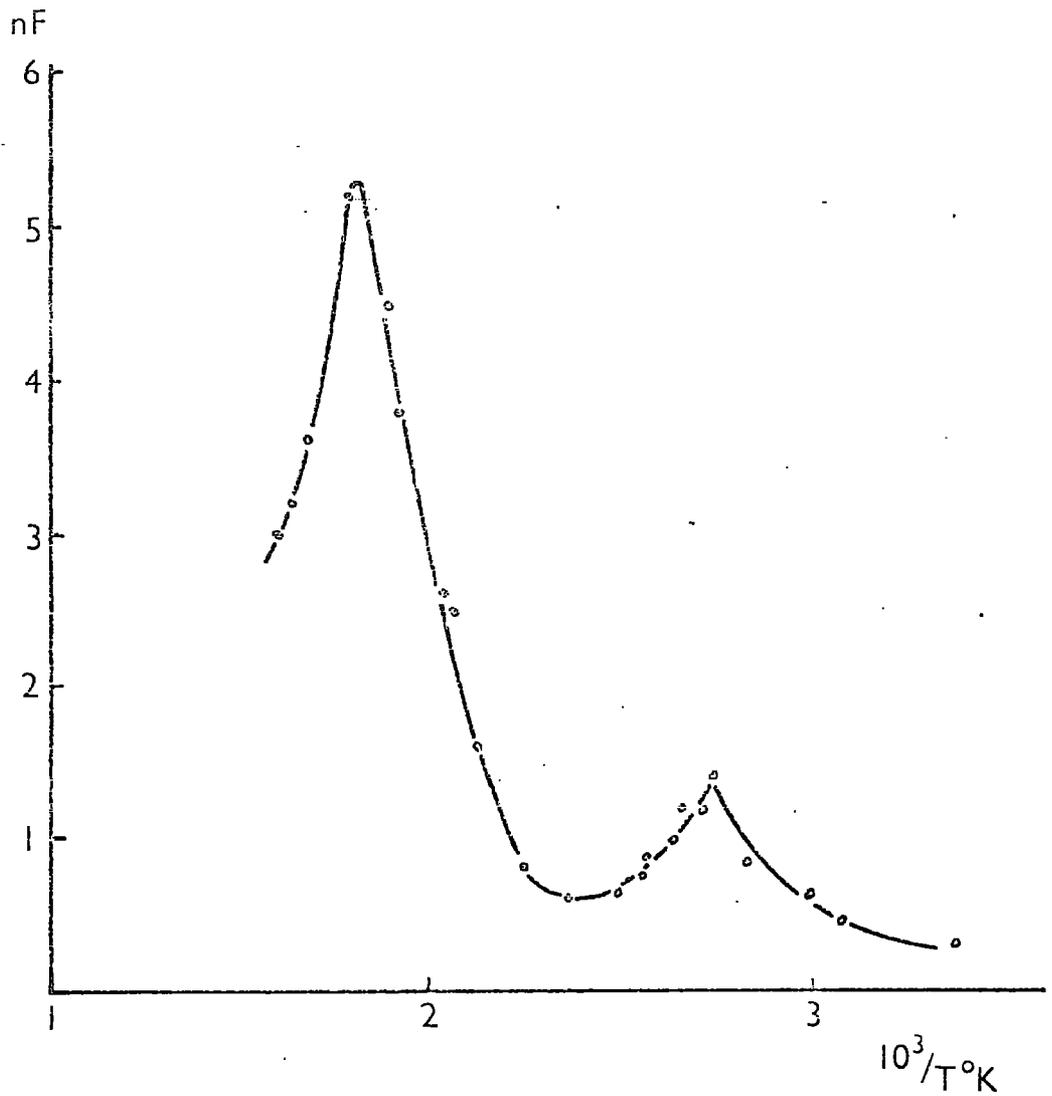
Fig. 8.f.   Capacitance of specimen heat treated in air.

being only about 140 at the Curie point peak and 560 at the high temperature peak. These are low compared with previously measured values in pure crystals but it is possible that the effective contact area on the crystal is less than the physical size of the contact.

The peak in dielectric constant combined with a peak in the resistivity, of course, lead to a dip in the loss tangent of the specimen. It is perhaps instructive to plot the loss tangent as a function of temperature. This is shown in fig.8.g. The dips due to the Curie point effect and to the high temperature effect are clearly seen.

LOG$_{10}$ $1/\omega CR$

Curie
point

TEMPERATURE
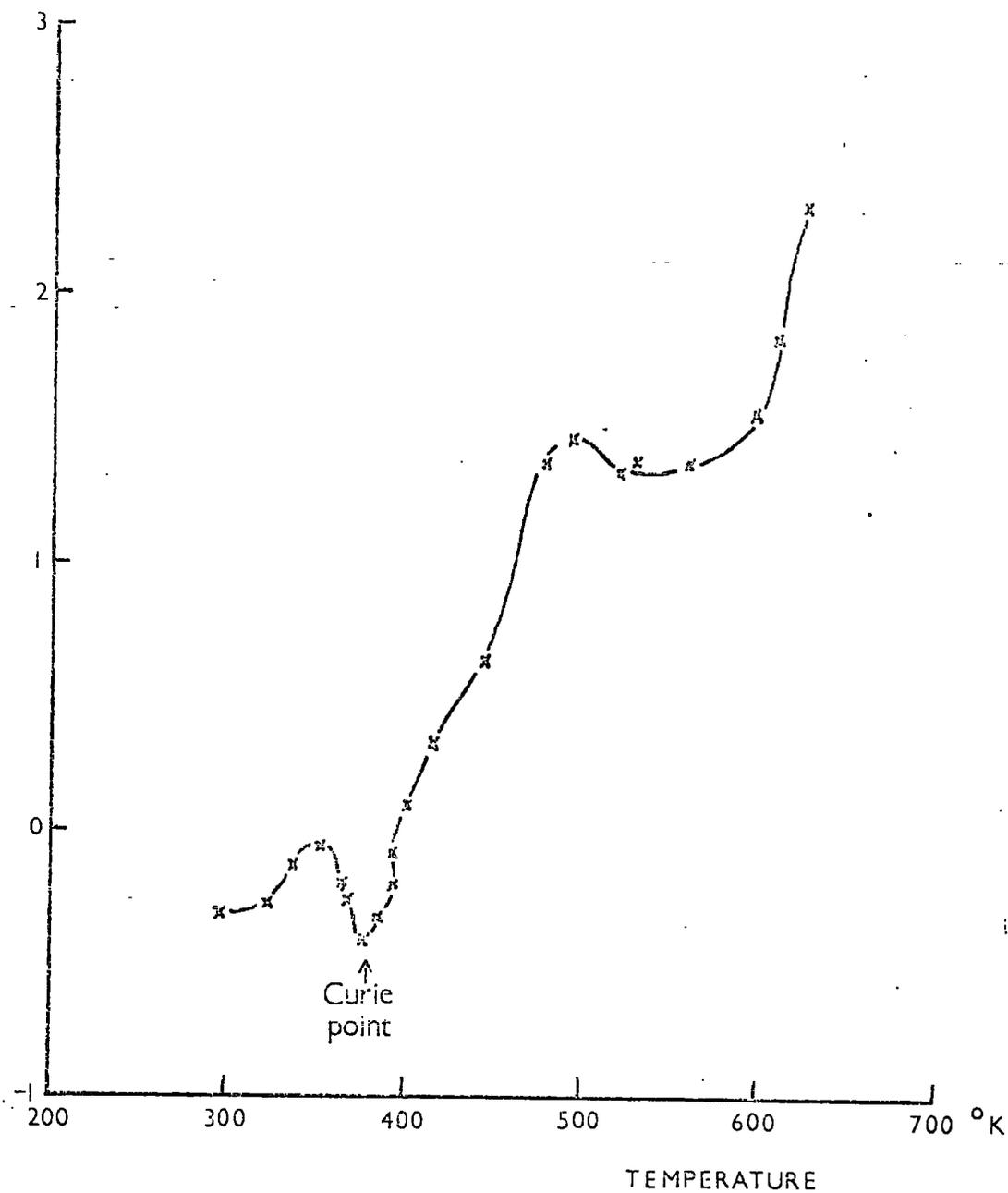
Fig. 8.g.   Dielectric loss tangent of specimen heat treated in air.

Chapter 9

Discussion, conclusion and suggestions

1.General discussion.

It is, generally, difficult to make any definite statement
about the conduction parameters in a conventional semiconductor
until the three basic measurements, resistivity, Hall coefficient
and Seebeck coefficient are made. In the present case, the
Hall coefficient proved elusive but it is possible to obtain
some information using the effective mass obtained by Berglund
and Baer (2.21.). Using this effective mass in the Seebeck
coefficient expression (equation 7A) and making suitable
guesses about the carrier scattering mechanism, the number of
carriers could be determined. The mobility could then be
obtained from the resistivity. It will be seen that this
analysis leads to two interesting features of the present
results. Firstly, the values of mobility which were obtained
were about two orders of magnitude less than the Hall mobilities
obtained by Berglund and Baer and, secondly, the mobility was
found to increase with increasing temperature in an exponential
way.

These two features indicated that a small polaron mechanism
was more likely to provide a successful explanation of the
results. In view of this it will now be of use to consider
polaron theory in general terms; how the polaron comes about;
what the particular features of small polaron theory are; how
the results of this theory differ from a classical Bloch-type
semiconductor.

2.The small polaron.

When a free electron exists in an ionic lattice, the ions in that lattice are disturbed. Coulomb forces draw positive ions towards the electron and repel negative ions from it. The crystal is, in fact, polarized. In this way, there is a region of the solid in the vicinity of the electron in which the phonon spectrum of the lattice is noticeably perturbed. If the electron moves through the crystal, the region of polarization moves with it, contributing an extra term to the inertia of the electron. The electron together with its polarization field, that is, with the phonon disturbance which it creates is called a polaron. In covalent semiconductors, or in those in which the ionicity is not high, the disturbance caused by the electron as it moves in the crystal lattice is negligible, but in strongly ionic crystals like barium titanate, the effect could be strong. Indeed, if the coupling between electron and phonons is sufficiently large, then the inertia of the polaron can become sufficiently high that the electron becomes localised. The electron is trapped by the polarization field which surrounds it. For this to happen, the spatial extent of the polaron is small (of the order of one lattice constant or less). If an electron is to be trapped in such a way, then it is clearly energetically more favourable for it to be trapped in the neighbourhood of a positive ion site (or, for a hole, at a negative ion site). The trapped electron can still move through the lattice if the polarization field is temporarily broken down by thermal fluctuations. Under these conditions,

however, the electron will be trapped again at the next
positive ion site. The motion of a small polaron in the
"hopping" mode then consists of a series of jumps from one
positive ion site to the next.

Since it was found that the present results are best
fitted by a small polaron hopping model, the rest of this
discussion will be confined to this part of polaron theory.
The author has found that an article by Klinger (9.1.)
provides a readable account of small polaron hopping transport.
This article sets out all the relevant results of the theory.

It is clear that the jumps from one site to the next are
thermal in origin. This leads to a thermally activated mobility.
The activation energy, ξ, is the energy required by the electron
to jump from one site to the next or, more exactly, the energy
required to break down the polarization barrier. This energy
is expected to be of the order of 10^{-1} to 10^{-2} eV. Klinger
gives the full temperature dependence of the mobility as

$$\mu \propto T^{-3/2} \exp(-\xi/kT) \qquad \qquad 9.A,$$

The three-halves dependence on temperature dominates at high
temperatures giving a maximum in the mobility at a temperature
$T_m = 2\xi/3k$. The magnitude of the mobility is always expected
to be low ($\gtrsim 1$ cm^2/Vs) due to the difficulty of exciting an
electron from one site to the next. More importantly, there is
no simple relationship between the drift mobility, μ_{xx}, and the

Hall mobility, μ_H , as is the case in conventional band theory (equation 6B). Small polaron theory shows that in the hopping regime, the Hall mobility is much greater than the drift mobility and that their ratio is not constant.

The activated mobility leads to a characteristic peak in carrier mobility (and hence in the real part of the a.c. conductivity) at a frequency $\omega_m = 4\xi/h$. This leads to an optical absorption peak (usually in the infra-red).

The Seebeck coefficient is simplified in small polaron theory from that in conventional semiconductor theory. The conventional Seebeck coefficient measures the position of the Fermi level through the term E_F/kT in equation 7A. The term

$$(5/2 + s)F_{(3/2 + s)} \, / \, (3/2 + s) \, F_{(1/2 + s)}$$

comes from considerations of the dynamic properties of the conduction electrons. In the small polaron hopping case, however, the electrons move with such difficulty that the dynamic term disappears and the final expression for the small polaron hopping Seebeck coefficient is

$$\alpha = k/e \, \log_e N/N_o \qquad\qquad 9.B.$$

where N is the concentration of polarons. In standard semiconductor theory, N_c is the density of states available to the electrons in the conduction band. This is temperature dependent and leads

to the temperature dependence of the Seebeck coefficient
even when the number of carriers is saturated. In small
polaron hopping theory, however, the density of states is
given by the total concentration of positive ion sites (see
Jonker and van Houten 9.2.) since it is possible for the
electron to be trapped at any such site. N_c is essentially
independent of temperature in small polaron hopping theory
so that the Seebeck coefficient is also independent of
temperature except in the intrinsic regime where N varies
with temperature.

3. The present results in conventional band theory.

As was outlined in section 1 of this chapter, an attempt
was made to explain the present results on the basis of
conventional band theory. Using the effective mass quoted
by Berglund and Baer, and the Seebeck coefficient results
described in chapter 7, an estimate of the number of carriers
was made. The resistivity results then gave the mobility.

Berglund and Baer (2.21.) performed resistivity, Hall
coefficient and Seebeck coefficient measurements on hydrogen
reduced crystals grown from the melt. From the Hall coefficient
measurements, they obtained the concentration and sign of the
majority carriers. They then calculated the Hall mobility from
the resistivity. Their Seebeck coefficient results, coupled
with the electron concentrations already obtained enabled them
to estimate the effective mass, m^*, (which is contained in the

expression for N_c which follows equation 7B). In order to make the estimate of effective mass, it is necessary to know the type of scattering mechanism operating (so that the term

$$(5/2 + s) \; F_{(3/2 + s)} \; / \; (3/2 + s) \; F_{(1/2 + s)}$$

of equation 7.A. can be determined). This is usually obtained from the temperature dependence of the mobility which is expected to be a simple power law. In the case of Berglund and Baer's results, however, this was not possible. Their results show an anisotropy in the mobility. The results for current parallel to the c axis shows mobility increasing with temperature and for current perpendicular to the c axis shows mobility decreasing with increasing temperature (fig.2.k.). Neither of these dependences is a simple power law. Berglund and Baer, nevertheless, assume that some mixture of optical mode and acoustic mode lattice vibrations dominated the scattering and quote the extreme values of $m^* = 4.5m_o$ and $m^* = 8.5m_o$ for the cases where scattering is entirely due to optical mode ($s=\frac{1}{2}$) and acoustic mode ($s=-\frac{1}{2}$) vibrations respectively.

The author considers that in a largely ionic material such as barium titanate, optical mode scattering should dominate and hence the value of $m^* = 4.5m_o$ was assumed in the following analysis. The Seebeck coefficient results of fig.7.c. show a manifestly high degree of scatter, such that the temperature dependence for each reduction time is difficult to determine.

The values obtained after 3 minutes reduction are so high that they could not be incorporated into any scheme involving realistic values for mobility, effective mass or scattering parameter. This will be discussed further later.

————The results for 7 and 15 minutes heat treatments, however, lead to reasonable fits if the electron concentrations were assumed constant throughout the temperature range measured, if the scattering parameter is taken to be $s=\frac{1}{2}$ as for optical mode scattering and if the effective mass is taken to be $4.5m_o$. The values of electron concentrations for which these fits were obtained were $7.5 \times 10^{19} cm^{-3}$ at 7 minutes heat treatment and $3.0 \times 10^{19} cm^{-3}$ at 15 minutes heat treatment. Fig.9.a. shows the Seebeck coefficient results for 7 and 15 minutes heat treatment replotted from fig.7.c. with the curves calculated from these concentrations shown as solid lines.

If these electron concentrations are used with the resistivity results of fig.6.h., the mobilities can be calculated. Fig.9.b. shows the mobilities obtained for both 7 and 15 minute heat treatments plotted against temperature. They show good agreement with each other, but, as mentioned in section 1 of this chapter, they show two very interesting points. Firstly, the mobilities (which are, of course, drift mobilities) are about 100 times smaller than the Hall mobilities given by Berglund and Baer. Secondly, the mobility increases with temperature.

There is another situation in semiconductor physics where the mobility increases with increasing temperature. This
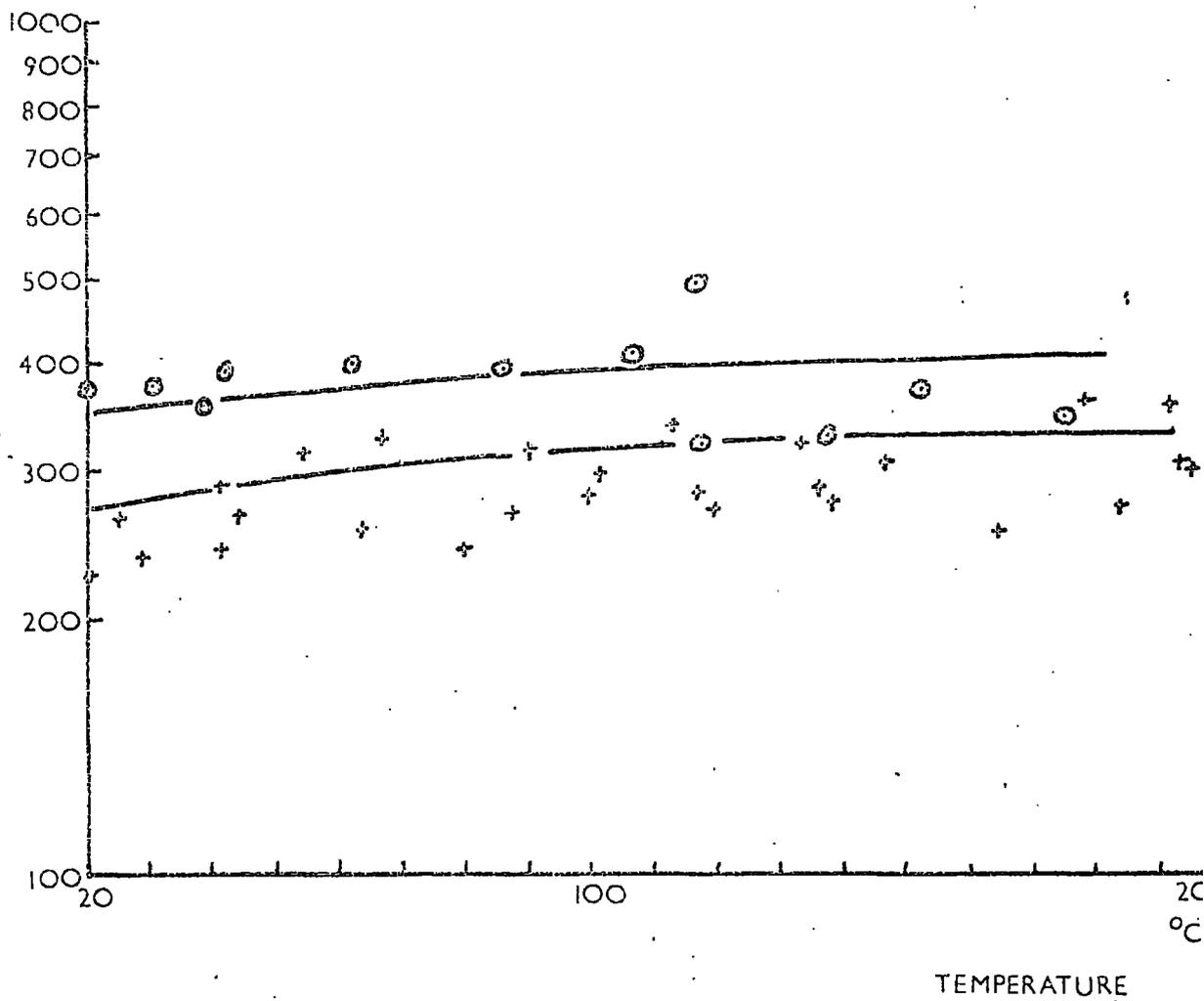
Fig. 9.a.   Seebeck measurements with calculated lines.

MOBILITY

cm^2/Vs

5 $\times 10^{-3}$

4

3

2

○ 7 min   n = 7·5 × 10^{19}

+ 15 min   n = 3   × 10^{19}

1

O   100   200   °C

TEMPERATURE
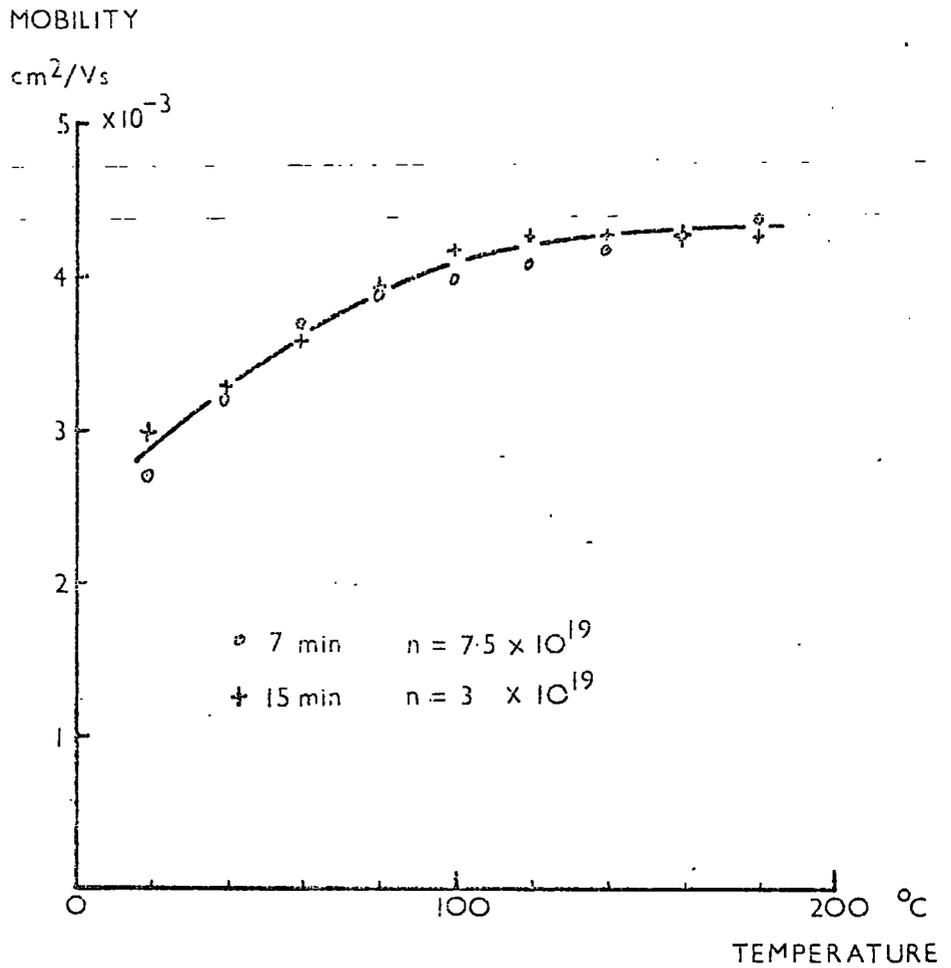
Fig. 9.b.   Mobility of reduced crystals.

is the case of impurity mode scattering, when the mobility is proportional to $T^{3/2}$. To verify that this mode was not operating in the present case, log μ was plotted against log T. This plot was not a straight line and the curve obtained had a slope less than 3/2 throughout its length. Impurity scattering was therefore discounted.

It should be pointed out that an attempt was made to explain the temperature dependence of the resistivity results reported in chapter 6 on the basis of a changing electron concentration and a constant mobility. This would lead, however, to Seebeck coefficients incompatible with the results of fig.7.c.

If the results of the three minute heat treatment Seebeck measurements are considered anomalous (a hypothesis which will be supported later), then it might be reasonable to assume from the mobilities shown in fig.9.b. that the mobility is not affected by the heat treatment. This would be supported to some extent by the fact that the resistivity curves of fig.6.h. show similar temperature dependences at all reduction levels. If this is so, we can use the mobility curves of fig.9.b. as a single curve and apply it to each of the reduction levels for which resistivity results are shown in fig.6.h. This will then show the effect of heat treatment in hydrogen upon the electron concentration. Having done this, the following electron concentrations were obtained:-

Heat treatment time at 800°C in hydrogen. (minutes)	Extrapolated electron concentration (cm^{-3})
3	1.0×10^{19}
5	2.3×10^{19}
7	7.5×10^{19}
10	4.1×10^{19}
15	3.0×10^{19}

These electron concentrations are plotted in fig.9.c. It can be seen that the initial rise followed by a subsequent drop in electron concentration agrees tolerably well with the results of Arend and Coufova described in chapter 2, section 6. The author's publication (9.3.) is based on these calculations.

The results of fig.9.b. are replotted in fig.9.d. in logarithmic form. It is seen that the results follow a

$$\mu \propto \exp\left(-\xi/kT\right)$$

dependence in two regimes which correspond approximately to the ferroelectric and paraelectric phases. This, coupled with the discrepancy between the Berglund and Baer Hall mobility and the author's drift mobility indicates strongly that a small polaron hopping model might explain the current results more adequately.

4. The present results in small polaron theory.

Analysis of Seebeck coefficient measurements in the small polaron hopping case is considerably simplified compared with
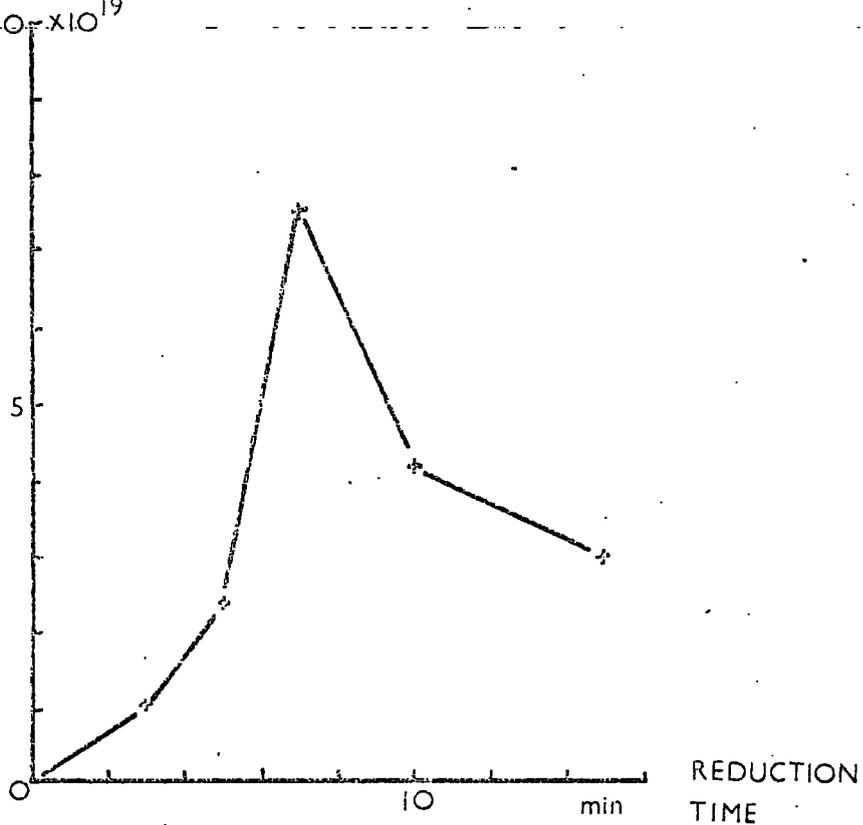
Fig. 9.c.   Electron concentration in reduced barium titanate.
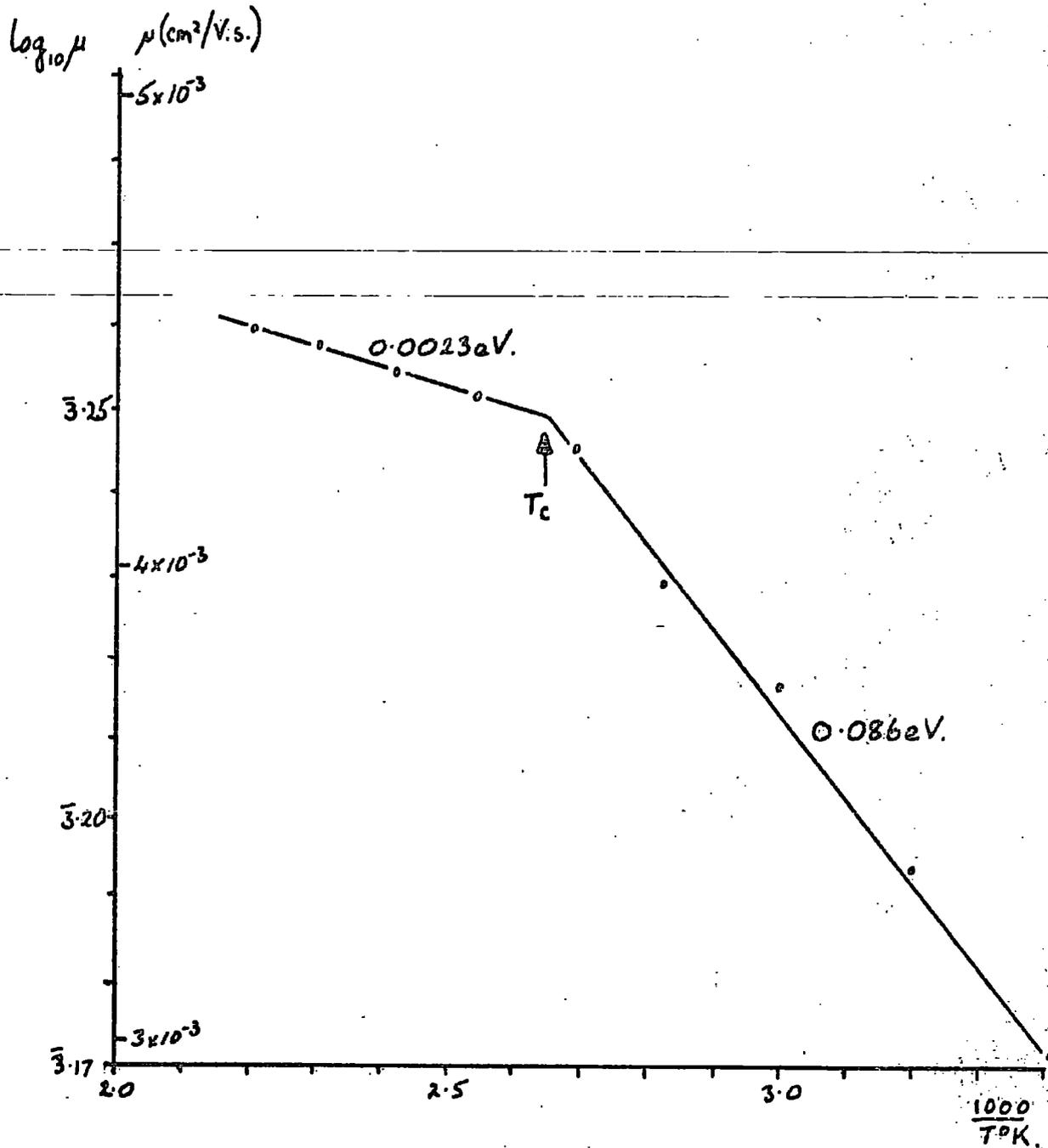
Fig.9.d. Logarithm of mobility calculated according to conventional
band model as a function of reciprocal temperature.

the analysis of the last section. Firstly, the dynamic term
has disappeared from the Seebeck coefficient expression, which
is now temperature independent and, secondly, the value of N_c
is known since it is given by the concentration of titanium
ions in the lattice. All that is necessary in the present case
is to find reasonable values of Seebeck coefficient which are
compatible with the results over the whole temperature range.
The value of N_c was taken to be 1.56 x 10^{22} cm^{-3} which is the
theoretical concentration of titanium ions in the stoichiometric
material. It was found that for Seebeck coefficients of
300 μ V. $^{\circ}$C^{-1} at 7 minutes heat treatment and 380μ V. $^{\circ}$C^{-1} at
15 minutes heat treatment, the polaron carrier concentrations
calculated from equation 9.B. are 4.76 x 10^{20} cm^{-3} and
2.18 x 10^{20} cm^{-3} respectively.

When these values of carrier concentration are used to
calculate the drift mobility from the resistivity, the curves
for the two heat treatment levels are the same to within the
experimental error. These are shown in fig.9.e. It can be seen
that the abrupt change in activation energy which appeared in
fig.9.d. is no longer apparent. The slope now changes continuously
throughout the temperature range shown. This departure from the
logarithmic dependence of μ_{xx} on 1/T is not difficult to explain
on the small polaron hopping model. It was seen in section 2
of this chapter, that the full expression for μ_{xx} involves a
term in $T^{-3/2}$ which will become important at temperatures of
the order of $2\xi/3k$. The slope of the curve of fig.9.e. at its
low temperature end where it is most likely to have meaning is
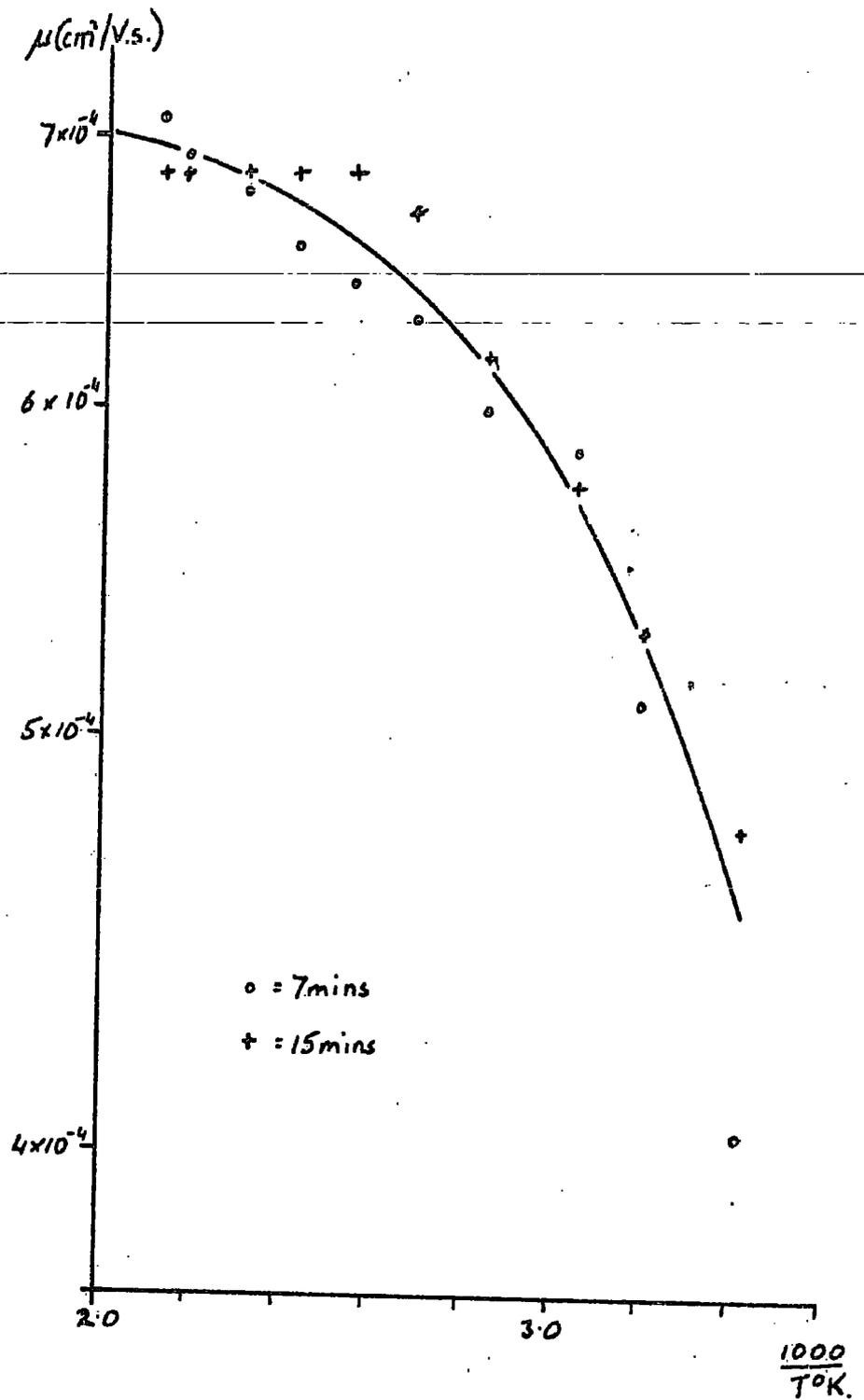
Fig.9.e. Small polaron mobility.

0.1 eV. This means that the temperature T_m at which the mobility is expected to be a maximum is about $380^\circ C$. The high temperature end of the present measurements being $200^\circ C$, it is concluded that the effect of the $T^{-3/2}$ factor would be apparent in these measurements.

In order to remove the effect of the $T^{-3/2}$ factor, $\log (\mu_{xx} T^{3/2})$ is plotted against reciprocal temperature. This plot is shown in fig.9.f. and is a tolerable straight line whose slope indicates a hopping activation energy of 0.074 eV. This modifies the above estimate of T_m to $300^\circ C$ which is consistent with the curve of fig.9.e.

From the value of ξ found above, we can deduce the wavelength λ_m at which the real part of the a.c. conductivity is a maximum. This is given by $\lambda_m = \pi\hbar c/2\xi$ (where c is the velocity of light) and is calculated to be $4.2\,\mu m$. The reflectance of reduced barium titanate single crystals has been measured by Reik and Heese (2.25). They have analysed their results on the basis of the small hopping model and have obtained a maximum in the real part of the a.c. conductivity at approximately $4\,\mu m$.

It is of interest to note that the application of the small polaron hopping model gives even lower values of drift mobility than were obtained in section 2 with conventional band theory.

The ratio between the Hall mobility measurements of Berglund and Baer and the drift mobility results obtained above is now about 700.
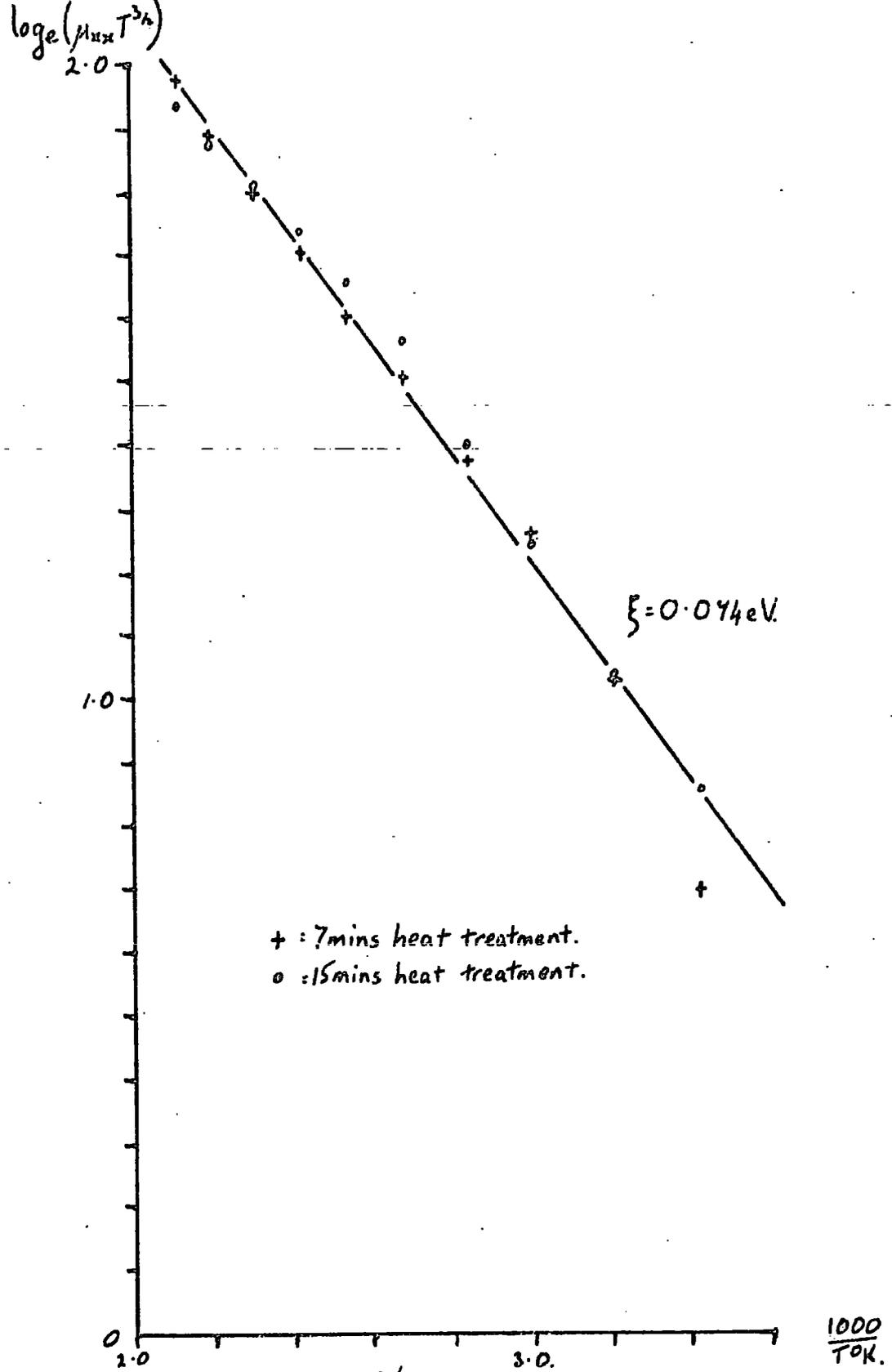
Fig.9.f. Plot of $\log_e(\mu_{xx} T^{3/2})$ against reciprocal temperature demonstrating small polaron hopping transport.

$\log_e(\mu_{xx} T^{3/2})$

$\xi = 0.074\,eV.$

+ : 7mins heat treatment.
o : 15mins heat treatment.

$\dfrac{1000}{T^{\circ}K}$

Holstein (9.3.) has obtained the complete expression for the hopping mobility. The mobility is given by

$$\mu_{xx} = \frac{ea^2}{kT} P \qquad\qquad 9.C.$$

where e, k, and T have their usual meaning, a is the polaron hopping distance (in this case, the Ti – Ti interionic distance). P is the hopping probability which is given in turn by

$$P = \frac{1}{h} \left[\frac{\pi}{\mathscr{E}kT} \right]^{\frac{1}{2}} J^2 \exp(-\mathscr{E}/kT) \qquad\qquad 9.D.$$

where J is a quantity with units of energy which is given various names in the literature but which is associated with resonant exchange of electrons between ions. In these two equations, the only unknowns for the samples of the present work are P and J. At $20^{\circ}C$, P is calculated from equation 9.C. to be 7.4×10^9 sec^{-1}. Then J is calculated from 9.D. and is found to be 0.0086 eV. It should be pointed out that Reik and Heese (2.25.) calculated the value 0.15 eV. The discrepancy presumably arises from their use of Hall mobility rather than drift mobility.

It is predicted both by Holstein and Klinger that with decreasing temperature, there is a transition to band-type motion at a temperature, T_b, which is approximately given by $\hbar\omega_o/2k$ (where ω_o is the angular frequency associated with the wavelength λ_o). In order to verify that the measurements reported in this work are within the range in which small polaron hopping motion can occur, this temperature was calculated and found to

~~be about 20°K. This transition therefore makes no limitation
on the analysis of this section.~~

In section 3, for the conventional band case, the hypothesis
was made that the mobility is unaffected by the hydrogen heat
treatment. It would appear that the same hypothesis would be
appropriate in the small polaron hopping case, since the
mobilities at 7 and 15 minutes heat treatment still agree.
In this case, we can again estimate the variation of carrier
concentration with time of heat treatment using the resistivity
curves of fig.6.h. and the mobility results of this section.
The concentrations arrived at are as follows:-

Heat treatment time at $800°C$ in hydrogen. (minutes)	Extrapolated polaron concentration. (cm^{-1})
3	6.9×10^{19}
5	1.48×10^{20}
7	4.18×10^{20}
10	2.40×10^{20}
15	1.89×10^{20}

These results are similar to those of fig.9.c. but are
numerically higher by a factor of about six. These results
are shown in fig.9.g.

5. Arend's chemical reactions.

We have seen in chapter 2, section 6 how Arend and Coufova
(2.11.) used chemical methods to determine the free electron
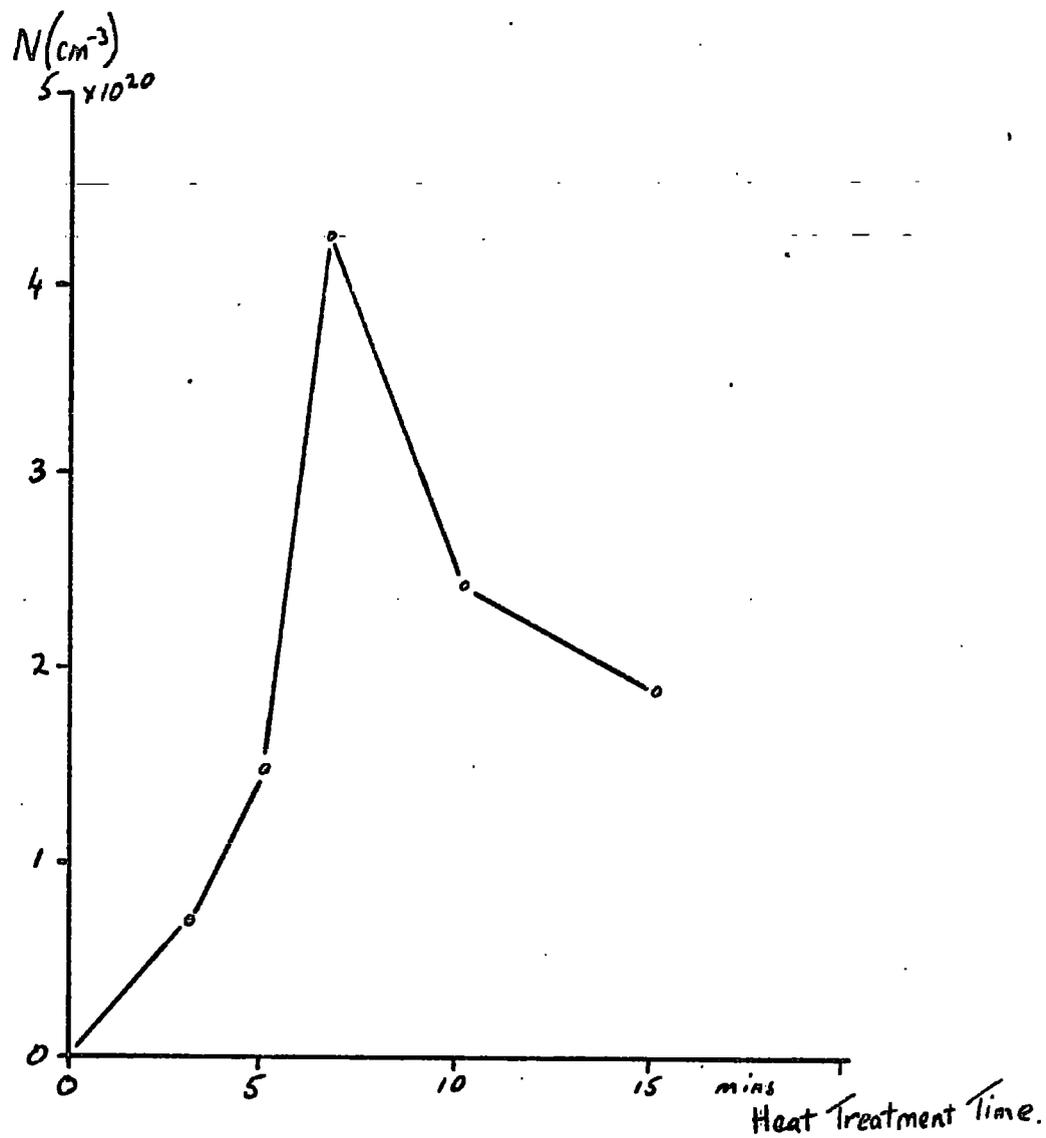
Fig.9.g. Number of small polarons per cm^3.

concentrations in flux grown barium titanate single crystals grown by the flux melt method. Their conclusions were that three chemical processes were responsible for the electrical properties of the crystals during the early stages of the hydrogen reaction. Initially, there is a reaction of the hydrogen with the fluorine impurity in the crystals giving a rapid formation of HF and liberating electrons. Secondly, the volatilization of TiF_3 leads to a reduction in the concentration of electrons. Lastly, a slow reaction takes place in which oxygen ions are removed to form water, giving a steadily rising electron concentration.

On the assumption that the mobility is unaffected by the chemical reactions involved in the heat treatment, the carrier concentrations have been calculated in sections 3 and 4 above for the band and small polaron hopping cases respectively. In both cases, the form of the results was the same, that is, there was found to be an initial rise in carrier concentration, followed by a fall in carrier concentration after about seven minutes heat treatment at $800^{o}C$ in hydrogen. Fig.9.h. shows both these curves together with the curve obtained by Arend and Coufova at $1100^{o}C$. The similarity between the curves obtained by the author and those obtained by Arend and Coufova is apparent. The results of Arend and Coufova show faster reactions as would be expected at a higher temperature. It must also be remembered that the reaction rates will depend on crystal thickness and on initial impurity concentrations, so that the author's results are not to be expected to be in exact agreement with those of Arend and Coufova.

CARRIER CONCENTRATION 10^{21} (cm^{-3})

D.L.R. (Polaron theory) 800°C.

AREND & COUFOVA 1100°C.

D.L.R. (Band theory) 800°C.

10^{20}

10^{19}

5   10   15   mins   20

Reaction time in Hydrogen.
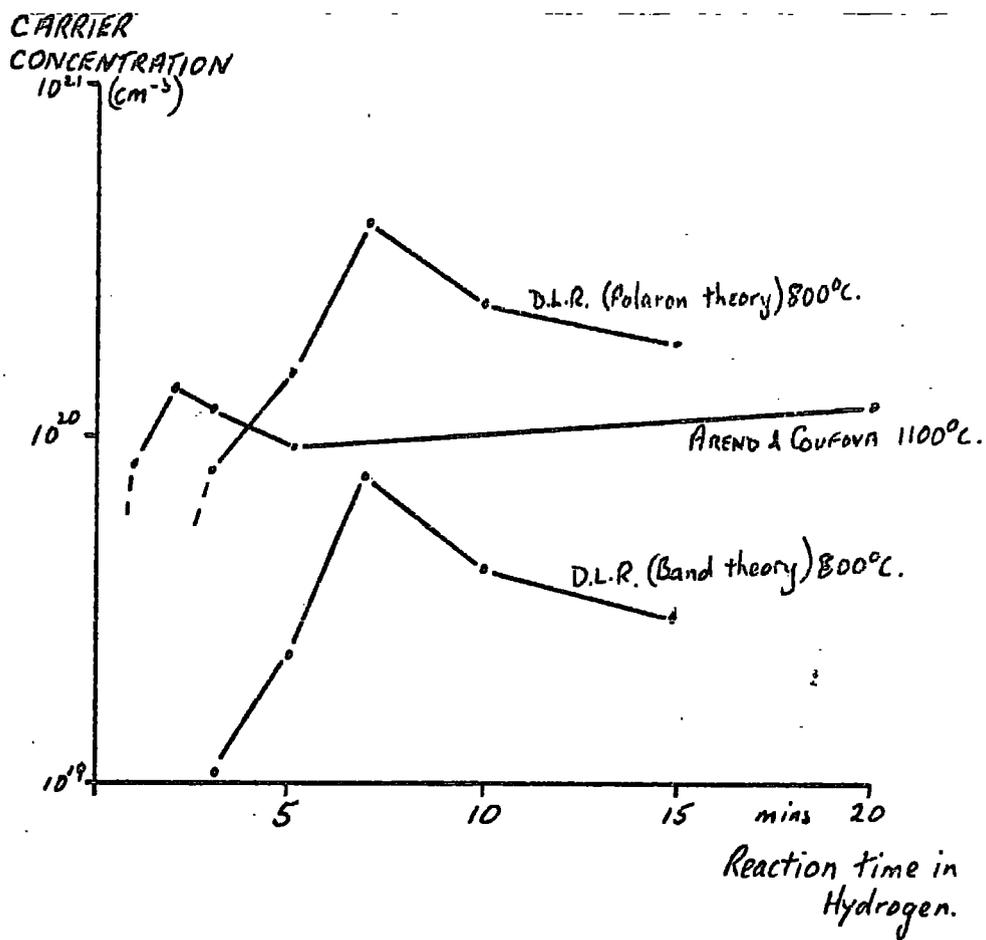
Fig.9.h. Comparison of results of band and polaron theories
with the results of Arend and Coufova.

If the explanation of these curves is as suggested by
Arend and Coufova, it is then possible to see why the Seebeck
coefficient result at three minutes heat treatment is anomalously
high. Throughout these reactions, the crystals will be chemically
and electrically non-uniform since they are not in equilibrium
with their surroundings. All the results obtained therefore
for Seebeck and resistivity measurements will be to some extent
in error. It is possible to show that if the mobility is
independent of carrier concentration as is being suggested
here, then van der Pauw resistivity measurements with current
flow in the plane of the crystal plate will yield a correct
mean carrier concentration. The reasoning behind this will not
be given here but is reproduced in appendix 2.

In the case of Seebeck coefficient measurements however,
inaccuracies will arise if the carrier concentration is non-
uniform. The degree to which this is important will depend both
on the direction and magnitude of the concentration gradients.
In the present case, the crystal reduced for 3 minutes will have
frozen into it the concentration gradients of the initial fast
hydrogen fluoride reaction. There will be strong concentration
gradients since the reaction is so fast and this will lead to
a relatively high error in the Seebeck coefficient results.
The following slower reaction involving the liberation of TiF_3,
will tend to rapidly cancel the gradients set up during the
first reaction since the concentration will decrease most quickly
at the surface where the first reaction has made it highest.
From then on, the reaction is much slower so that the concentration

gradients will be relatively small. It can be seen then how
a series of reactions such as these can give rise initially
to highly erroneous results to Seebeck measurements but
consistent results thereafter.

The analysis of the data for the 3 minute reduced crystal
is further complicated by the rapidly changing conductivity
since it is not certain that the 3 minute resistivities of
fig. 6.h. can be applied to the 3 minute Seebeck results of
fig. 7.c. These results were not obtained on the same crystal
and it is only on crystals reduced for 5 minutes and more that
the resistivities have been shown to agree well between one
sample and another.

It is important at this stage to appreciate where the
conduction electrons come from in these reactions. The complete
reaction equation as formulated by Arend and Coufova is given
in chapter 2, section 6. It is:-

$$(Ba_{1-a}K_a)Ti(O_{3-a}F_a) + (y+u)H_2 = xTiF_4 + 2yHF + uH_2O +$$

$$(Ba_{1-a}K_a)(Ti_{1-x-z}(TiV)_{x-z})$$
$$(O_{3-a-u}F_{a-4x-2y-3x}(AV)_{4x-2y-3z-x})$$

$$+ (2y-z-2u)\ e^-$$
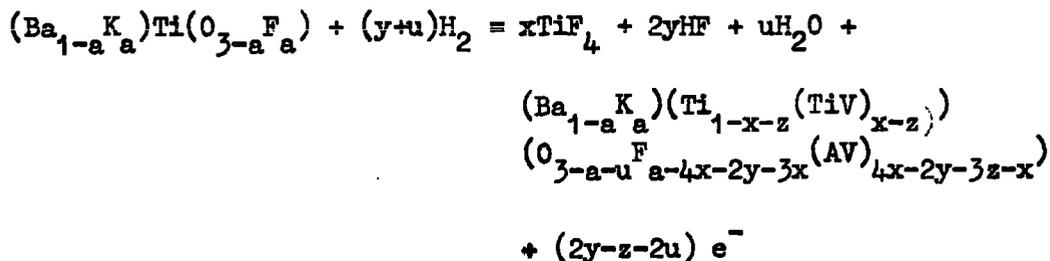
During the first reaction, that of HF formation, the removal
of fluorine leads to the formation of anion vacancies and
electrons. One cannot distinguish between anion vacancies which
have been formed by removal of an impurity ion and those formed
by removal of the oxygen ion. The electrons generated by this

process can be considered therefore as if they had come from
the oxygen 2p levels.

The second process is rather more complicated. The removal
of one titanium ion and three fluorine ions gives rise to one
cation vacancy and three anion vacancies respectively. The
formation of the three anion vacancies liberates three electrons
all of which are used to neutralise the cation vacancy. A
further electron is trapped to complete the cation neutralisation.
No new electrons are liberated therefore but there is a reduction
in the concentration of carrier electrons.

The third process is a simple reduction process. Oxygen
is removed, leaving an oxygen vacancy and liberating one electron.
This electron clearly comes from the oxygen 2p levels.

In this way, it can be seen that at all stages, the electrons
which are available for conduction have come from the oxygen
2p levels (the valence band, in fact). It was seen in chapter 4,
sections 3 and 4 that Jaynes' theory of ferroelectricity is the
only one which could explain the large drop in Curie point shown
in fig.4.c. In this theory, Jaynes attributed the ferroelectric
properties to the oxygenvalence octahedra. The next section will
show how the loss of electrons from the oxygen 2p levels accounts
for the curve of fig.4.c.

There is a further piece of evidence for the three process
theory of Arend. It can be seen from the complete chemical

equation above that it is only the first and last reactions (the formation of HF and of H_2O) which are dependent on the hydrogen atmosphere. The second reaction, that of volatilization of TiF_3 is dependent only on a fluorine impurity in the crystal. The effect of this reaction alone is to remove electrons from the conduction states (the sign of ze is negative). It was reported in chapter 8, section 2 that two probe resistance measurements were made during heat treatment in an argon atmosphere. The resistance was found to increase monotonically for treatment times up to 50 minutes as shown in fig.8.b. This is what one would expect if electrons are removed steadily from the conduction states (assuming the mobility to remain constant throughout).

6.Ferroelectricity in reduced $BaTiO_3$.

Jaynes' theory of ferroelectricity in barium titanate attributes the ferroelectric phenomenon to field splitting of the oxygen 2p levels. We have seen in section 5, that the concentration of electrons in these levels is reduced by the heat treatment process in hydrogen, these electrons being made available for conduction.

In chapter 4, an account of Jaynes' theory was given and it was shown that the Curie point temperature was dependent on the degree to which electrons were removed from the 2p levels. Equation 4.J. gives the Curie temperature in terms of the factor K :-

$$2K/(1 + K) = \tanh(\varepsilon/kT_c)$$

$$\frac{2K}{1+K} = \tanh \left(\varepsilon/kT_c \right)$$

It was shown that K is proportional to the number of electrons in the 2p levels and that this equation makes T_c very sensitive to changes in the electron concentration within the 2p levels. The total concentration of 2p electrons is 3 per unit cell, that is, 4.67×10^{22} cm^{-3}. The peak polaron concentration quoted in section 4 of this chapter is 4.18×10^{20} cm^{-3} so that the oxygen 2p levels have at this stage of the heat treatment process been depleted by 0.9%. The estimate made in chapter 4 of the depletion of these levels was 0.001% but this estimate was based on the Berglund and Baer's Hall mobility and we have now seen that the drift mobility is 1000 times smaller than this. In chapter 4, it was shown that the observed drop in Curie temperature would in fact be explained by a depletion of about 1% in the oxygen valence electrons. It would appear therefore that Jaynes' theory could provide a suitable explanation of the observed change in the Curie point on the basis of the calculated polaron concentrations. On this basis, the changes in Curie point to be expected at various heat treatment levels according to equation 4.J. have been calculated using the polaron concentrations of fig.9.g. The predicted Curie temperatures (assuming that the untreated crystals have a Curie point of 114°C) are shown in the following table together with the measured values.

Heat treatment time at 800°C in hydrogen	Curie point Predicted	Measured
3 mins	108.5°C	108.5°C
5 mins	105.0°C	100.0°C
7 mins	99.5°C	101.5°C
10 mins	102.5°C	–
15 mins	104.0°C	106.0°C

The measured values are replotted in fig.9.i. (solid line)
with the predicted points (broken line) for comparison. The
agreement is certainly within the experimental error. This
agreement verifies not only that the Jaynes' theory is applicable
to these crystals but also confirms that the small polaron
hopping treatment is more appropriate than the band treatment
which would only account for about one or two degrees drop in
Curie temperature. Furthermore, since the Curie point measurements
agree so well with the polaron concentrations determined in
section 5, it suggests that the assumptions on which those
polaron concentrations were calculated are in fact correct.
In calculating the polaron concentrations, it was assumed that
the mobility is unaffected by the chemical processes taking place.
This is, therefore, verified by the Curie point measurements.

7.Conclusions.

The conclusions of this work can be summarised as follows:
1. Electrical conduction in flux grown barium titanate single
crystals takes place in the small polaron hopping mode. This
is determined from the temperature dependence of the drift
mobility which follows a $T^{-3/2} exp(\xi/kT)$ relationship and is
confirmed by the large ratio between the Hall mobility determined
by Berglund and Baer and the drift mobility determined by the
author. The drift mobility is considered to be unaffected by the
chemical reactions which take place during heat treatment in
hydrogen.
2. The electron concentrations in hydrogen heat treated specimens
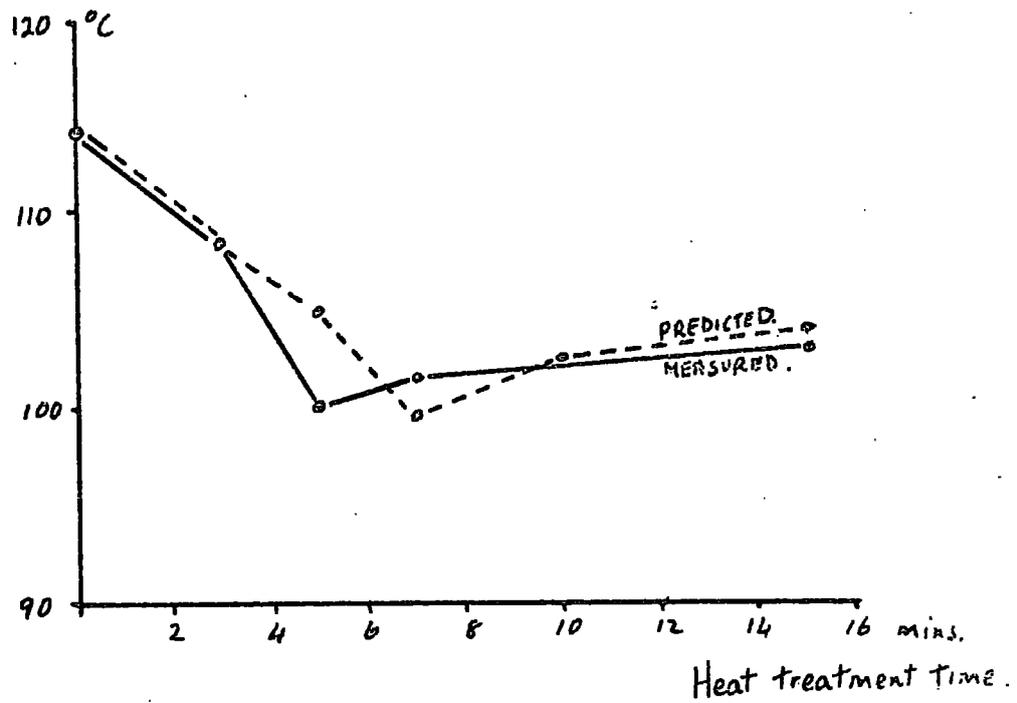
Fig.9.i. Comparison of predicted and measured Curie temperatures.

have been determined on the basis of small polaron hopping motion and have been confirmed by the analysis of measurements of the ferroelectric Curie temperature. The concentrations so obtained are of the same form over the range of heat treatments studied as the electron concentrations derived by Arend and Coufova by chemical methods. This confirms the results of Arend and Coufova and verifies their suggestion that there are three chemical processes which dominate the hydrogen heat treatment of flux grown barium titanate crystals. There are an initial reaction of fluorine impurities with the hydrogen to form HF, followed by the evolution of TiF_3 and finally the removal of oxygen to form water.

3. Two probe measurements of resistance and dielectric constant indicate an anomaly at about $400^\circ C$ in the electrical characteristics of specimens heat treated in air at about $800^\circ C$. No suggestions are made concerning the nature of this effect since it was not extensively studied.

8. Suggestions.

There are a number of points arising from the work reported in this thesis which suggest further research work.

Firstly, those fields in which the author carried out only superficial work require further investigation. Notable among these are the two probe measurements on specimens heat treated in air. The anomaly which occurs at about $400^\circ C$ has not been reported elsewhere and it is felt that its investigation could

throw further light on oxidation/reduction processes in flux melt crystals.

Concerning the main body of work carried out by the author, there are a number of points which require confirmation. The resistivity and ferroelectric Curie temperature measurements should be extended to longer reduction times in order to confirm the third chemical process suggested by Arend and Coufova, that of removal of oxygen. These measurements should show a steadily decreasing resistance after about 15 to 20 minutes reduction and this should be accompanied by a steadily decreasing Curie temperature.

The process of conduction by small polarons has been fairly well established in the present work, but this would be confirmed if the resistivity measurements were extended both to higher and lower temperatures. Higher temperatures should show the maximum in mobility at around $300^{o}C$ and lower temperatures should show an exponential variation of mobility with temperature at temperatures much lower than T_m. The best confirmation which could be obtained of the mobilities which are reported here would be direct measurements of the drift mobility in drift experiments with ultra-violet or electron beam excitation.

Appendix 1

The Sulphide Analogues of Barium Titanate

The existence of barium titanium sulphide has been reported previously by Hahn and Mutschke (A.1.1.). Very little is known about the material but since it is the sulphide analogue of barium titanate, there is some likelihood that it may be isomorphous with and have similar properties to barium titanate. In order to gain some information on this, sintered specimens of the double sulphide, $BaTiS_3$, and also of the thiotitanate, $BaTiSO_2$ were made (see note (a) below).

Equimolar proportions of BaS and TiS_2 in one case and of BaS and TiO_2 in the other, were ground, intimately mixed and pressed into pellets measuring $\frac{3}{4}$ in. in diameter and about 1/16 in. thick. These were then placed in a stainless steel bomb and fired at $800^{\circ}C$ for several days.

The specimen of the double sulphide which was prepared in this way was subjected to X-ray powder photography. After elimination of the lines due to excess barium sulphide, the pattern agreed well with that reported by Hahn and Mutschke. Hahn and Mutschke indexed the lines on the basis of a hexagonal structure with a = 6.781 and c = 5.686. It was found in the course of the present work, however, that there was also evidence of a tetragonal structure with a = 4.087 and c = 6.687.

Whether or not the mixed sulphide is hexagonal, it is unlikely to be ferroelectric since in the perovskite ferroelectrics,

one expects the axial ratio to be nearly unity (c.f. barium titanate where $c/a = 1.01$).

Further evidence that the material is not ferroelectric is provided by measurements of the capacitance of the disc which indicated a dielectric constant of less than 10.

The thiotitanate has not been reported to exist. The reacted material corresponding to its composition, however, showed X-ray powder lines which were unidentifiable from the A.S.T.M. index. No definite analysis of these lines could be made but there was some evidence among some of the stronger lines of an orthorhombic structure. Again there was no evidence of a high dielectric constant.

The main conclusion to be drawn from this work is that barium titanium sulphide and, if it exists, barium thiotitanate are probably not similar in structure or electrical properties to barium titanate. In view of this no further work was performed on them.

(a) In the literature, the compound $BaTiS_3$ has been referred to as the thiotitanate. Strictly speaking, this nomenclature should be reserved for a compound in which only one oxygen atom per molecule is replaced by sulphur.

In this appendix, therefore, in order to differentiate between the two compounds and to preserve correct chemical usage, the complete sulphide is referred to as barium titanium sulphide and the compound $BaTiSO_2$ is given the prefix thio-.

Appendix 2

Mean electron concentration from non-uniform crystals

It would seem that the results of the present measurements agree with the chemical measurements of Arend and Coufova and that their chemical processes took place in the author's heat treatment experiments. If this is so, then there is an important point to remember in the interpretation of the electrical results. That is, that at no time during these chemical reactions are the crystals in equilibrium with their surroundings. The consequence is that at all times there will be impurity concentration gradients and hence carrier concentration gradients in the crystals. This appendix shows how this affects the resistivity measurements.

Fig. A.2.1. shows a slab of material which can be considered to be made up of an infinite number of layers in each of which the mobility is the same but the electron concentration is different. We designate the number of electrons in the mth slice as n_m. If contacts are applied on the periphery of the slab, the conductance of the mth slice, Σ_m, is proportional to n_m.

$$\Sigma_m = kn_m eu$$ where k is a function of the geometry of slice and contacts, and is the same for all slices.

The total conductance, Σ , of the slab is obtained by summation over all m,

$$\Sigma = keu(n_1 + n_2 + n_3 + \dots \text{ etc}).$$

$$\Sigma = keun$$ where n is the total number of conduction

current flow

mth slice containing
n_m electrons per c c
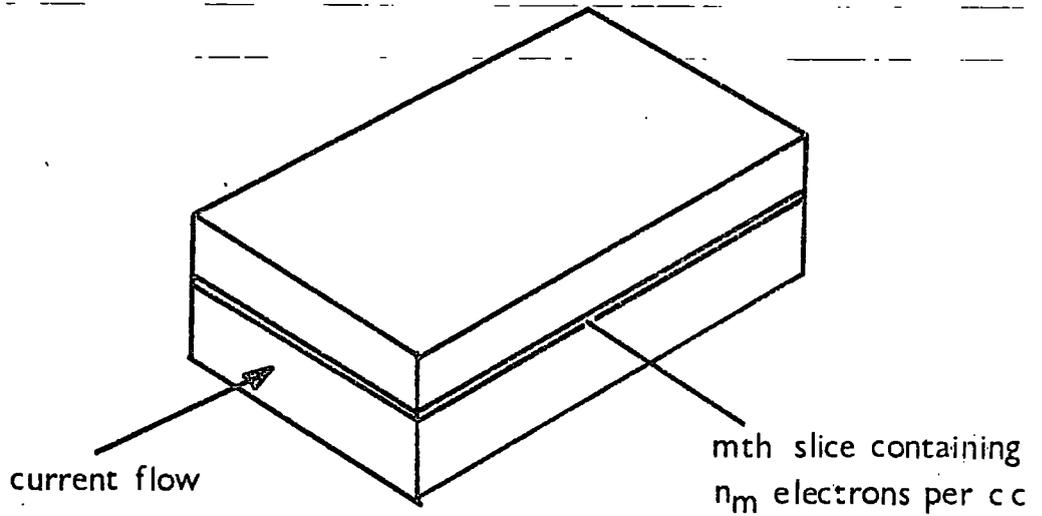
Fig. A.2.1 Crystal plate with non-uniform electron concentration.

electrons in the crystal. It can be seen therefore that in the rather special case of conductivity measured in the plane of a slice where carrier concentration gradients are essentially perpendicular to the current flow, the measured resistivity will be the same as if the electrons present **had** been uniformly distributed. The measurement of crystal plates by van der Pauw's method fulfils this special case. During the chemical processes involved, the reactions will take place at the surface and the impurities involved in the reactions will diffuse outwards towards the surface. Apart from a relatively small correction for reaction at the edges, the concentration gradients will be perpendicular to the flat faces of the crystals. The resistivity measurements of chapter 6, can be assumed therefore to have involved all the electrons available for conduction and so the results are comparable with the chemical results of Arend and Coufova.

Bibliography

1.1.   Bulletin of the Institute of Physics   18,302,(1967).

2.1.   Von Hippel et al.   Ind.Eng.Chem.,38,1097,(1946).
2.2.   Wul & Goldman   C.R.Acad.Sci.U.R.S.S.46,139,(1945).
                               C.R.Acad.Sci.U.R.S.S.49,177,(1945).
                               C.R.Acad.Sci.U.R.S.S.51, 21,(1945).
2.3.   Rase & Roy   J.Am.Ceram.Soc.,38,102,(1955).
2.4.   Megaw   Nature,155,484,(1945).
2.5.   Rhodes   Acta.Cryst.,2,417,(1945).
                                     Acta Cryst.,4,105,(1951).
2.6.   Mason & Matthias   Phys.Rev.,74,1622,(1948).
        and Mason   Piezoelectric crystals (Van Nostrand,N.Y.)(1949).
2.7.   Devonshire   Phil.Mag.series 7,40,1040,(1949).
2.8.   Slater   Phys.Rev.,78,748,(1950).
2.9.   Jaynes   Phys.Rev.,79,1008,(1950).
        and Ferroelectricity,(Princeton University Press)
                                                        (1953).
2.10.   Cross   Phil.Mag.series 7,44,1161,(1953).
2.11.   Arend,Coufova & Novak   J.Amer.Ceram.Soc.,50,22,(1967).
2.12.   Novak & Arend   J.Amer.Ceram.Soc.,47,530,(1964).
2.13.   Heywang   J.Amer.Ceram.Soc.,47,484,(1964).
2.14.   Jonker   Sol.St.Electronics,7,895,(1964).
2.15.   Brown & Taylor   J.Appl.Phys.,35,2554,(1964).
2.16.   Ikegami & Ueda   J.Phys.Soc.Jap.,19,159,(1964).
2.17.   Branwood & Tredgold   Proc.Phys.Soc.76,93,(1960).
2.18.   Kawabe & Inuishi   Jap.J.Appl.Phys.,2,590,(1963).
2.19.   Ueda & Ikegami   J.Phys.Soc.Jap.,20,546,(1965).
2.20.   Ikegami, Ueda & Ise   J.Phys.Soc.Jap.,16,572,(1961).

2.21. Berglund & Baer   Phys.Rev.

2.22. Kosek & Arend   Phys.Stat.Sol.$\underline{24}$,K.69,(1967).

2.23. Cox, Roberts & Tredgold   Brit.J.Appl.Phys.,$\underline{17}$,743,(1966).

2.24. Arend & Coufova   Czech.J.Phys.,$\underline{B13}$,55,(1963).

2.25. Reik & Heese   Phys.Stat.Solidi,$\underline{24}$,281,(1967).

2.26. Gerthsen, Groth, Hardtl,
       Heese & Reik   Sol.St.Comm.,$\underline{3}$,165,(1965).

2.27. Kahn & Leyendecker   Phys.Rev.,$\underline{135}$,A1321,(1964).

3.1. Gallagher & Schrey   J.Amer.Ceram.Soc.,$\underline{46}$,567,(1963).

3.2. Rase & Roy   J.Amer.Ceram.Soc.,$\underline{38}$,102,(1955).

3.3. Horn   J.Appl.Phys.,1616,(1961).

3.4. Sasaki   Jap.J.Appl.Phys.,$\underline{4}$,24,(1965).

3.5. Brown & Todt   J.Appl.Phys.,$\underline{35}$,1594,(1964).

3.6. Remeika   U.S.Patent No.2,852,400,(Sept.1958).
                  and   J.Amer.Ceram.Soc.,$\underline{76}$,940,(1954).

3.7. de Vries   G.E.^{C}.Res.Labs.Rep.No.59-RL-2188(1959).

3.8. Saburi   J.Phys.Soc.Jap.,$\underline{14}$,1159(1959).

3.9. Brown & Taylor   J.Appl.Phys.,$\underline{35}$,2554,(1964).

3.10. Ikegami & Ueda   J.Phys.Soc.Jap,$\underline{19}$,159,(1964).

3.11. Branwood,Hughes, Hurd & Tredgold
                       Proc.Phys.Soc.,$\underline{79}$,1161,(1962).

3.12. Turner & Sauer   J.Electrochem.Soc.,$\underline{107}$,250,(1960).

3.13. Pearlstein   Metal Finishing,$\underline{59}$,(1955).

3.14. Landis   J.Appl.Phys.$\underline{36}$,2000,(1965).

3.15. Morgan   Ph.D.Thesis,University of Durham (1966).

4.1. Jaynes   Ferroelectricity(Princeton University Press)(1953).

4.2. Mason & Matthias   Phys.Rev.$\underline{74}$,1622,(1948).

4.3. Devonshire   Phil.Mag.series 7,$\underline{40}$,1040,(1949).

4.4. Slater   Phys.Rev.,$\underline{78}$,748,(1950).

5.1. Dvorak   Czech.J.Phys.,B11,253(1961).

5.2. & 5.4. Kupfer,(ed)   Polarons & Excitons.

5.3. Elliott

6.1. Smith   Semiconductors,(C.U.P.)(1959).

6.2. Putley   The Hall Effect & Related Phenomena
                                           (Butterworth)(1960).

6.3. van der Pauw   Phillips Res.Reps.,13,1,(1958).

6.4. Allen   M.Sc.Thesis.University of Newcastle-upon-Tyne
                                              (1965).

9.1. Klinger

9.2. Jonker & van Houten   Sonderdruck aus Halbleiterprobleme,
                                           Band VI (1961).

9.3. Holstein   Ann.Phys.,8,343,(1959).

A.1.1. Hahn & Mutschke   A.S.T.M. Index.
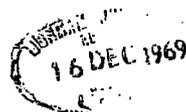
Electrical Conductivity during Hydrogen Reduction of Barium Titanate Single Crystals

In recent years, considerable research effort has been directed to a better understanding of electrical processes in oxygen-deficient barium titanate [1-7] and particularly in single crystals grown by the process described by Remeika [8]. It is well established that single crystals grown by this technique suffer from the incorporation of appreciable concentrations of impurities, notably potassium and fluorine from the solvent.

It has been recently shown by Arend et al [7] that these impurities play an important role in the chemical processes which take place during the early stages of the hydrogen reduction of these single crystals. The method employed by Arend involved chemical analysis of crystals reduced in hydrogen at temperatures of 900° C and above for periods from a few minutes to a few hours. This established that there are three regions in which different chemical processes are involved.
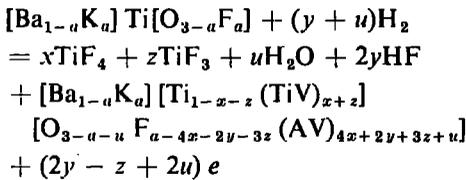
Initially, the hydrogen reacts with fluorine present in the crystal to produce hydrogen fluoride. This results in the fast liberation of electrons into the conduction band of the material.

Subsequently, a slower process of volatilis-

ation of titanium fluoride becomes dominant. The release of titanium fluoride is accompanied by a drastic reduction in the number of free electrons in the material.

Finally, when all the fluoride ions in the crystal have been exhausted by these processes, the slow process of formation of water by reduction of the barium titanate forming an oxygen-deficient crystal becomes detectable although the number of electrons liberated by this process remains relatively small at temperatures of 900° C even up to reduction times of 20-h.

Arend gives the reaction equation including all observed processes as

$$[Ba_{1-a}K_a] Ti[O_{3-a}F_a] + (y + u)H_2$$
$$= xTiF_4 + zTiF_3 + uH_2O + 2yHF$$
$$+ [Ba_{1-a}K_a] [Ti_{1-x-z} (TiV)_{x+z}]$$
$$[O_{3-a-u} F_{a-4x-2y-3z} (AV)_{4x+2y+3z+u}]$$
$$+ (2y - z + 2u) e$$

where (TiV) and (AV) indicate titanium and anion vacancies respectively.

Concurrent experiments have been performed by the present writers in which flux-grown barium titanate crystals were reduced in hydrogen at 800° C for times up to 15 min. In some of these experiments, platinum paste contacts were applied to opposite faces of the crystal plates allowing two-probe resistance measurements to be made during the reduction process. The result of such an experiment in which the specimen resistance reached a minimum after 5 min reduction is shown in fig. 1. Subsequent reduction up to 20 min resulted in an increased resistance.

Further specimens (obtained from the Harshaw Chemical Co) were reduced without contacts applied, and were allowed to cool to room temperature after varying reduction times. Four-probe resistivity measurements were made on these specimens with current flow in the plane of the crystal plates. Although the crystals are expected to be non-uniformly reduced, since the chemical reactions occur at the surface, a representative average figure for the concentration of electrons should be obtained if the current flow is parallel to the principal faces of the crystal. On this basis, Hall and Seebeck coefficient measurements were made on these plates. The apparatus used was unable to detect a Hall signal indicating a mobility of less than 10^{-5} m^2/Vsec. Seebeck coefficient measurements
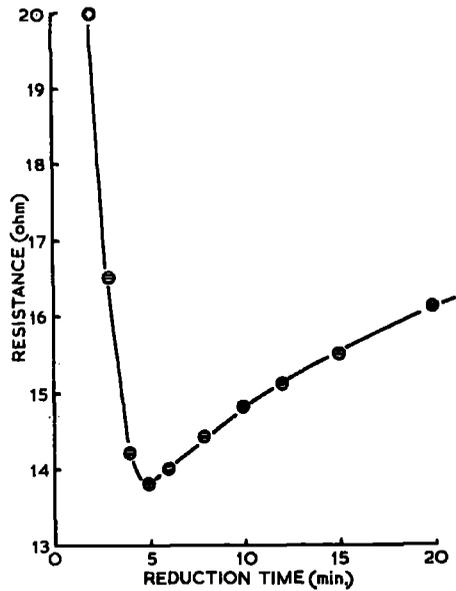
336

Figure 1 Two-probe resistance of barium titanate flux-grown crystal measured during reduction in hydrogen at 800° C.

at 300° K on crystals reduced for more than 5 min were used to determine the electron concentration assuming an electron effective mass of 4.5 m_0 (Berglund and Baer [9]), and a scattering parameter $S = +\frac{1}{2}$. The resulting concentrations were approximately proportional to the conductivity, indicating a mobility near 3×10^{-7} m^2/Vsec. The Seebeck results for crystals reduced for less than 5 min did not lead to similar mobilities, and this may be due to the very high concentration gradients in the crystals during the initial fast reaction.

The representative electron concentrations calculated from the resistivities using the mobilities obtained at reduction times greater than 5 min are shown in fig. 2 with the results of Arend et al for comparison. Agreement between these results is close since the crystals were probably grown under somewhat different conditions and therefore probably contain different initial concentrations of impurities. Furthermore, the shape of the curves depends on the thickness of the crystals. The lower curve of fig, 2 is based on crystals with thickness between 100 and 150 μm.

Further evidence to support the reaction mechanisms proposed by Arend is obtained from measurements made during heat treatments in an inert atmosphere. Of the three reactions proposed by Arend, only the first and last are dependent on
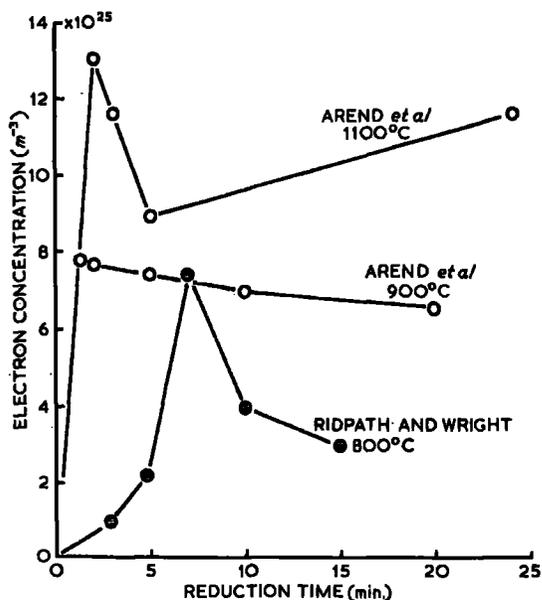
Figure 2 Electron concentration of reduced crystals compared with the results of Arend *et al* [7].

a hydrogen atmosphere. The second, the volatilisation of TiF_3, is expected to take place on heat treatment in the absence of hydrogen. Two-probe resistance measurements have been made
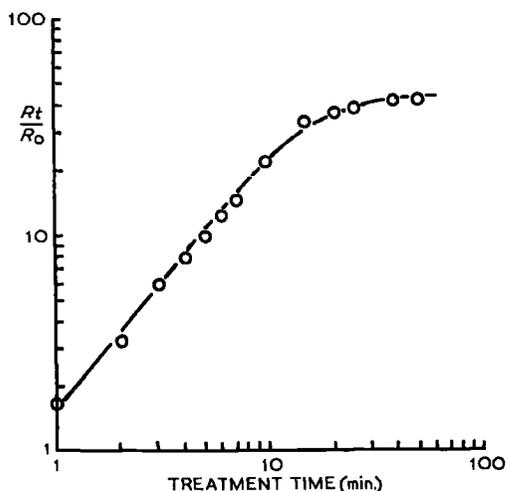
in a similar way to that described for the two-probe measurements during reduction, with an ambient of argon at atmospheric pressure. The results are shown in fig. 3, the resistance being expressed as a multiple of the initial resistance. It can be seen that the resistance now increases monotonically as a function of time. This follows from the equation above where y and u are now zero and the change in electron concentration is $-z$.

These electrical resistance measurements correlate directly with the analytical measurements of Arend *et al* and support their proposal that the heat treatment of flux-grown barium titanate in hydrogen results in three reactions, the formation of HF, the volatilisation of TiF_3 and the formation of water.

Acknowledgements

Figure 3 Increase in resistance of flux-grown $BaTiO_3$ during heat treatment in argon at 800° C.

References

1. K. KAWABE and Y. INUISHI, *Jap. J. Appl. Phys.* **2** (1963) 590.
2. H. IKUSHIMA and S. HAYAKAWA, *ibid* **6** (1967) 454.
3. S. IKEGAMI, I. UEDA, and Y. ISE, *J. Phys. Soc. Jap.* **16** (1961) 572.
4. S. IKEGAMI and I. UEDA, *ibid* **19** (1964) 159.
5. H. AREND and P. COUFOVA, *Czech. J. Phys.* **B13** (1963) 55.
6. V. DVORAK, *ibid* **B11** (1961) 253.
7. H. AREND, P. COUFOVA, and J. NOVAK, *J. Amer. Ceram. Soc.* **50** (1967) 22.
8. J. P. REMEIKA, *J. Amer. Chem. Soc.* **76** (1954) 940.
9. C. N. BERGLUND and W. S. BAER, *Phys. Rev.* **157** (1967) 358.

16 February 1968   D. L. RIDPATH*
D. A. WRIGHT
Department of Applied Physics
University of Durham
South Road, Durham City, UK

*Current address: Central Electricity Research Laboratories, Cleeve Road, Leatherhead, Surrey, UK